**GABRIEL MARQUES PONTES**

# **Ocean-Atmosphere interactions in the mid-Pliocene global warming:** Lessons for the 21st century climate

São Paulo
2021

GABRIEL MARQUES PONTES

# **Ocean-Atmosphere interactions in the mid-Pliocene global warming:** Lessons for the 21st century climate

A thesis submitted to the Instituto Oceanográfico of the Universidade de São Paulo in partial fulfilment for the requirements for the degree of **Doctor of in Sciences**, Oceanography, with emphasis in Physical Oceanography.

Supervisor: **Prof. Dr. Ilana Wainer**

São Paulo
2021

GABRIEL MARQUES PONTES, **Ocean-Atmosphere interactions in the mid-Pliocene global warming:** Lessons for the 21st century climate. A thesis submitted to the Instituto Oceanográfico of the Universidade de São Paulo in partial fulfilment for the degree of Doctor of Sciences, Oceanography, with emphasis in Physical Oceanography.

Approved on: ___/___/_____

Examination Board

Prof. Dr. Ilana Wainer Instituição: IO-USP

Presidente Assinatura _____

Prof. Dr._____ Instituição: _____

Conceito_____ Assinatura _____

Prof. Dr. _____ Instituição: _____

Conceito_____ Assinatura _____

Prof. Dr. _____ Instituição: _____

Conceito_____ Assinatura _____

To my beloved wife, Ana Carolina.

# ACKNOWLEDGEMENTS

First of all, a special thanks to my supervisor, Professor Ilana Wainer, for always believing in my capability of achieving this objective and contributing to my maturity in the scientific field.

A very special thanks to Professor Andréa S. Taschetto for supporting all my ideas and hypotheses and also for all of the help while I was abroad undertaking my academic internship at the University of New South Wales.

To Professors Alex Sen Gupta and Agus Santoso for the amazing discussions.

To the OC2 crew for making of this lab an enjoyable environment and, of course, for the fun and afterhours beers.

To my family for all of the support during all these years.

To the Oceanographic Institute for providing all necessary infrastructure.

To the São Paulo Research Foundation for granting this PhD scholarship and all the financial support for the development of this research (processes number 2016/23670-0 and 2019/08282-1).

This study was financed in part by the Coordenação de Aperfeiçoamento de Pessoal de Nível Superior - Brasil (CAPES) - Finance Code 001.

And, to the most special person, my wife, Ana Carolina, whose love and partnership gave me extra energy during the most difficult times throughout this journey.

Each time politics is mixed up with science,

humanity gives a thousand steps behind.

# ABSTRACT

PONTES, Gabriel Marques. **Ocean-Atmosphere interactions in the mid-Pliocene global warming:** Lessons for the 21st century climate. 2021. 219 f. Thesis (Doctorate) – Oceanographic Institute, University of São Paulo, São Paulo, 2021.

During the mid-Pliocene (~3 million years before present), annual mean temperatures were approximately 3°C higher than present, which is similar to the projected global warming for the end-of-century climate. Furthermore, carbon dioxide ($CO_2$) concentrations in the atmosphere were similar to present day (~400 ppm). Paleoclimate studies have been investigating whether there was a past warm climate that would serve as an analogue for the current warming. As such, the mid-Pliocene climate arises as a candidate to a possible future scenario. This thesis investigates key aspects of the Southern Hemisphere climate in the mid-Pliocene through the simulation results of the Pliocene Model Intercomparison Project and climate model sensitivity experiments to evaluate whether the mid-Pliocene is comparable to the projected future warming. Firstly, higher rates of warming in the northern hemisphere create an interhemispheric temperature gradient that enhances the southward cross-equatorial energy flux by up to 48% in the mid-Pliocene. This intensified energy flux reorganizes the atmospheric circulation leading to a northward shift of the Inter-Tropical Convergence Zone (ITCZ) and weakened and poleward displaced Southern Hemisphere Subtropical Convergences Zones. These changes result in drier-than-normal Southern Hemisphere tropics and subtropics, with rainfall reductions in South America of up to 25%. Second, the modes of variability based on Atlantic sea surface temperature were overall weaker and less frequent, indicating increased climate stability in the mid-Pliocene. In particular, a weaker Atlantic Meridional Mode was associated with increased inter-hemispheric SST gradient and northward ITCZ shift. Lastly, a northward shift of the Pacific ITCZ reduced the activity of the El Niño Southern Oscillation by 25%. These results highlight the key role of the ITCZ position in driving climate change in the tropics and subtropics of the Southern Hemisphere. Observations and numerical studies of the ongoing warming, on the other hand, show a southward shift in the Pacific and Atlantic ITCZs, which indicate that the mid-Pliocene global warming differs from the current warming. Thus, significant climate aspects represented by the current set of Pliocene climate simulations are not being experienced in 20th/21st century warming of the planet. Nonetheless, this thesis highlights the effects of meridional shifts of the ITCZ to the Southern Hemisphere climate.

Keywords: Climate Science, paleoclimatology, climate modelling, modes of variability, Atlantic Ocean, South America.

# RESUMO

PONTES, Gabriel Marques. **Interações Oceano-Atmosfera no aquecimento global do Plioceno Médio:** Lições para o clima do século 21. 2021. 219 f. Tese (Doutorado) – Instituto Oceanográfico, Universidade de São Paulo, São Paulo, 2021.

Durante o Plioceno Médio (~3 milhões de anos atrás) temperaturas médias anuais eram aproximadamente 3°C acima das atuais e com concentrações de $CO_2$ na atmosfera equivalentes à moderna (~400 ppm). Estudos paleoclimáticos tem investigado a possibilidade de haver algum clima passado que sirva de análogo para o atual aquecimento global. Assim, o Plioceno Médio surge como um potencial candidato a um clima futuro mais quente. Nesta tese são investigados processos importantes para o clima do Hemisfério Sul, através de resultados das modelagens numéricas do *Pliocene Model Intercomparison Project* associados a experimentos numéricos com modelos climáticos, para avaliar se o clima do Plioceno Médio pode ser considerado um análogo para as iminentes mudanças climáticas. Primeiramente, os resultados desta tese mostram que elevadas taxas de aquecimento no Hemisfério Norte intensificaram o gradiente inter-hemisférico de temperatura assim como o fluxo de energia do Hemisfério Sul para o Norte no Plioceno Médio, o que levou a uma reorganização da circulação atmosférica resultando em um descolamento para norte da Zona de Convergência Inter-Tropical (ZCIT) e a Zonas de Convergência Subtropicais mais fracas e deslocadas para sul. Estas mudanças resultaram em um Hemisfério Sul mais seco que o atual, com reduções na precipitação da América de 25%. Ainda, a análise dos modos de variabilidade do Oceano Atlântico baseados na temperatura da superfície do mar indica maior estabilidade climática no Plioceno Médio. Em especial, o aumento no gradiente inter-hemisférico de temperatura e o deslocamento para norte da ZCIT estão associados à menor amplitude do modo meridional do Atlântico no Plioceno Médio. Por último, o deslocamento para norte da ZCIT no oceano Pacífico resultou em maior estabilidade do fenômeno El Niño Oscilação Sul. Os resultados apresentados nesta tese destacam o papel fundamental da ZCIT em gerar mudanças no clima das regiões tropicais e subtropicais do Hemisfério Sul. Estudos observacionais e numéricos sobre o aquecimento global atual mostram um deslocamento para sul das ZCITs nos oceanos Atlântico e Pacífico, os quais indicam que apesar da semelhança entre as magnitudes do aquecimento global do Plioceno Médio e o atual (~3ºC), a resposta do sistema Terra nestes dois cenários é diferente. Sendo assim, as atuais simulações do clima no Plioceno Médio apresentam aspectos que divergem do aquecimento do sistema terrestre atual, e, portanto, devem ser usados com cautela como um análogo do clima atual. No entanto, os resultados desta tese destacam as implicações das migrações meridionais da ITCZ para importantes processos associados ao clima do Hemisfério Sul.

Palavras-chave: Ciência do clima, paleoclimatologia, modelagem do sistema climático, modos de variabilidade, Oceano Atlântico, América do Sul.

# LIST OF FIGURES


| | | |
|---|---|---|
| Figure 1 | Earth's chronology ring and important climatic stages | 15 |
| Figure 2 | Temperature trends of the past 65 Ma | 17 |
| Figure 3 | Data-model comparison of mid-Pliocene SST anomalies | 18 |
| Figure 4 | Cumulative probability functions for binomial distributions | 28 |
| Figure 5 | Data-model comparison of Sea Surface Temperatures anomalies | 33 |
| Figure 6 | Summertime rainfall change and Subtropical Convergence Zones | 40 |
| Figure 7 | Subtropical high intensification | 42 |
| Figure 8 | STCZs-ITCZ-Monsoon relationship | 45 |
| Figure 9 | Atmospheric Meridional circulation changes | 48 |
| Figure 10 | Schematic of the drivers of reduced rainfall in the Southern Hemisphere | 49 |
| Figure 11 | Simulated variability in the mid-Pliocene | 56 |
| Figure 12 | Multi-model analysis of the Atlantic Multidecadal Variability | 60 |
| Figure 13 | AMOC changes | 64 |
| Figure 14 | Multi-model analysis of the Atlantic Meridional Mode | 67 |
| Figure 15 | Tropical Atlantic mean state changes | 68 |
| Figure 16 | Multi-model analysis of the South Atlantic Subtropical Dipole | 71 |
| Figure 17 | Simulated Mid-Pliocene tropical variability changes | 83 |
| Figure 18 | Equatorial Pacific Ocean changes | 85 |
| Figure 19 | Increased ENSO stability | 88 |
| Figure 20 | ENSO-ITCZ inter-model relationship | 91 |
| Figure 21 | Changes to potential ENSO triggers | 93 |
| Figure 22 | Energetics constraints for the ITCZ position | 96 |
| Figure 23 | Schematic of the drivers of suppressed ENSO activity in the mPWP | 98 |
| Figure 24 | Schematic of the drivers of the changes in ocean-atmosphere processes in the mPWP | 101 |

# LIST OF TABLES


| | | |
|---|---|---|
| Table 1 | PlioMIP1 and PlioMIP2 boundary conditions | 23 |
| Table 2 | Modelling groups participant in PlioMIP phases1 and 2 | 24 |

## ABBREVIATION LIST

| | |
|---|---|
| AEM | Atlantic Equatorial Mode |
| AGCM | Atmospheric General Circulation Model |
| AMM | Atlantic Meridional Mode |
| AMV | Atlantic Multi-decadal Variability |
| AMOC | Atlantic Meridional Overturning Circulation |
| BP | Before present |
| CAM | Community Atmospheric Model |
| CESM | Community Earth System Model |
| CMIP | Coupled Model Intercomparison Project |
| ENSO | El Nino Southern Oscillation |
| EOF | Empirical Orthogonal Function |
| ITCZ | Inter-Tropical Convergence Zone |
| ITF | Indonesian Through Flow |
| ka | Thousand years |
| Ma | Million years |
| MIP | Model Intercomparison Project |
| MMM | Multi-model mean |
| MMMe | Multi-model median |
| mPWP | mid-Pliocene Warm Period |
| NAD | North Atlantic Drift |
| NCAR | National Center for Atmospheric Research (USA) |
| PlioMIP | Pliocene Model Intercomparison Project |
| PRISM | Pliocene Reconstruction, Interpretation and Synoptic Mapping project |
| RCP | Representative Concentration Pathway |
| SAT | Surface Air Temperature |
| SACZ | South Atlantic Convergence Zone |
| SAMS | South American Monsoon System |
| SASD | South Atlantic Subtropical Dipole |
| SHB | Southern Hemisphere Booster |
| SICZ | South Indian Convergence Zone |
| SPCZ | South Pacific Convergence Zone |
| SPMM | South Pacific Meridional Mode |
| SST | Sea Surface Temperature |
| SSP | Shared Socioeconomic Pathway |
| STCZs | South Tropical Convergence Zones |
| TNA | Tropical north Atlantic |
| WES | Wind-Evaporation-SST |

## CONTENTS


**1 INTRODUCTION 14**

1.1 THE PLIOCENE EPOCH – GEOLOGICAL CONTEXT 16

1.2 THE MID-PLIOCENE WARM PERIOD (MPWP) – PHYSICAL ENVIRONMENT 17

**2 SCIENTIFIC HYPOTHESIS – RATIONALE 20**

**3 OBJECTIVES 21**

3.1 CENTRAL OBJECTIVE 21

3.2 SPECIFIC OBJECTIVES 21

**4 MATERIALS AND METHODS 22**

4.1 THE PLIOCENE MODEL INTERCOMPARISON PROJECT (PLIOMIP) 22

*4.1.1 Multi-model analysis 25*

4.2 THE COMMUNITY EARTH SYSTEM MODEL (CESM) 29

*4.2.1 Experimental Design 29*

**5 RAINFALL REGIME IN THE SOUTHERN HEMISPHERE IN THE MPWP 31**

5.1 INTRODUCTION 32

5.2 METHODS 35

5.3 RESULTS 38

*5.3.1 Subtropical High Intensification 41*

*5.3.2 ITCZ-Monsoon-STCZs relationship 43*

*5.3.3 Large-scale forcing 46*

5.4 DISCUSSION 48

**6 ATLANTIC SST VARIABILITY IN THE MPWP 53**

5.1 INTRODUCTION 54

6.2 METHODS 57

6.3 RESULTS 59

*6.3.1 Atlantic Multidecadal Variability 59*

*6.3.1.1 The role of the Atlantic Meridional Overturning Circulation 62*

*6.3.2 Tropical Atlantic Modes 65*

*6.3.3 The South Atlantic Subtropical Dipole 69*

*6.3.4 Frequency 71*

6.4 DISCUSSION 72

**7 THE EL NIÑO-SOUTHERN OSCILLATION IN THE MPWP 76**

7.1 INTRODUCTION 77

7.2 METHODS 78

7.3 RESULTS 82

*7.3.1 Reduced ENSO amplitude 82*

*7.3.2 Role of equatorial Pacific Ocean changes 83*

*7.3.3 Increased ENSO stability 86*

*7.3.4 Role of off-equatorial Pacific changes 89*

*7.3.5 Large-scale forcing 94*

7.4 DISCUSSION 97

**8 CONCLUSION 100**

8.1 SCIENTIFIC PROGRESS 100

8.2 CONCLUDING REMARKS 101

**REFERENCES 104**

**APPENDIX A – SUPPLEMENTARY INFORMATION FOR CHAPTER 5 115**

**APPENDIX B – SUPPLEMENTARY INFORMATION FOR CHAPTER 6 119**

**APPENDIX C – SUPPLEMENTARY INFORMATION FOR CHAPTER 7 128**

# 1 Introduction

During Earth's 4 billion years' history, it has undergone a number of changes and a variety of climate states. Paleo archives indicate that Earth has experienced extremely cold climates, the so called 'snowball Earths' (Figure 1), with estimates that 70% of the surface was covered by ice (i.e., Hoffman et al. 1998). There were also periods at which Earth's temperature reached 10-15 ºC above present levels, which are known as 'hothouse Earths' (Figure 1; Kennett and Stott 1991). In addition to these extreme stages, Earth's climate has also experienced a number of intermediary stages, such as the relatively recent glacial and interglacial cycles (Figure 1; Jouzel et al. 1987). The analysis of paleo archives confirms that Earth's climate was naturally variable since its formation.

Up until now, all climatic changes that occurred on Earth were driven by natural phenomena. The most important driver of past changes in Earth's climate was the Sun, which is responsible for the majority of the energy input into the climate system. The Sun drives changes in climate through variations in insolation, such as the ones caused by changes in Earth's orbital parameters (i.e. Milankovitch cycles), which have driven the Pleistocene glacial cycles (Jouzel et al. 1987). Another natural source of perturbations in Earth's climate occurs due to volcanic activity. It is hypothesized that intense volcanic activity during ancient Earth was responsible for the formation of the first atmosphere, which then generated warm conditions on Earth's surface through the 'greenhouse effect' (Rubey 1951). However, nowadays the probability of occurrence of such volcanic activity is very low, the impact of sporadic eruptions in the climate system may not last for more than a few decades (Mann et al. 2021). Today we add an additional driver to Earth's climate that is anthropogenic activity (IPCC 2007). Human activity has been shown to affect climate especially through fossil fuel burning,

which adds Signiant amount of greenhouse gases into the atmosphere and intensifies the natural greenhouse effect.

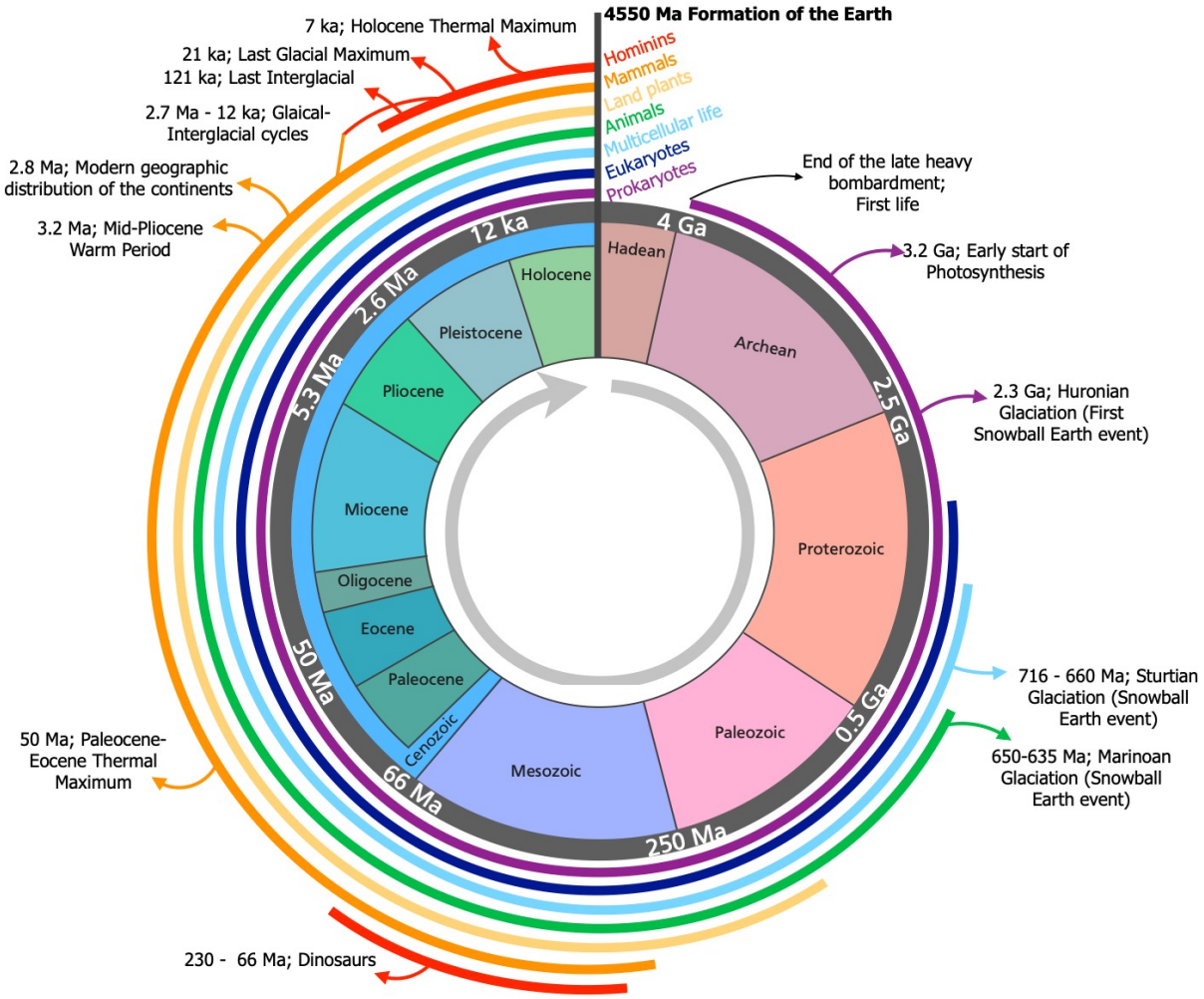


**Figure 1.** Earth's chronology ring and important climatic stages. Inner circle: earth's eras and Cenozoic's periods. Outer lines: evolution of life on Earth. Important climatic stages are indicated around Earth's chronology ring. Ga: giga ($10^9$) years; Ma: million ($10^6$) years; ka: thousand ($10^3$) years. Source: adapted from https://en.wikipedia.org/wiki/History_of_Earth.

We are already experiencing climate change. The scientific community has joined efforts to identify possible changes and alert society about its risks (IPCC 2007). To achieve this, scientists have studied the climate system by investigating past, present, and future climates with paleo-reconstructions, instrumental records, theory, and numerical simulations. This thesis investigates the past warm climate of the mid-Pliocene through paleo-

reconstructions and numerical simulations to improve our understanding on the climate system response to conditions warmer than present.

## 1.1 The Pliocene Epoch – Geological Context

The Pliocene begins at 5.3 Ma BP with surface air temperature (SAT) anomalies of approximately +4 K relative to the Common Era (pre-industrial climate at ~1850; Figure 2; Lisieckand Raymo 2005). These anomalies have progressively reduced to approximately –1 to –2 K at the end of the Pliocene Epoch (Figure 2), which terminates at the Northern Hemisphere Glaciation (~2.6 Ma BP). The following Period, namely Quaternary, comprises two Epochs: the Pleistocene and the Holocene (Figure 2). The former is marked by high climate variability due to the glacial cycles driven by changes in the Earth's orbit at periods of $10^5$ years. During Interglacial stages Earth's temperature reached +1 to +2 K relative to the Common Era (Figure 2). The later, Holocene, started at ~12 thousand years (ka) BP and consists in the ongoing interglacial period, which has lasted longer than previous interglacial periods and, thus, has been distinguished from the Pleistocene Epoch. During the mid-Holocene (~ 7 ka BP) Earth warmed by approx. +0.5 to +1 K above Common Era levels due to increased insolation in the Northern Hemisphere (Mascott 2013).

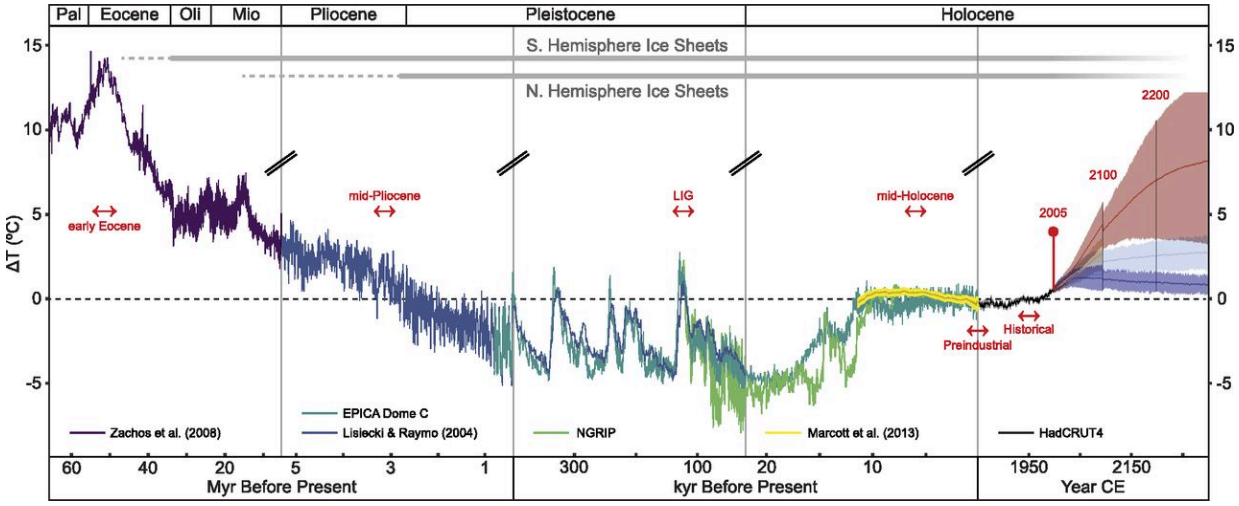


**Figure 2.** Temperature trends of the past 65 Ma and potential geohistorical analogues for future climates indicated by red arrows: early-Eocene (~55 Ma BP), mid-Pliocene (~3.2 Ma BP), Last-Interglacial (LIG; ~121 ka BP), mid-Holocene (~7 ka), pre-industrial (at 1850) and historical (between 1850 and 2005). Source: Burke et al. (2018).

## 1.2 The mid-Pliocene Warm Period (mPWP) – Physical Environment

Paleoclimate studies have been investigating whether there was a past warm climate that would serve as an analogue to the current warming. During the Pliocene cooling trend, recent research discovered anomalous high temperatures (approximately +3 ºC; Figure 3) in between 3.3 and 3 Ma BP (Dowsett et al. 1996), which was named mid-Pliocene Warm Period (hereafter referred as mid-Pliocene). As such, paleo scientists have joint efforts to provide further information about the physical environment of the mid-Pliocene. The availability of high confidence paleoenvironmental records for this period has further motivated the scientific community.

Studies found that the mid-Pliocene could share some characteristics of the future warming. During the mid-Pliocene, surface air temperature anomalies were ~3 K higher than present day (Dowsett et al. 1996). The most robust feature of the mid-Pliocene warming is the polar amplification, where Sea Surface Temperatures (SST) were as high as 9 ºC in the high

latitudes of Northern Hemisphere and 4 ºC in the Southern Ocean, while the tropical oceans faced a less pronounced warming (< 2 K; Dowsett et al. 2009; Figure 3). Polar ice was greatly reduced. The Greenland ice sheet experienced a retreat of ~50-70% while western Antarctica was ice free. The onset of these mid-Pliocene conditions is attributed to a rise in $CO_2$ levels (Lunt et al. 2012), which reached similar values to present day (~400 ppm; Seki et al. 2010).

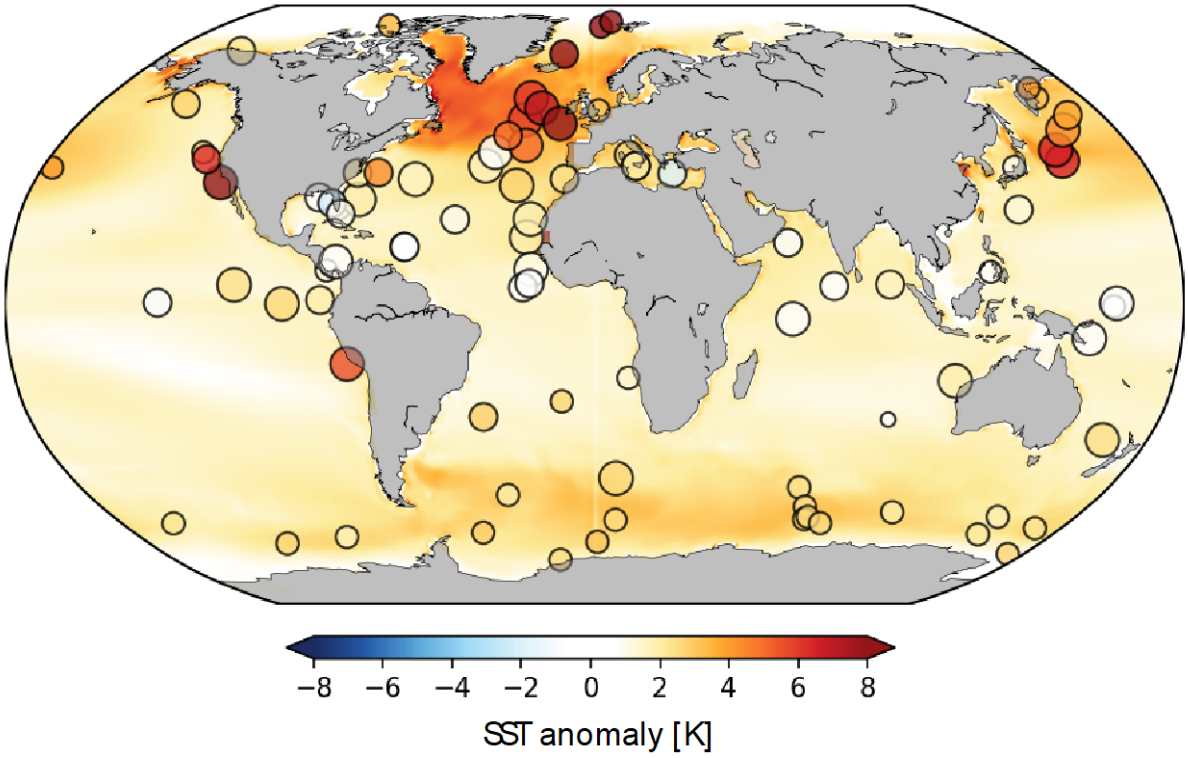


**Figure 3.** Data-model comparison of mid-Pliocene SST anomalies (relative to the pre-industrial climate). Shading indicates multi-model mean PlioMIP phase 2. Circle indicate reconstructed SST anomalies based on the compilation performed by the Pliocene, Research Interpretation, and Synoptic Mapping phase 3 (PRISM3) project. Circle size indicate site confidence: low, medium, high and very-high.

During the Pliocene the modern distributions of the continents was established, giving rise to the current large-scale ocean circulation (De Schepper et al. 2013). In the early Pliocene the geographic distributions of the continents were similar to present day, but with a few important differences. First, the water flux from the Pacific to the Indian Ocean through the Indonesian archipelago, namely Indonesian Through Flow (ITF), was significantly higher as the Australian tectonic plate was displaced southwards. Secondly, there was a significant water

exchange between the Atlantic and Pacific Oceans as the Central American Seaway, also known as Isthmus of Panama, was widely opened. Finally, fluxes through the Bering Strait in the North Pacific were southward, entering into the Artic Ocean. At ~3.3 Ma BP (beginning of the mid-Pliocene), the Australian plate had already displaced northwards, reducing the ITF, the Isthmus of Panama was nearly closed (~100m deep), and the flux through the Bering Strait changed towards north. Thus, stablishing the modern pattern of the ocean circulation and facilitating comparisons between the mid-Pliocene and present and future climates.

Throughout the 300 thousand years interval of the mid-Pliocene, orbital forcing was quite variable (Naish et al. 2009). Thus, not every warm peak during this interval is of relevance to future climate change, as many occurred due to changes in orbital parameters, unlike today (Haywood et al. 2016a). To overtake this issue it was identified the KM5c interglacial peak at 3.205 Ma BP when orbital parameters were similar to present day and are thought to have reduced effect on paleo reconstructions (Haywood et al. 2016a).

Due to the mid-Pliocene characteristics described above it was considered of high relevance for climate change. Firstly, the mid-Pliocene experienced annual mean SATs of approximately +3 ºC with $CO_2$ concentrations (~400 ppm) and orbital forcing similar to present day. Furthermore, the large-scale pattern of the oceanic circulation was similar to modern as the continents have reached their present position. Therefore, partially motivated by similarities between mid-Pliocene and scenarios of future warming, the Pliocene Model Intercomparison Project (PlioMIP) initiative was developed. This thesis investigates climate features and physical processes of the mid-Pliocene warming through model output of the participants in the PlioMIP and sensitivity climate model experiments.

# 2 Scientific Hypothesis – Rationale

The mid-Pliocene shares a similar degree of warming (approx. +3 ºC) as projected for the end-of-century climate by the climate models participants of the Coupled Model Intercomparison Project phase 5 (CMIP5) and 6 (CMIP6), under a "business-as-usual" scenarios (RCP8.5 and SSP8 scenarios, respectively). Significant effort has been made by paleo-scientists to obtain environmental information of the mid-Pliocene climate, which have provided reconstructions of ice sheets, soils, lakes, vegetation and SST at some sites. These provide valuable information about the mid-Pliocene climate, however; it is not possible to evaluate physical processes and understand mechanisms for the mid-Pliocene warmth through proxy-based reconstruction. Nonetheless, this information about the warm nature of the mid-Pliocene can be used to force climate models for completeness. And, thus, the next step of the scientific progress to understand the mid-Pliocene climate was to provide a set of climate model simulations through the PlioMIP initiative. Today, how the Pliocene warming has affected important climate processes remain unclear, especially regarding to the Southern Hemisphere climate.

Here, the effect of the mid-Pliocene warming on processes which are important to the Southern Hemisphere is investigated, with special attention to the South American climates. It is one of the goals of this study to verify whether this past warm climate can be considered a useful analogue to future projected warming.

# 3 OBJECTIVES

## 3.1 Central Objective

To investigate key physical processes that have affected the Southern Hemisphere and South American climates during the mid-Pliocene (~ 3 Ma BP) warming in order to evaluate whether their response and mechanisms is analogue to the future projected warming (see section 3.2 below). This is proposed to be achieved through analysis of model output of the modelling groups participants in the Pliocene model Intercomparison Project (PlioMIP) phases 1 and 2 and numerical simulations with NCAR-CESM1.2 model (National Center for Atmospheric Research USA – Community Earth System Model version 1.2). The NCAR-CESM1.2 model is used to decouple ocean-atmosphere-ice processes when evaluating physical mechanisms.

## 3.2 Specific Objectives

- To evaluate the mean Southern Hemisphere hydroclimate with respect to important atmospheric features (i.e., the Inter-Tropical Convergence Zone, Subtropical Jets and South Atlantic Subtropical High-pressure system) and the oceanic influence over atmospheric processes and climate features;
- To evaluate the impact of the mid-Pliocene warming over the modes of SST that affect the variability of the South American hydroclimate. In particular the response of the main mode of climate variability are investigated. In particular the Atlantic multi-decadal variability (AMV), the Atlantic Equatorial Mode (AEM; also known as the Atlantic Niño), the South Atlantic Subtropical Dipole (SASD) and the El-Niño Southern Oscillation (ENSO).

# 4 Materials and Methods

In order to achieve the objectives defined in the chapter above cmodel output from the Pliocene Model Intercomparison Projects (PlioMIP) phase 1 and 2 are combined with sensitivity numerical experiments using the Community Earth System Model version 1.2 (CESM1.2).

## 4.1 The Pliocene Model Intercomparison Project (PlioMIP)

The PlioMIP initiative was developed to investigate the climate of the interglacial mid-Pliocene. Here, model output from PlioMIP phases 1 and 2 are used. In PlioMIP1, coupled climate models were tasked to simulate average climate conditions for the period between ~ 3.3 and ~ 3 million years ago (Haywood et al. 2011). In these simulations, the greenhouse gas (GHG) forcing is set to 405 ppm $CO_2$, the orbital configuration is not changed from modern configuration, and the remainder prescribed boundary conditions, which include orography, ice sheets, vegetation, and land-sea mask, are given by the PRISM reconstructions (Dowsett et al. 2010; Table 1). The western Antarctica ice sheet experienced ice-free conditions during the mid-Pliocene while the Greenland ice sheet was estimated to be reduced by 50%. The major changes in vegetation include the expansion of the tropical rain forests. For example, the Amazon rainforest expanded southwards and the vegetation in the Sahel region expanded northwards (Dowsett et al. 2010). The control simulation is run with boundary conditions of the pre-industrial period where the$CO_2$ concentration is set to 280 ppm (Table 2).

**Table 1.** PlioMIP1 and PlioMIP2 boundary conditions. LSM: land-sea mask. Topo: topography.

| | LSM | Topo. | Soils | Lakes | Ice Greenl. | Ice Antarc. | Vegetation | $CO_2$ | Orbital paramet. |
|---|---|---|---|---|---|---|---|---|---|
| **Pre-industrial** | Modern | Modern | Modern | Modern | Modern | Modern | Modern | 280 | Modern |
| **PlioMIP1** | Plio | Plio | Modern | Modern | Plio - | Plio | Plio | 405 | Modern |
| **PlioMIP2** | Plio – enhanced* | Plio – enhanced* | Plio – enhanced | Plio – enhanced | Plio – enhanced | Plio | Plio | 400 | Modern |

*MRI-CGCM2.3 was the only model that could not apply the enhanced reconstruction from PRISM4 in PlioMIP2 with respect to land-sea mask and topography and, thus, applied the previous, standard, reconstruction.

PlioMIP2 apply rather similar boundary conditions to PlioMIP1 (Table 1). Nonetheless there were significant differences at some regional locations, which could potentially affect the large-scale climate (Haywood et al. 2011, 2016b, 2020). First, although both phases have not applied changes in orbital parameters, phase 1 was designed to simulate a time averaged global SST reconstruction between 3 and 3.3 Ma BP, while phase 2 focused on a narrower time slice (Marine Isotope Stage KM5c at 3.205 Ma BP) with almost identical orbital parameters to modern (Haywood et al. 2016a). As such, the 'enhanced' Prism dataset was developed to focus on the KM5c time-slice (Table 1). Both phases applied a mid-Pliocene land-sea mask, but PlioMIP2 land-sea mask accounts for glacial isostatic adjustments and changes dynamic topography. This resulted in a subaerial Canadian Archipelago, Bering Strait and emergence of the Sunda and Sahul shelves in the Indonesia and Australia region. Phase 2 models also applied soils and lakes reconstructions and a newer reconstruction of the Greenland ice sheet that now accounts for a 70% retreat, instead of the 50% retreat applied in phase 1. These reconstructions were derived from the U.S. Geological Survey PRISM dataset, specifically the most recent and fourth version iteration of the reconstructions (PRISM4; Dowsett et al. 2016). In PlioMIP2, modelling groups could choose from either using the vegetation reconstruction from Salzmann et al. (2008), same as PlioMIP1, or use dynamic

model vegetation option. COSMOS was the only model among PlioMIP2 participants to use dynamic vegetation. For a detailed description of each model's implementation, please see references in Table 2.

**Table 2.** Modelling groups participants in PlioMIP phases 1 and 2.

| | Institute | Ref. |
|---|---|---|
| **PlioMIP1** | | |
| CCSM4 | National Center for Atmospheric Research - USA | (Rosenbloom et al. 2013) |
| COSMOS | Alfred Wegener Institute – Germany | (Stepanek and Lohmann 2012) |
| FGOALS-g2 | LASG – China | (Zheng et al. 2013) |
| GISS-E2-R | Goddard Institute for Space Studies – USA | (Chandler et al. 2013) |
| HadCM3 | University of Leeds – United Kingdom | (Bragg et al. 2012) |
| IPSL-CM5A | Laboratoire des Sciences du Climat et de l'Environnement - France | (Contoux et al. 2012) |
| MIROC4m | Centre for climate change research, Uni. Tokyo - Japan | (Chan et al. 2011) |
| MRI-CGCM2.3 | University of Tsukuba – Japan | (Kamae and Ueda 2012) |
| NorESM-L | Norwegian Research Centre – Norway | (Zhang et al. 2012) |
| **PlioMIP2** | | |
| CCSM4-UofT | University of Toronto – Canada | (Chandan and Peltier 2017) |
| CCSM4-2deg | Utrecht University – The Netherlands | - |
| CCSM4-1deg | National Center for Atmospheric Research – USA | (Feng et al. 2020) |

| | | |
|---|---|---|
| CESM1.2 | National Center for Atmospheric Research – USA | (Feng et al. 2020) |
| CESM2.1 | National Center for Atmospheric Research – USA | (Feng et al. 2020) |
| COSMOS | Alfred Wegener Institute – Germany | (Stepanek et al. 2020) |
| EC-EARTH3.3 | Stockholm University – Sweden | (Zheng et al. 2019) |
| GISS-E2-1-G | Goddard institute for Space Studies – USA | - |
| HadCM3 | University of Leeds – United Kingdom | (Hunter et al. 2019) |
| IPSL-CM6A-LR | Laboratoire des Sciences du Climat et de l'Environnement - France | (Lurton et al. 2020) |
| IPSL-CM5A | Laboratoire des Sciences du Climat et de l'Environnement - France | (Tan et al. 2020) |
| IPSL-CM5A2 | Laboratoire des Sciences du Climat et de l'Environnement - France | (Tan et al. 2020) |
| MIROC4m | Centre for climate change research, Uni. Tokyo - Japan | (Chan and Abe-Ouchi 2020) |
| MRI-CGCM2.3 | University of Tsukuba – Japan | (Kamae et al. 2016) |
| NorESM-L | Norwegian Research Centre – Norway | (Li et al. 2020) |
| NorESM1-F | Norwegian Research Centre – Norway | (Li et al. 2020) |

### *4.1.1 Multi-model analysis*

Model Intercomparison Projects (MIPs) were developed targeting on reducing model uncertainties (Jansen et al. 2007). This kind of uncertainty is generated within each climate model by model biases and differing parametrizations and resolutions. Different resolutions

also determine which processes can be solved by models and, thus, affecting their physics (Jansen et al. 2007). Modelling groups participants in MIPs are tasked to apply the same boundary conditions in a given simulation with their respective climate models. This is to assure comparability among the differing models.

The objectives of the multi-model analysis are to identify processes that are common across models in a given simulation and provide confidence intervals. When working with a single simulation of a single model, there will be only one value (or map) for each analysis' results. In this case, significance analyses can be obtained through Monte Carlo experiments (i. e. Pausata et al. 2017); however, this only gives the perspective of a single model. In multi-model analysis, each model's simulation provides a sample of the distribution (all models), which gives the opportunity to apply statistical analyses that assume the independency of the samples, although climate models still share some common physical equations (Stellema et al. 2019). Results from multi-model ensembles can be evaluated through either parametric or non-parametric statistics. In parametric statistics the most-likely value and confidence intervals of the distribution are obtained through the computation of mean and standard deviation, respectively, while in non-parametric statistics these are median and, for example, interquartile range (IQR).

The focus of the present thesis is to evaluate how different the mid-Pliocene climate was from pre-industrial climate. As such, a powerful metric is to evaluate multi-model mean (MMM) differences between these two simulations (mid-Pliocene minus pre-industrial). This analysis highlights changes between the mid-Pliocene and pre-industrial simulations that are common across models.

Multi-model ensembles allow us to assess the statistical significance of the changes. There are three most common procedures in the literature to assess this: standard deviation of the changes, analysing the magnitude of the multi-model mean of normalized change and model

agreement on the sign of the change. Power et al. (2012) evaluates that all three methods are equivalent. In this work, the last method is used. Model agreement on the sign of the change assess the statistical significance based on a binomial distribution of equal probability (p=q=0.5) associated with an equal probability of a given model simulating a positive or negative change. Depending on the analysis, the number of models may change, due to the data availability in the PlioMIP database (from 7 to 25 models), and so the threshold for statistical significance (Figure 4). For N=7 (models) the significance level of 95% is achieved when at least 5 models (72%) agree on the sign of the change (Figure 4). For N=9 the same significance is achieved with 7 models (77%) and for N=12 this is 9 models (75%; Figure 4). For higher N, the 95% level is achieved when ~70% of the models agree on the sign of the change. To keep consistency with the choice of this method, all values cited in Chapters 5, 6 and 7 correspond to the multi-model median and inter-quartile range (IQR), unless otherwise stated. The IQR accounts for the range between the $25^{th}$ and $75^{th}$ quantiles of the distribution. When indicating changes, if the IQR does not cross the zero value, it indicates that there is at least a 75% model agreement on the sign of the change (usually significant at the 95% level; Figure 4). Here, the use of the word 'significant' will be always associated to statistical significance.

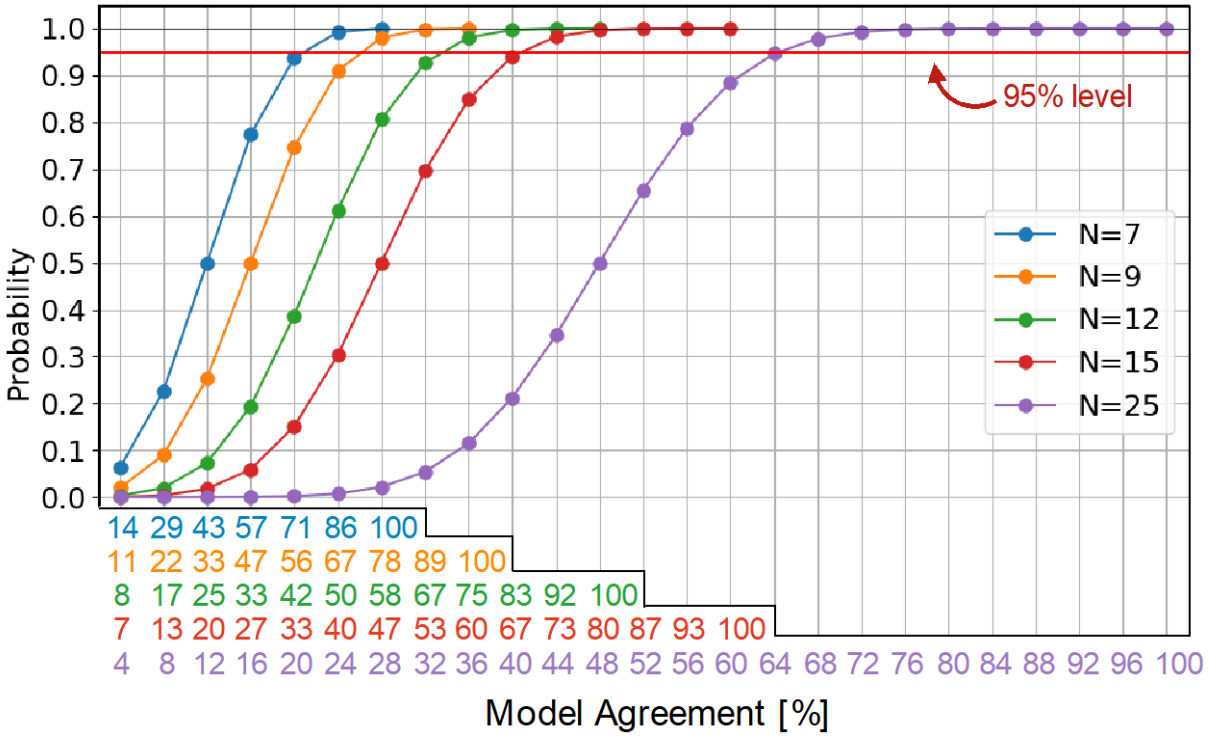


**Figure 4.** Cumulative probability functions for binomial distributions with p = q = 0.5 and N = 7,9,12,15 and 25. In this study, 'N' is associated to the number of models used in each analysis. The x-axis changes for each curve. The number highlighted in the x-axis indicates the model agreement [in %] required to reach the 95% significance level. For N ≥ 12, an ~70% model agreement is significant at the 95% level. Source: the author.

A valuable analysis when investigating physical mechanisms is the inter-model relationship. This is the dispersion diagram between two processes that are hypothesized to be linked to one another. For example, when investigating the causes of the mean changes in the hydroclimate of South America, one may hypothesize that a northward shift of the Inter-tropical Convergence Zone (ITCZ) is linked to weakened South American Monsoon System (SAMS) in the mid-Pliocene. If this hypothesis holds one is expected to find a relationship among the models between the changes in these two processes (i.e., the models that show higher ITCZ shifts would be associated with major decreases in the SAMS). A significant inter-model relationship is a robust metric as it states that the two processes hold a link regardless the differences in model's parametrizations, resolutions, climate sensitivity and even boundary conditions, as this can be applied to different MIPs in the same analysis (i.e., in Chapters 5 and 7). It is worth noting that all analyses are first performed within each model and only the final

result is compared among models. For example, when computing changes in the transport of the Atlantic Meridional Overturning Circulation (AMOC), the AMOC transport is first computed for each simulation of each model, then the difference (mid-Pliocene minus pre-industrial) is calculated also for each model to obtain a final value for each individual model. The MMM change of the AMOC transport is, thus, the mean of this final distribution.

## 4.2 The Community Earth System Model (CESM)

The Community Earth System Model version 1.2 (CESM1.2) is the updated version of the Community Climate System Model version 4 (CCSM4) developed by the National Center for Atmospheric Research (NCAR, USA). CESM1.2 is a fully coupled global climate model. It includes active components for ocean, atmosphere, sea-ice, ice sheets, vegetation, and rivers. The differing component models are coupled through the CESM1 coupler that uses the Model Coupling Toolkit. The CESM family of models is used to run the PlioMIP phases 1 and 2 experiments (CCSM4, CESM1.2 and CESM2; Table 2).

### *4.2.1 Experimental Design*

In order to explore the impact of reduced global sea-ice volume and increased SST on tropical rainfall, a set of sensitivity experiments based on the PlioMIP simulations was performed. The intention here is to evaluate the atmospheric response to an imposed SST field, thus, the atmospheric component is run isolated (namely Community Atmospheric Model version 4 [CAM4]), instead the fully coupled mode. Also, as the focus is to evaluate the large-scale response, the 2º resolution version of the model is used.

A total of 4 experiments were executed. In the first experiment, CAM4 was forced with pre-industrial SST and sea-ice climatology based on multi-model mean PlioMIP1 pre-industrial control simulation. CO2 was set at its pre-industrial value of 280.4 ppmv. In

experiment 2, CAM4 was forced with mid-Pliocene SST and sea-ice climatology based on the multi-model mean PlioMIP1 simulations. No changes over continental areas were included and the $CO^2$ concentration was kept at its pre-industrial value. Experiments 3 and 4 consists of reproducing experiments 1 and 2, respectively, but with multi-model mean SST and sea-ice from PlioMIP2. Each experiment consisted of a 5-member ensemble to account for uncertainties due to different initial conditions. Each member was initialized in a different starting date in order to have a different initial condition. Each member was run for 31 years. The first year of each member was excluded as it includes the atmospheric spin-up. The choice of a 5-member with 31 years each relies on the fact that the focus is to evaluate changes in the mean climatological state.

# 5 Rainfall Regime in the Southern Hemisphere in the mPWP

In this chapter, changes in the Southern Hemisphere hydroclimate during the mid-Pliocene are evaluated and their possible causes are investigated. Examining changes in the hydroclimate allow to evaluate how Earth has responded to the mid-Pliocene warming, as these can be caused by both thermodynamical and dynamical processes.

The results presented in this chapter were published in the journal *Scientific Reports* in August 2020.

---

**Pontes, G. M.** *et al.* Drier tropical and subtropical Southern Hemisphere in the mid-Pliocene Warm Period. *Sci. Rep.* **10**, 13458 (2020). http://www.nature.com/articles/s41598-020-68884-5

---

## 5.1 Introduction

Understanding atmospheric circulation and precipitation during past warm climates is useful to produce constraints on possible future changes. Rainfall proxy archives do not exist for the tropics and Southern Hemisphere subtropics in the mid-Pliocene. As such, the PlioMIP models may provide important estimates of how rainfall may have looked in the mid-Pliocene. To date, there has been no detailed investigation of Southern Hemisphere rainfall changes in the mid-Pliocene. Most studies have focused on the Northern Hemisphere monsoon systems (Zhang et al. 2013, 2015, Sun et al. 2016) or global land monsoons (Li et al. 2018). These studies reported intensified western African, Asian and Australian monsoons and a weakened South American monsoon.

SST changes indicated by both PlioMIP ensembles and proxy-data from the mid-Pliocene (Figure 5a) suggest possible changes in the atmospheric circulation through changes in the meridional heat transport. These data clearly indicate a Northern Hemisphere warmer than Southern Hemisphere during the mid-Pliocene (Figure 5a,b). Theoretical and observational studies indicate that in response to changes in the interhemispheric SST gradient, there is strengthening of the cooler hemisphere Hadley cell and displacement of the Inter-Tropical Convergence Zone (ITCZ) towards the warmer hemisphere (Chiang and Friedman 2012, Schneider et al. 2014). In addition, changes in the intensity and position of the Hadley Cells and low-level winds can have a substantial impact on rainfall at subtropical latitudes. Indeed, Southern Hemisphere tropics and subtropics are the only regions that are simulated to be drier in the wetter atmosphere of the mid-Pliocene (Figure 5c).

A closer examination in the tropical and subtropical Southern Hemisphere (Figure 5d) indicates that reduced rainfall in the subtropical Southern Hemisphere is also related to a minimum SST increase. In the subtropical South Pacific, there is a strengthening of rainfall in

the west and a weakening in the central-east coincident with SST changes. A warmer tropical Northern Hemisphere across all basins is also consistent with its increased rainfall due to the thermodynamical effect (Held and Soden 2006; 'wet-wetter' theory). Furthermore, the non-uniform tropical warming results in increased tropical inter-hemispheric SST gradient, indicating that dynamical changes could also have contributed to changes in rainfall. As such, local changes in SST may also play a role in drying the subtropical Southern Hemisphere climate and amplifying the large-scale inter-hemispheric contrast.

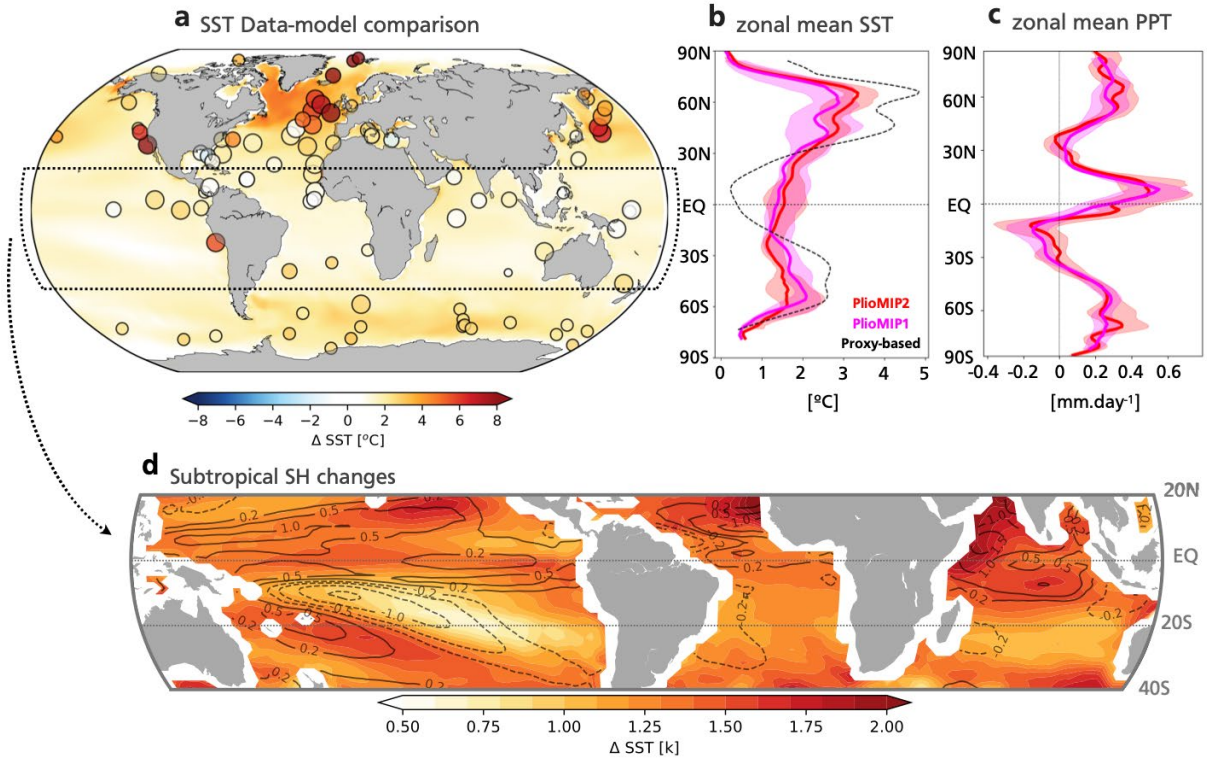


**Figure 5.** Data-model comparison of Sea Surface Temperatures anomalies during the mid-Pliocene and PlioMIP precipitation. (**a)** Multi-model mean SST anomaly in the PlioMIP2 (mid-Pliocene minus pre-industrial). Circles indicate location of sites and SST anomalies compiled by PRISM (Dowsett et al. 2010). Size of the circles indicate confidence level. Small: low confidence. Medium: medium confidence. Large: High confidence. (**b)** zonal mean SST anomaly from PRISM (dashed black) and multi-model medians PlioMIP1 (magenta) and PlioMIP2 (red). (**c)** as per 'b' but for precipitation. Banding indicates interquartile range. d) as per 'a' but including contours (black) of precipitation changes in mm.day$^{-1}$.

The largest changes in rainfall in the Southern Hemisphere are likely associated with changes in the Inter-Tropical Convergence Zone (ITCZ) and Subtropical Convergences Zones (STCZs; Figure 5d). In modern Southern Hemisphere climatology more than 50% of the annual rainfall occurs during the extended austral summer period (November to March) in most regions (Nicholson 2000, Vera et al. 2006). The ITCZ and STCZs largely contribute to this. Firstly, the ITCZ that moves south during austral summer and increases rainfall in the Southern Hemisphere Tropical regions (Vera et al. 2006). In addition, the STCZs are a summertime feature of the subtropics that can have rainfall rates comparable to the ITCZ (up to ~ 400 mm month$^{-1}$; Trewartha 1968).

The STCZs are bands of intense cloudiness and convection that set up transversally from tropical latitudes to the subtropics, commonly visible via satellite images. They develop when troughs of the subtropical jet penetrate the subtropics and poleward low-level winds prevail at the western limit of the subtropical highs (Kodama 1992, Widlansky et al. 2011, van der Wiel et al. 2015). In addition, these systems become intensified when moisture fluxes from the ITCZ and monsoon systems feed into the northern portion of the STCZs (Kodama 1993, Liebmann et al. 1999, Carvalho et al. 2002). These convergence zones are more intense in the Pacific and Atlantic basins, namely the South Pacific Convergence Zone (SPCZ) and the South Atlantic Convergence Zone (SACZ), respectively, while they are less notable in the Indian Ocean (Kodama 1993, van der Wiel et al. 2015).

In this chapter, model output from PlioMIP phases 1 and 2 are combined to results from sensitivity experiments using the Community Atmospheric Model version 4 (CAM4) to understand the drivers of Southern Hemisphere summertime rainfall patterns during the mid-Pliocene.

## 5.2 Methods

A key regional change occurs in the location of the Subtropical Convergence Zones (STCZs). Therefore, the position of the STCZs is defined as the maximum rainfall latitude, at each longitude, between 15°S–40°S and 160°W–190°W (0–20°S and 160°E–160°W) for the SPCZ diagonal (zonal) sector and 55°W–20°W for the SACZ. The COSMOS model was not able to simulate the poleward diagonal projection of the STCZs in its pre-industrial simulations in both phases of the PlioMIP (Appendix A) and, thus, its results were not included in this chapter. Additionally, to identify possible meridional displacements of the mean position of the STCZs a cross section was defined for the SPCZ, from 145°W/35°S to 165°W/15°S, and SACZ, from 50°W/38°S to 30°W/18°S. The intensity of the STCZs were computed as the total November-to-March mean rainfall along the STCZ length.

In evaluating the causes of the STCZs changes, three atmospheric features are of major importance: the subtropical jet, the ITCZ and subtropical high systems. The position of the subtropical jet is computed as the Weighted mean latitude of U-wind (at 200 hPa) based on latitudes where the intensity was greater than 50% of its maximum in the zonal mean.

The position of the ITCZ is defined as the precipitation weighted mean latitude based on latitudes where precipitation is greater than 50% of its maximum in the zonal mean. Pacific and Atlantic ITCZs are computed over their respective oceans only (land areas not included). This method may include double-ITCZ and double-ITCZ biases if the double ITCZ associated precipitation is greater than 50% of the maximum. The double-ITCZ bias is an artificial feature produced by most climate models that overestimates the tropical precipitation south of the equator. Here the ITCZ bias is defined as the difference between simulated pre-industrial Pacific ITCZ position and the observed position averaged from 1979 to 2020. Although the PlioMIP models suffer from double-ITCZ bias (mean bias: -4.1 ± 2.1 sd). It is worth noting that

the ITCZ bias is evaluated by comparing the pre-industrial model simulations with modern climate, which is already under the influence of global warming.

The intensity of the atmospheric subtropical highs is usually evaluated through sea level pressure (Reboita et al. 2019). However, quantifying the intensity of the subtropical highs is not a simple task when dealing with different climate backgrounds (+~3K) as the global pressure weakens in a warmer atmosphere. To overcome this pressure issue, it is computed the stream function at 850 hPa to identify the position and intensity of the Subtropical High systems. The stream function can be derived from the geostrophic balance:

$$f \times \vec{v} = -\frac{1}{\rho}\nabla_H \mathrm{p}$$

where $\vec{v} = (u_g, v_g)$, p, $f$ and $\rho$ are the velocity vector, pressure, Coriolis function, and density, respectively. Knowing that for a fluid of horizontally uniform density, the geostrophic flow in an f-plane is non-divergent, i.e.

$$\frac{\partial u_g}{\partial x} + \frac{\partial v_g}{\partial y} = 0 \quad \text{for} \quad \rho = \rho_0(g) \quad \text{and} \quad f = f_0 = 2\Omega sin\theta,$$

we can define a stream function which yields to

$$u_g = -\frac{\partial \psi}{\partial y} = -\frac{1}{\rho_0 f_0}\frac{\partial p}{\partial y} \quad \text{and} \quad v_g = \frac{\partial \psi}{\partial x} = \frac{1}{\rho_0 f_0}\frac{\partial p}{\partial x}$$

It is worth noting that in the Southern Hemisphere, increased pressure gradients over geostrophic flows result in intensified anticyclonic circulation (negative stream function). To define the centre of the atmospheric subtropical highs, it is first computed a zonal cross section in the latitude of the maximum stream function (at 850 hPa) value in the subtropics (20°S–40°S). In this cross section, it is then computed the weighted mean longitude based on longitudes where the intensity was greater than 90% of its maximum.

In evaluating precipitation changes over the continent two monsoons system are of major importance to this study: the South American Monsoon System (SAMS) and the Australian Monsoon (AusM). The strength of these systems is computed as the total November-to-March precipitation in between 10–25°S and 35–65°W for the SAMS and 15–25°S and 130–150°E for the AusM.

Further, the causes of changes in the ITCZ position are evaluated through energetic constraints (Schneider et al. 2014). Considering a long enough period (i.e. ≥ 30 years) so that the energy storage in the atmospheric system and on land surfaces are negligible and neglecting the relatively small kinetic energy of atmospheric motions, the divergent of the zonally averaged atmospheric energy balance is given by the residual between the surface and top-of-atmosphere energy fluxes (Neelin et al. 1987):

$$\frac{\partial \mathcal{H}(\theta)}{\partial \theta} = 2\pi a cos\theta(\mathcal{R}^{TOA} - \mathcal{O}) \quad (1)$$

Where the annually- and zonally-averaged heat transport is given by $\mathcal{H} = \langle \overline{vh} \rangle$. The moist statistic energy $h$ is defined as the sum of dry static energy $s = C_p T + gz$ and latent energy $l = L_v q$, where $L_v$ is the laten heat of vaporization and $q$ is the specific humidty. $\mathcal{R}^{TOA}$ is net radiation at the top-of-the-atmosphere and $\mathcal{O}$ is the energy uptake by oceans.

Integrating from the south pole ($\theta = -\pi/2$) and applying the boundary condition that the transport at the pole must vanishes, as a non-zero transport at the pole is physically meaningful, gives us the formula to obtain the heat transport at any latitude, by integrating the imbalance from the south pole:

$$\mathcal{H}(\theta) = 2\pi a^2 \int_{-\pi/2}^{\theta} cos\theta(\mathcal{R}^{TOA} - \mathcal{O})\, d\theta \quad (2)$$

The ITCZ dynamically separates both hemispheres. Towards north, the Northern Hemisphere Hadley cell exports heat towards high latitudes in the Northern Hemisphere,

implying a positive energy transport. The same occurs in Southern Hemisphere, however, implying a negative energy transport towards high latitudes in the Southern Hemisphere. Assuming that the latitude at which meridional winds change sign is constant with altitude and eddy fluxes around the equator are negligible, the zonal mean ITCZ is located close to the latitude $\delta$ at which the meridional atmospheric energy transport $\mathcal{H}(\theta)$ changes sign (Kang et al. 2009). As such, expanding $\mathcal{H}(\theta)$ in Taylor Series at a low-latitude $\delta$ around the equator, we obtain, to first order:

$$0 \approx (\mathcal{H}(\theta))_\delta = (\mathcal{H}(\theta))_0 + \delta\left(\frac{\partial \mathcal{H}(\theta)}{\partial \theta}\right)_0 \tag{3}$$

Where the subscript 0 denotes quantitites evaluated at the the equator. Solving for $\delta$ and accounting for Equation 1 at the equator results in the ITCZ position (Bischoff and Schneider 2014):

$$\delta = -\frac{1}{2\pi a^2}\frac{\mathcal{H}(\theta)_0}{\mathcal{R}^{TOA}{}_0 - \mathcal{O}_0} \tag{4}$$

This relationship shows that the ITCZ position $\delta$ is proportional to the negative of the energy flux across the equator ($\mathcal{H}(\theta)_0$) and that the sensitivity of this relationship is determined by the energy input in the equatorial atmosphere ($\mathcal{R}^{TOA}{}_0 - \mathcal{O}_0$).

## 5.3 Results

The PlioMIP simulations show that one of the most notable changes in the Southern Hemisphere summertime rainfall in the mid-Pliocene compared to pre-industrial conditions occurs in the subtropical regions along the STCZs (Figure 6). Reduced precipitation is simulated along portions of both the SPCZ and SACZ (Figure 6 b,c) and a clear southward shift of these bands is seen (Figure 6d–g; see Methods for how the position of the STCZs are obtained; for individual models see Appendix A). Another change is associated with a

northward shift of the ITCZ due to consistent increased rainfall in the Northern Hemisphere tropics, which is best observed in the Pacific Ocean for both PlioMIP phases (Figure 6b,c).

The total November-to-March mean rainfall along the STCZs decreases in both PlioMIP1 and PlioMIP2 models (Appendix A). All PlioMIP1 and PlioMIP2 models exhibit a weakened SPCZ (− 6% to − 11% and − 10% to − 16%, respectively; numbers define the interquartile range; see Methods). The SACZ weakening is only evident in the PlioMIP1 (− 9% to − 15%) while in the PlioMIP2 the change is not as obvious (− 3% to 6%). It is important to note that the SACZ comprises land and ocean sectors. The land sector is more dependent on moisture fluxes from the Amazon and evapotranspiration processes, while the ocean sector is more dependent on the subtropical high system (Carvalho et al. 2004). In the PlioMIP2 the changes in the SACZ ocean sector are more consistent than in the land sector (Figure 6c). The reduced rainfall along the STCZs indicates weakened deep convection at these regions. The STCZ in the Indian Ocean, namely the South Indian Convergence Zone (SICZ), represents a less robust feature of the observed Southern Hemisphere monsoon system (Kodama 1993) and, thus, a clear SICZ is usually not well seen in observations nor simulated in most climate models (Figure 6a; see Appendix A for individual models).

In addition to a weakening, the Southern Hemisphere STCZs significantly shifts southwards in both PlioMIP1 and PlioMIP2 models (Figure 6d,e,f,g). In all models, the SPCZ displaces southwards (Figure 6d,e): in the PlioMIP1 by − 1.9° to − 0.8°, and in the PlioMIP2 by − 4.1° to − 1.2°. The poleward shift in the SACZ position is more extreme in the PlioMIP1 models with a displacement of − 4.5° to − 0.6° compared to − 1.3° to − 0.4° in the PlioMIP2 simulations (Figure 6f,g).

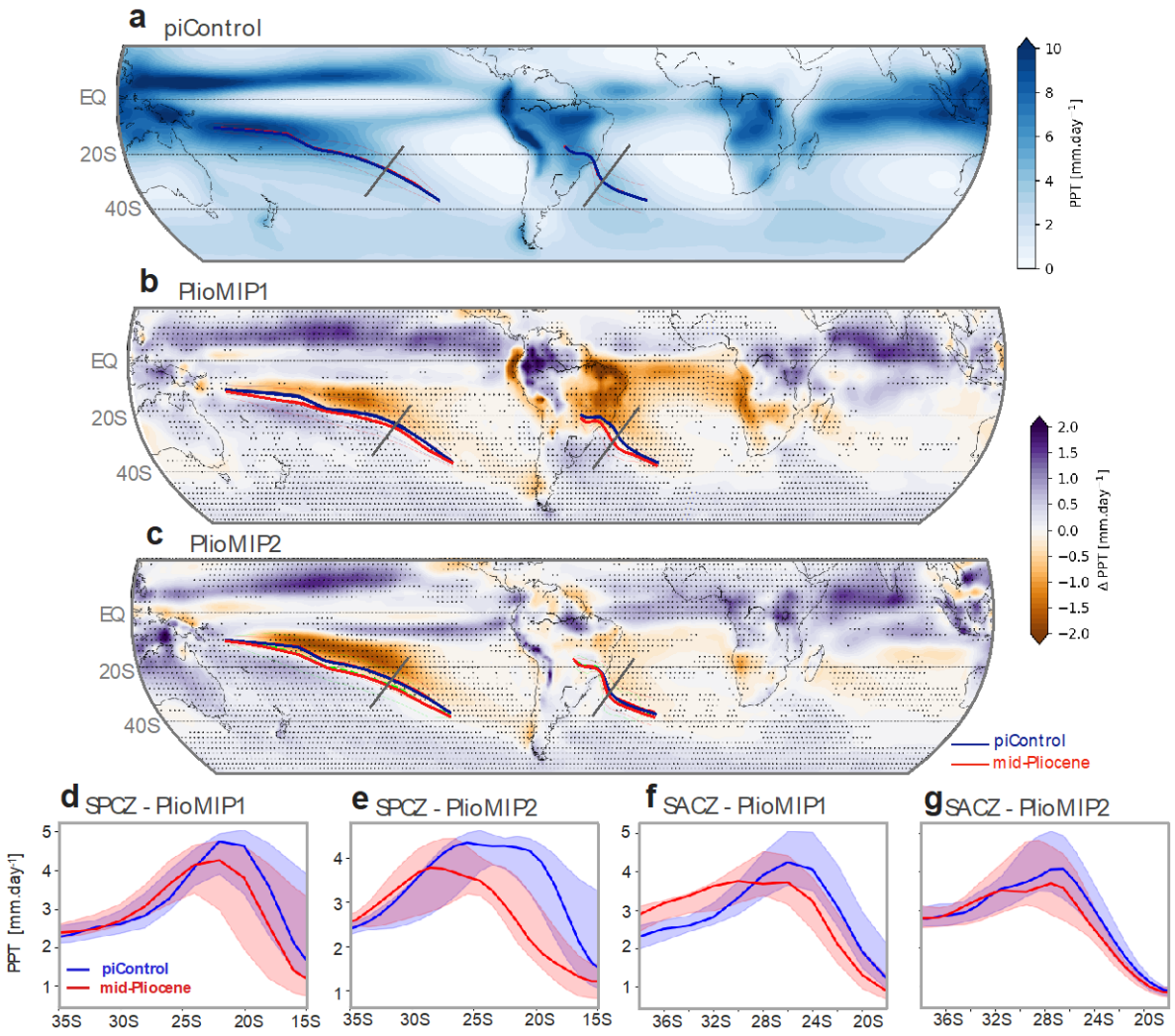


**Figure 6.** Summertime rainfall change and Subtropical Convergence Zones. (**a**) Multi-model mean November-to-March precipitation in the PlioMIP2 pre-industrial control simulation. Dark blue line indicates the position of the SPCZ and SACZ in the Pacific and Atlantic oceans, respectively. Banding indicates standard deviation range. Grey lines indicate the position of the cross section whose results are shown in the lower panels. (**b**) Multi-model mean change in the southern hemisphere precipitation from PlioMIP1 simulations relative to their pre-industrial control. Dark blue (red) lines indicate the position of the SPCZ and SACZ in the pre-industrial control (mid-Pliocene) simulation. (**c**) as 'b' but for PlioMIP2. Stippling indicates 72% model agreement in the sign of the change for PlioMIP1 and 75% for PlioMIP (see Methods). Panels (**d**) to (**g**) show the rainfall change along the cross sections indicates in panels 'a' to 'c'. (**d**) and (**e**) show the change in SPCZ cross section in PlioMIP1 and 2, respectively. (**f**) and (**g**) as per 'd' and 'e' but for SACZ. Banding indicates interquartile range.

### *5.3.1 Subtropical High Intensification*

Two important features that regulate the intensity, duration and position of the STCZs are the position of the subtropical jet and the strength and the location of the atmospheric subtropical high pressure systems (Kodama 1992, Widlansky et al. 2011, van der Wiel et al. 2015, Zilli et al. 2019). Therefore, one may suppose that the weakening and southward shift of the STCZs in mid-Pliocene are related to a southward shift in the position of the subtropical jet. In this scenario, it would be expected less penetration of the subtropical jet troughs at subtropical latitudes. This weakens the zonal pressure gradient that is necessary for the occurrence of poleward low-level flows (Kodama 1992). However, the subtropical jet shifts equatorward by a small amount in PlioMIP1 (0° to 0.6°; Table S3) while the PlioMIP2 models do not show uniform changes (− 0.1° to 1.2°; Table S3). In contrast, Atmospheric General Circulation Models (AGCM) experiments forced with reconstructed mid-Pliocene SST field from PRISM have simulated a southward shift in the position of the Southern Hemisphere subtropical jet (Li et al. 2018), which would contribute to weakened STCZs in the mid-Pliocene.

The second cause for the STCZ changes might relate to an expansion and/or intensification of the Subtropical High pressure systems. An expanded Subtropical High prevents intrusions of the subtropical jet and weakens the continental heat lows that occur during summer months and contribute to an intensified zonal pressure gradient (Zilli et al. 2019). Quantifying the intensity of the subtropical highs is not a simple task when dealing with different climate backgrounds (+ 2–3 °C) as the global pressure weakens in a warmer atmosphere (Held and Soden 2006). As such, it is computed the stream function at 850 hPa to identify the position and intensity of the pressure systems at low levels relative to the background state (c.f. Methods). The results show that the Subtropical High pressure systems were more intense in the mid-Pliocene in both PlioMIP phases (Figure 7a,b).

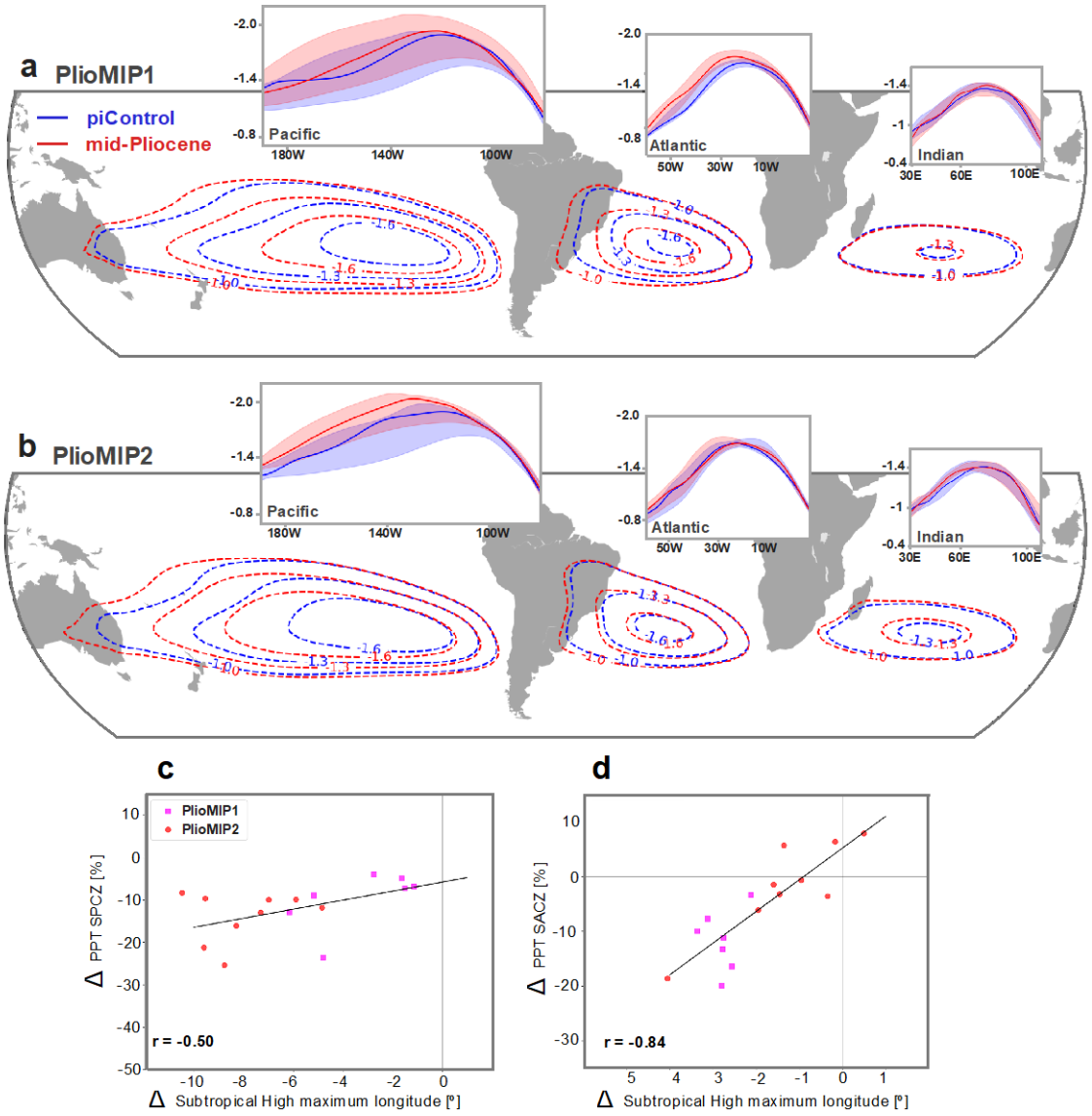


**Figure 7.** Subtropical high intensification. (**a)** PlioMIP1 MMM stream function at 850 hPa. Units $10^{-7}$ $m^2$ $s^{-1}$. Inner panels show the multi-model median stream function at the latitude of the maximum stream function for the Pacific, Atlantic and Indian oceans (Methods). Banding indicates inter-quartile range. (**b)** as 'a' but for PlioMIP2. (**c)** relationship between the change in the position of the subtropical high maximum and the change in the SPCZ precipitation along its diagonal sector. The subtropical high maximum position is computed as the weighted average longitude of the 850 hPa stream function shown in the inner panels of 'a' and 'b' (see methods). (**d)** as per 'c' but for SACZ.

Across all models there is a strong relationship between the change in the position of the Subtropical High and the change in the intensity of the STCZs (Figure 7c,d), where the models that simulate larger westward displacements of the subtropical high tend to be associated with larger rainfall reduction along both STCZs. The SPCZ comprises two sectors:

a western zonal sector, which sometimes merges with the ITCZ in the western Pacific Warm Pool; and, an eastern NE to SW oriented sector (Vincent 1994), extending south-eastward to Cook Islands. Here, there are only significant correlations associated with rainfall changes in the eastern sector. Changes in rainfall at the western SPCZ may be more influenced by changes in the position and temperature of the Western Pacific Warm Pool.

The South Pacific Subtropical High intensification and westward shift is more severe in the PlioMIP2 simulations (Figure 7) with a westward shift of 7° to 9.5° compared to a shift of 1.5° to 5° in the PlioMIP1 simulations. In the Atlantic basin results for both PlioMIP phases show a westward shift; however, with larger values for the PlioMIP1 (− 2.7° to − 3°) compared to the PlioMIP2 (− 0.3° to − 1.6°).

One may question whether the STCZs changes are associated with changes in local SSTs (Xie et al. 2010). In the South Atlantic basin, there is no clear agreement between the changes in precipitation and SSTs (Figure 5d). In fact, the local SST in the southwestern South Atlantic has been shown to be a response to the SACZ (Chaves 2004), and acts to dampening the SACZ strength (De Almeida et al. 2007). In contrast, the South Pacific SST changes project onto the SPCZ location, suggesting that local forcing may have played a role in the Pacific convergence zone (Figure 5d). However, it is difficult to evaluate whether the regional SST change is the main driver of the SPCZ changes as significant changes. The local SST could be a result of significant changes in winds more broadly, associated with the subtropical high system (Figure 7), through the wind-evaporation-SST (WES) footprinting mechanism (Vimont et al. 2001).

### *5.3.2 ITCZ-Monsoon-STCZs relationship*

Observational studies have shown that when moisture fluxes from the ITCZ and monsoons can penetrate into the STCZs, it can result in more intense deep convection at the

convergence zone (Kodama 1993, Carvalho et al. 2002, Vera et al. 2006). Although the SPCZ and SACZ are formed regardless of the influence of the ITCZ and monsoon systems (Kiladis et al. 1989, Kodama 1992).

A coherent northward shift in the Pacific ITCZ is simulated in both PlioMIP phases. The austral summer position of the Pacific ITCZ moved northwards by + 0.9° to + 1.8° in the PlioMIP1 models and by + 1° to + 2.4° in the PlioMIP2 models. All PlioMIP1 models show a northward ITCZ shift in the Atlantic of + 0.4° to + 2°, while in the PlioMIP2 this change is less clear (− 0.1° to + 1.3°).

The change in the Pacific and Atlantic ITCZ positions are linearly related to the changes in rainfall along the diagonal sector of the SPCZ and the SACZ, respectively (Figure 8). Here, there is only a significant relationship of the ITCZ with the most remote part of the SPCZ (diagonal sector; Figure 8a) and not the section of the SPCZ that comes into more direct contact with the ITCZ (zonal sector). This is likely due to an indirect effect via atmospheric changes from equator to the subtropics and is different from the direct mechanism proposed earlier (Vincent 1994). The ITCZ is a large-scale atmospheric feature whose position is tied to the meridional atmospheric circulation and, thus, meridional heat fluxes (discussed below). As such, the ITCZ migrates northwards as the southward energy flux at the equator (also called "energy flux equator") intensifies. These changes intensify the Southern Hemisphere Hadley circulation and the Subtropical High system, which in its turn is closely linked to the diagonal sector of the SPCZ (Figure 7c).

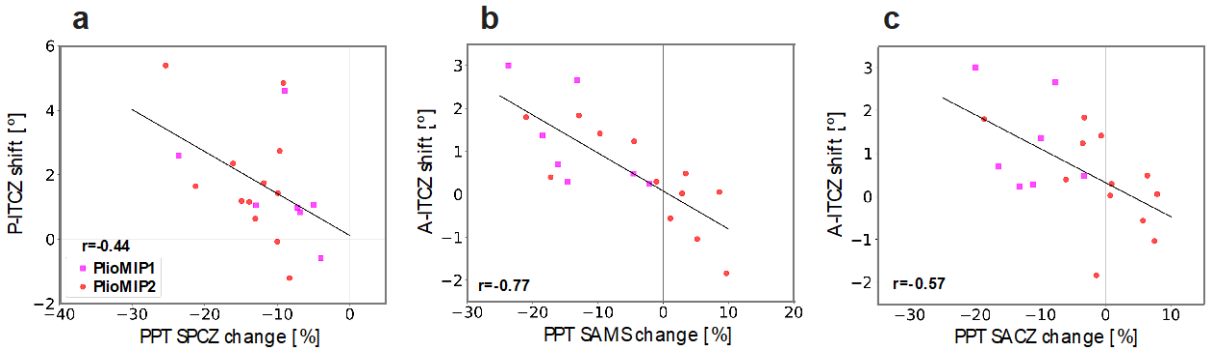


**Figure 8.** ITCZ-Monsoon-STCZs relationship. (**a)** relationship between the Pacific ITCZ shift and the change in the SPCZ precipitation along its diagonal section. (**b)** relationship between the Atlantic ITCZ shift and the mean change in the South American Monsoon system (SAMS) precipitation (25°S–10°S; 35°W–65°W). (**c)** relationship between the Atlantic ITCZ shift and change in the precipitation along the SACZ.

Furthermore, it is worth noting that in the Pacific region the ITCZ, Australian Monsoon and SPCZ are not all necessarily attached to one another. For example, two models (NorESM-L in PlioMIP1and CCSM4 in PlioMIP2) that show extreme northward shifts of the Pacific ITCZ (4.6° and 4.8°, respectively; outliers in Figure 8a) do not weaken the SPCZ accordingly (−9% and −9%, respectively) but show great intensification of the Australian Monsoon (26% and 33%, respectively). This means that the Australian Monsoon can still intensify and provide moisture to the SPCZ even if the ITCZ shifts northward.

In the Atlantic sector, the moisture flux from the ITCZ to the SACZ is more direct than in the Pacific sector due to the topographical characteristics of South America (Carvalho et al. 2004, Vera et al. 2006). During summertime, the ITCZ moisture flux flows into the Amazon basin up until reaching the Andes Mountain chain in the western Amazon. This moisture flux is then guided by the Andes towards south-eastern South America establishing the South American Monsoon System (SAMS; Jones and Carvalho 2002, Carvalho et al. 2004). As such, a northward shift of the Atlantic ITCZ during summertime directly implies in weakened SAMS ($r = 0.77$; Figure 8b). In this way, a more northward ITCZ position also suppress the equatorial

moisture flux from reaching subtropical latitudes and, thus, weakens the SACZ system ($r = 0.57$; Figure 8c).

The PRISM reconstruction provides further evidence of a northward ITCZ shift in the mid-Pliocene (Dowsett et al. 2010). It is well established that variations in tropical Atlantic SST directly influences the position of the ITCZ and precipitation in west African countries (Mcgee et al. 2018) and Northeast Brazil (Utida et al. 2019). The PRISM includes three high-level confidence sites in the north-western African upwelling region (Figure 5a,d). These sites reveal an SST warming in between 1 °C to 2.2 °C relative to the Common Era (~ 1850). This indicates weakened upwelling in this region which in turn is suggested to be linked to decreased north-eastern trades winds due to a northward displacement of the Atlantic ITCZ (Mcgee et al. 2018).

### *5.3.3 Large-scale forcing*

The similarity of changes across the ocean basins (Subtropical High intensification and northward ITCZ shift) suggests a common large-scale driver. Changes in the inter-hemispheric heat contrast have been shown to affect tropical and subtropical atmospheric circulation through changes in the meridional heat flux (Chiang and Friedman 2012, Schneider et al. 2014, Bakker and Prange 2018). To evaluate whether the atmospheric changes in the PlioMIP models are consistent with these earlier studies, sensitivity experiments using the National Centre for Atmospheric Research (NCAR) Community Atmospheric Model version 4 (CAM4) are performed. The CAM4 model is forced with multi-model mean monthly climatology of SST and sea-ice from PlioMIP1 and PlioMIP2. Land areas (i.e. land-ice, vegetation and soils) and $CO_2$ concentrations were kept as pre-industrial (see Methods). CAM4 is also forced with model-based SST and sea-ice from PlioMIP pre-industrial controls as a comparison.

The AGCM experiments show qualitatively similar rainfall changes to those simulated by the fully-coupled PlioMIP models (Appendix A). The experiments were able to capture the

large-scale changes in rainfall in the tropics and subtropics, particularly in the Pacific and Atlantic Oceans associated with the STCZs, and in most of South America and Southern Africa. Disagreements occur over regional areas in Western Africa, Tropical Indian Ocean and Australia. It is important to note that the PlioMIP models include prescribed changes in vegetation (PlioMIP1 and PlioMIP2) and soils (PlioMIP2 only; Table S2) and the AGCM experiments do not. Therefore, the AGCM experiments indicate that a large part of the mid-Pliocene precipitation change is associated with large-scale changes in SST and sea-ice (Supplementary Fig. S4).

The changes in meridional circulation are in agreement with the PlioMIP simulations (Figure 9). Changes in the zonal mean meridional stream function indicates an intensification and northward expansion of the Southern Hemisphere Hadley cell, while its Northern Hemisphere counter-part weakens (Figure 5a,b). This results in a northward ITCZ displacement and increased cross-equatorial southward energy flux (CAM4-PlioMIP1: 0.09PW or 48%; CAM4-PlioMIP2: 0.07PW or 44%; Figure 5c). The energy flux across the equator in the forced pre-industrial experiments agrees with the observed value of − 0.2 PW (Marshall et al. 2014; − 0.2 PW forced with PlioMIP1 and − 0.16PW forced with PlioMIP2; Figure 9c). These changes are consistent with a warmer Northern Hemisphere compared to Southern Hemisphere as indicated by proxy data and models (Figure 5a,b) and enhanced Southern Hemisphere high pressure systems, which likely drive weakened STCZs.

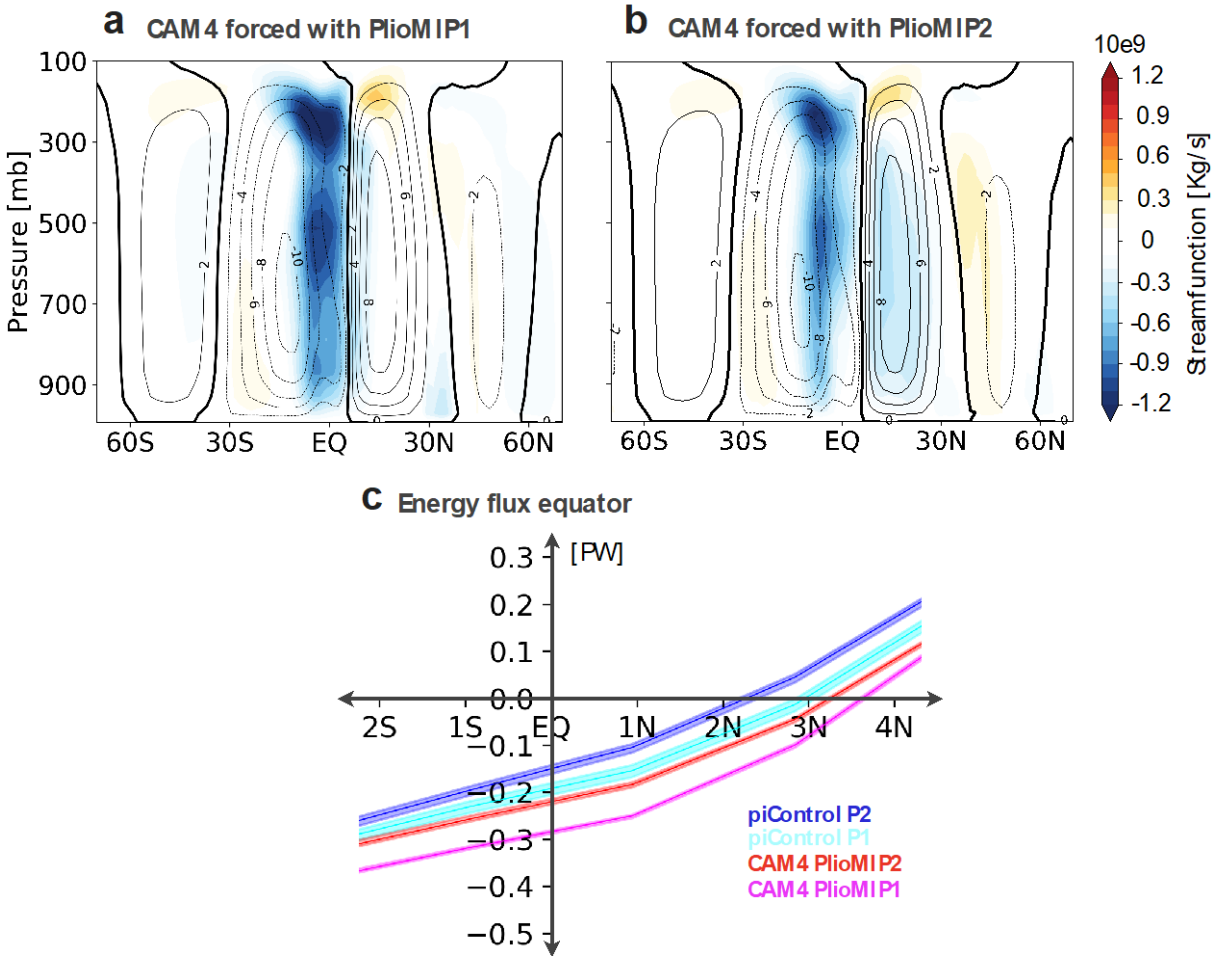


**Figure 9.** Atmospheric Meridional circulation changes. **(a)** 5-member ensemble mean of the zonally averaged meridional stream function simulated by the CAM4 model forced with model-based PlioMIP1 SST and sea-ice. Contours indicate piControl stream function: contour interval $2 \times 10^{-9}$. Shading indicates change (mid-Pliocene minus piControl). Units: $10^{-9}$ kg $s^{-1}$. (**b)** as 'a' but for the simulation forced with model-based PlioMIP2 SST and sea-ice. (**c)** integrated atmospheric meridional heat transport. Banding indicates ensemble range.

## 5.4 Discussion

A warmer atmosphere holds more moisture and as such would be expected to be associated with more rainfall. Indeed, all PlioMIP models increase global mean rainfall in the mid-Pliocene. However, the mid-Pliocene simulations show large spatial differences in rainfall and a mostly drier tropical and subtropical Southern Hemisphere.

This chapter provides a consistent picture of changes associated with the Southern Hemisphere summertime rainfall in the mid-Pliocene (Figure 10). PlioMIP simulations indicate

that the convergence zones in the South Pacific and South Atlantic weakened and displaced south during mid-Pliocene relative to pre-industrial conditions. These changes were associated with changes in interhemispheric SST gradient and consequently differences in large-scale atmospheric circulation. In particular, during the mid-Pliocene the northern hemisphere was warmer than the southern hemisphere. This interhemispheric temperature difference enhanced the southward energy flux equator as well as intensified the Southern Hemisphere Hadley circulation. As a result, the ITCZ shifted northward, and the Subtropical Highs in the Southern Hemisphere strengthened during the mid-Pliocene. Since the Subtropical Highs are related to the formation and location of the convergence zones, the intensified Pacific and Atlantic Subtropical Highs weakened the SPCZ and SACZ. As the ITCZ moves northward, the moisture inflow from the tropics to the subtropics over South America decreases, leading to a drier-than-normal SACZ. The ITCZ-SPCZ relationship is more complex and probably illustrates the link between the SPCZ weakening with changes in the large-scale circulation.

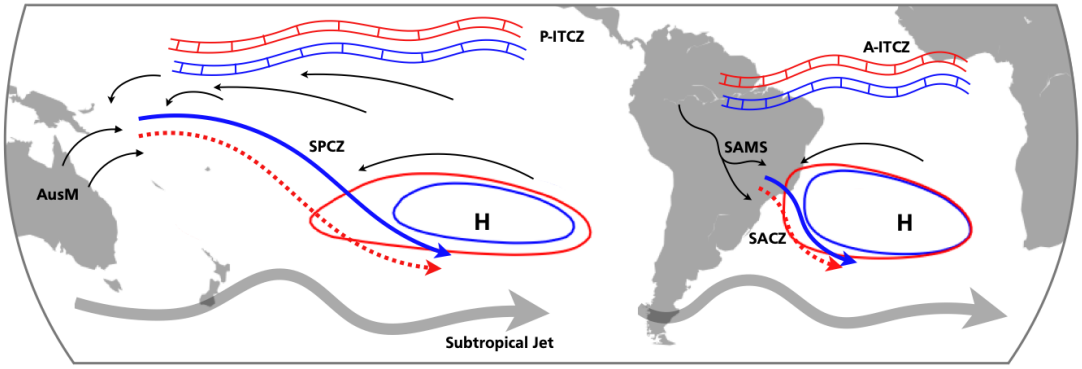


**Figure 10.** Schematic of the drivers of reduced rainfall in the Southern Hemisphere: subtropical high, ITCZ, STCZs and monsoon systems. Thicker grey arrows indicate the position of the subtropical jet. Thin black arrows indicate sources of moisture to the STCZs. AusM: Australian Monsoon. SAMS: South American Monsoon System. P-ITCZ: Pacific ITCZ. A-ITCZ: Atlantic ITCZ.

These results suggest that the asymmetric warming between the two hemispheres may contribute to the tropical and subtropical changes in precipitation. In the PlioMIP experiments there is a large imposed change in the polar ice distribution. The change is considerably larger

in the northern hemisphere compared to the southern hemisphere and gives rise to a large-scale asymmetric change in temperature (Hill et al. 2014). Previous studies have shown that such an asymmetric change can give rise to an ITCZ shift (Chiang and Friedman 2012, Schneider et al. 2014; and references therein). Additionally, local SST appears to play an important role in the ITCZ shift. However, the coupled changes to SST, atmospheric circulation and precipitation within the tropics could be in turn a response to large-scale remote changes. SST and precipitation are strongly coupled in the tropics and ocean–atmosphere feedbacks could have played an important role in both amplifying (i.e. WES and upwelling; Mcgee et al. 2018) and damping (i.e. tropical ocean circulation; Schneider 2017) ITCZ shifts. Thus, tropical changes in rainfall are also consistent with an increased tropical inter-hemispheric SST gradient (McGee et al. 2014; Figure 5b,c,d). Another confounding factor that may have contributed to changes in local precipitation within the tropics is the expansion of the tropical rainforests in the PlioMIP simulations. For instance, a northward expansion of the tropical vegetation in Africa is known to increase precipitation in the Northern Hemisphere tropics, decrease trade winds and, thus warm the tropical North Atlantic (Pausata et al. 2020). It is important to note that the PlioMIP initiative focuses on a single interglacial time slice (KM5c at ~ 3.2 Ma) within the mid-Pliocene Warm Period (3–3.3 Ma). Thus, it is not possible to evaluate the sequencing of events that have triggered the mid-Pliocene rainfall shifts within the PlioMIP. Additionally, the relative effect of local versus remote SST forcing on tropical and subtropical rainfall during the mid-Pliocene requires further investigation.

The SACZ changes are less intense in the PlioMIP2 simulations than in PlioMIP1. A major difference between PlioMIP phases is that the second phase includes changes in soils, while the first phase uses modern-day distributions (PlioMIP phases 1 and 2 boundary conditions are described in Table 1). The PRISM reconstruction indicates a southward expansion in the tropical rainforests. As a consequence, this change is more evident in PlioMIP1

than in PlioMIP2 (Salzmann et al. 2008; i.e. modern soils at subtropical latitudes used in PlioMIP1 are mostly replaced with soils from tropical rainforests which likely add a source of moisture in the subtropics in PlioMIP2). Both phases apply the same changes in vegetation. These regional differences in soils may offset the large-scale forcing, especially in South America where the SACZ is located mostly over the continent (Carvalho et al. 2004, 2011). It is worth noting that the changes in vegetation (both phases) and soils (PlioMIP2 only) do not increase rainfall in south-eastern South America as one would expect due to the southward expansion of the Amazon rainforest. The effect of different soil types from PlioMIP1 to PlioMIP2 is clear over central Brazil: 100% of the PlioMIP1 models show weaker SAMS, while there is less agreement among PlioMIP2 with only 55% models showing reduced SAMS. These regional changes could also be related to the spread among models with respect to the northward shift in the Atlantic ITCZ in the PlioMIP2.

Here, in addition to thermodynamically induced rainfall changes, changes in gradients drive shifts of important atmospheric features that result in a mostly drier subtropical Southern Hemisphere. This highlights that dynamical changes can be as important as thermodynamical ones in a warmer scenario. The mid-Pliocene (proxy and models) illustrates a scenario where the Northern Hemisphere warming rates are higher than its Southern counterpart. Over the past four decades, the Arctic has been warming faster than the global average (Zhang 2005) with faster sea-ice melting than projected (Stroeve et al. 2007). At the same time, the Antarctic warming has been increasing in the western sector while a weak cooling has been observed in the eastern sector (Paolo et al. 2015) similarly to the mid-Pliocene (Naish et al. 2009). In this way the mid-Pliocene share some characteristics of the modern warming. The mid-Pliocene indicates that once differing warming rates between both hemispheres become important, dynamical atmospheric changes are likely to become relevant. In fact, the SACZ has been recently reported to be shifting poleward due to an intensified South Atlantic subtropical high

over the satellite era (post-1979; Zilli et al. 2019). Thus, the evaluation of the mid-Pliocene adds a constraint associated with differing rates of warming between hemispheres.

Limitations of the present study include the accuracy of proxy data used to force the models and climate model biases. Uncertainties remain in the extents of the Greenland ice sheet (Haywood et al. 2016b) and the distribution of biomes (vegetation and soils), especially in South America due to a lack of geological sites (Salzmann et al. 2008). Furthermore, climate models are thought to underestimate the magnitude of long-term warming due to a lack of polar feedback processes (Fischer et al. 2018). Indeed, most PlioMIP models underestimate the magnitude of the proxy-based polar amplification. As such, both proxy and modelling studies are needed for a better understanding of the mid-Pliocene climate. To isolate the influence of asymmetric interhemispheric temperature changes on the tropical circulation, future work could use partial coupling experiments where extratropical SST is prescribed, and the tropical ocean–atmosphere is allowed to evolve freely. For completeness, vegetation changes should also be taken into account.

# 6 Atlantic SST Variability in the mPWP

In this chapter changes and mechanisms for the global SST variability and Atlantic SST modes of variability are evaluated. The Atlantic SST variability has a high impact on the rainfall variability of South America and, thus, understanding the behaviour of ocean-atmosphere interactions in the warmer mid-Pliocene may shed light on future changes. At the moment of writing, only PlioMIP1 model output was available.

The results presented in this chapter were published in the journal *Climatic Change* in February 2020.

---

**Pontes, G. M.**, Wainer, I., Prado, L. & Brierley, C. Reduced Atlantic variability in the mid-Pliocene. *Clim. Change* **160**, 445–461 (2020). https://doi.org/10.1007/s10584-020-02675-9

---

## 5.1 Introduction

In this chapter, climate variability in the mid-Pliocene is investigated. the mid-Pliocene experienced reduced meridional SST gradients (Brierley et al. 2009) that have been hypothesized to impact climate variability (Rehfeld et al. 2018). Previous studies have looked at both proxy data and simulation results to assess the climate variability in the Pliocene. Draut et al. (2003) presented geological evidence that the Pliocene epoch (~ 5 Ma to ~ 2.7 Ma) was a period of relative climate stability, with reduced SST variability and the absence of abrupt changes, having a similar climate signature as those found for the Holocene (past ~ 12 ka) or Marine Isotope Stage 11 (424–374 ka). In addition, Dowsett et al. (2005), analysing PRISM estimates, reported greater SST variability at high latitudes. Most studies that examine climate variability during the Pliocene have focused on the El Niño Southern Oscillation (ENSO) (Haywood et al. 2007, Scroxton et al. 2011, Watanabe et al. 2011, Brierley 2015, Tindall et al. 2016). Watanabe et al. (2011) provided evidence of ENSO variability in the Pliocene by analysing coral-based SST. Brierley (2015) found a robust reduction in ENSO amplitude and a shift towards lower frequencies from simulation results of the Pliocene Model Intercomparison Project (PlioMIP). Tindall et al. (2016) analysed extended PlioMIP simulations of the Hadley Centre general circulation model (HadCM3) to detect changes in ENSO centennial-scale variability, showing that it was less frequent and longer in duration.

The impact of mid-Pliocene boundary conditions on climate variability varies for differing latitudinal regions (Figure 11). Brierley (2015) and Tindall et al. (2016) have investigated the variability of the Pacific and Indian oceans for this period. In agreement with these studies, Figure 11 shows how the spatial variability of SST is reduced for the Tropical Pacific in the PlioMIP models (Figure 1a). The changes for the tropical and subtropical Atlantic Ocean show a consistent pattern of reduced SST variability that has not been previously noted (Figure 1a). The globally averaged tropical variability decreases in all models with a multi-

model median (MMMe) of 7% (Figure 11b). The changes in variability in the Southern Hemisphere subtropics are small (Figure 11b), except if looking at the individual ocean basins. In the Northern Hemisphere mid-latitudes, the variability decreases by 5%. The mid-latitudes have experienced the greatest warming in the mPWP (Figure 11c), and the meridional SST gradient decreases between the equator and ~ 60° in both hemispheres (Figure 11d). This, in turn, might be associated with decreased variability in low latitudes and mid-latitudes (Rehfeld et al. 2018).

Polar regions in the PlioMIP models show increased variability in the Southern and Arctic oceans by 10% and 39%, respectively. It is important to note that all models show increased Arctic variability (Figure 11b). This could be associated with increased SST gradient poleward of 60° on both hemispheres. This gradient change is seen on both PlioMIP simulations and PRISM dataset (Figure 11d). The change in subtropical-to-polar SST gradient is approximately 5 times greater than the decrease seen between low latitudes and mid-latitudes. Thus, changes in SST gradient are likely to be modulating SST variability.

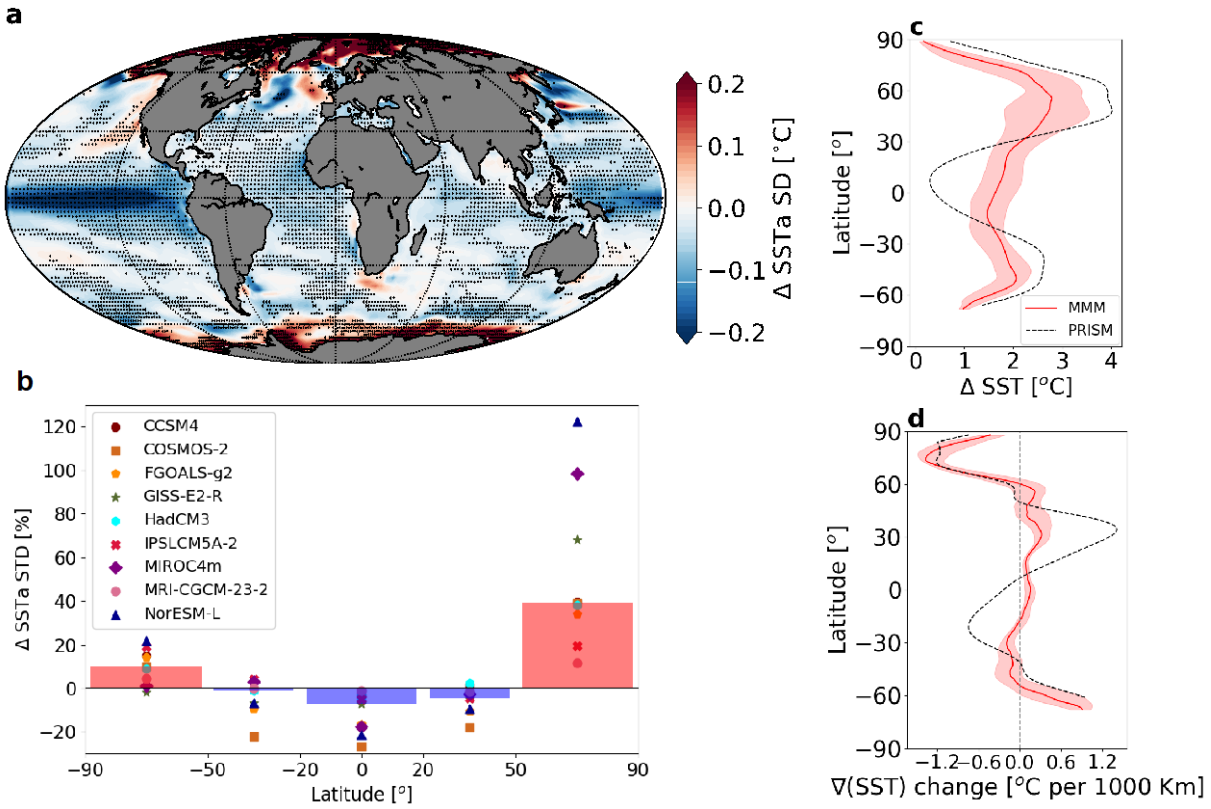


**Figure 11.** Simulated variability in the mid-Pliocene. **a** MMM SST anomaly (SSTa) standard deviation difference (mid-Pliocene minus piControl). Stippling indicates at least 7 out of the 9 PlioMIP models agree on the sign of the change (~ 80% model agreement). **b** MMMe zonally averaged SSTa standard deviation difference. It represents the change in variability from piControl to the mid-Pliocene at each latitudinal zone, as indicated by the column width. The simulated mid-Pliocene variability shows an overall decrease. It is represented by low- and mid-latitude regions. However, high latitudes have experienced increased variability. Symbols indicate each model's value for the Antarctic region (min − 2%; max 22%), Southern Hemisphere subtropics (min − 22%; max 4%), tropical regions (− 27% to − 1%), Northern Hemisphere subtropics (min − 18%; max 2%), and Arctic region (min 11%; max 122%). **c** PRISM SST reconstruction (black dashed line) and MMMe zonally averaged SST difference (red line). **d** PRISM (black dashed line) and MMMe change in the zonally averaged meridional SST gradient from pole to pole, computed between each two consecutive grid points (red line). Both negative values in the Southern Hemisphere and positive values in the Northern Hemisphere indicate a decreased gradient. Banding on panels **c** and **d** indicates interquartile range.

Patterns of Atlantic SST variability are known to have impacts over continental areas, mostly through changes in precipitation. The Atlantic Multidecadal Variability (AMV), which is defined as the basin-wide leading empirical orthogonal function (EOF) between the equator and 60° N in the North Atlantic, is associated with precipitation variability over North America

and Brazil (Enfield et al. 2001, Ting et al. 2011) and with the frequency of severe tropical Atlantic hurricanes (Trenberth and Shea 2006). In the tropical Atlantic, the Atlantic Equatorial Mode (AEM, also known as Atlantic Niño), which is defined by the leading EOF in the tropical Atlantic (20° S–20° N and 60° W–20° E; e.g., Deser et al. 2010), intensifies atmospheric convection at the equator, holding the Atlantic rain belt at its southern position (Giannini et al. 2003). The Atlantic Meridional Mode (AMM), which is represented by the EOF2 in the tropical Atlantic (Deser et al. 2010), is strongly associated with the meridional displacements of the Intertropical Convergence Zone (ITCZ; Wainer and Soares 1997). In the Southern Hemisphere, the South Atlantic Subtropical Dipole (SASD), represented by the leading EOF between 0°–50° S and 60° W–20° E (Morioka et al. 2011), has been associated with changes in precipitation of opposite polarity over northeastern and southeastern Brazil (Morioka et al. 2011, Wainer et al. 2014). These Atlantic modes of variability impact the location and distribution of precipitation. Therefore, an investigation of the changes in these modes in the mPWP may provide a useful constraint for possible future projections associated with a warmer world.

This chapter aims at evaluating changes in the spatial structure, frequency, and amplitude of the Atlantic SST variability modes using the output of all nine coupled model participants in the PlioMIP phase 1. PlioMIP2 data was not yet available at the time these analyses were performed. The modes to be analysed are AMV in the North Atlantic, AEM and AMM in the tropical Atlantic, and the SASD in the South Atlantic.

## 6.2 Methods

There are two well-accepted techniques to detect modes of variability based on SST: index-driven metrics and through the calculation of EOFs. Both techniques are computed with anomalies that are obtained by removing the average annual cycle from the original time series. The most common detection is made through index-driven metrics and is usually the mean over

a given area (e.g., Zebiak 1993) or the difference between two areas (e.g., Wainer et al. 2014). This metric assumes that the pole of variability does not change its position. Therefore, to be able to evaluate spatial changes in the SST modes, they are defined through the computation of EOFs. EOF analysis allows us to separately study changes in the spatial structure for both frequency and amplitude, which is achieved by normalizing the EOF spatial pattern by its spatial standard deviation (e.g. Brierley 2015). results based on the index metrics are still presented and discussed whenever appropriate. However, the change in the spatial pattern associated to the index-based time series, which is computed by regressing it into the SST anomaly field, is not comparable to the change in the EOF spatial pattern as the first is under the influence of amplitude changes. The amplitude of the modes of variability are defined as the time series standard deviation (as in Taschetto et al. 2014, Brierley 2015).

To evaluated changes in the frequency of the modes of variability the spectral analysis methodology described by Mudelsee (2014) using Welch's overlapped segment averaging procedure is adopted. Since the weight given by the EOF analysis for its respective time series may differ from model to model, all EOF time series were normalized by their own standard deviation before applying the spectral analysis. In this manner, it is possible to isolate the influence of amplitude, as well. The dominant frequency is defined as the frequency with the greatest power density in the spectrum.

It is worth noting that in this chapter multi-model medians are used. Multi-model means are used in two cases: (1) when plotting multi-model maps because the use of medians can distort the patterns and (2) when just a few models have the available variables for the analysis. Therefore, unless specified, all values presented are MMMe followed by the range of all models, which includes extreme models.

## 6.3 Results

### *6.3.1 Atlantic Multidecadal Variability*

All PlioMIP models have represented the AMV pattern in their respective leading EOFs over the North Atlantic in both pre-industrial and mid-Pliocene climates (Figure 12). These patterns are consistent with the horseshoe pattern observed in the HadISST dataset; however, some models show a bias in the position of the AMV pole at extratropical latitudes (Appendix B). The mid-Pliocene multi-model mean results show significant spatial changes, which can be observed in the difference map (mid-Pliocene minus piControl; Figure 12b). The difference shows that the positive AMV pole expands equatorward and eastwards in at least 7 out of 9 models (Figure 12b; individual models in Appendix B).

Alternatively, the AMV mode was also analysed through the index-based metrics. This is the area-weighted average SST anomaly over the North Atlantic (0°–60° N; 80° W–0°). The spatial pattern of this metric, computed by regressing the AMV index time series onto the SST anomaly field, cannot reveal structural changes. It, instead, indicates the regions with greatest changes in amplitude. This analysis shows increased variability in the northeastern North Atlantic and reduced variability in the Tropical North Atlantic (TNA; Appendix B).

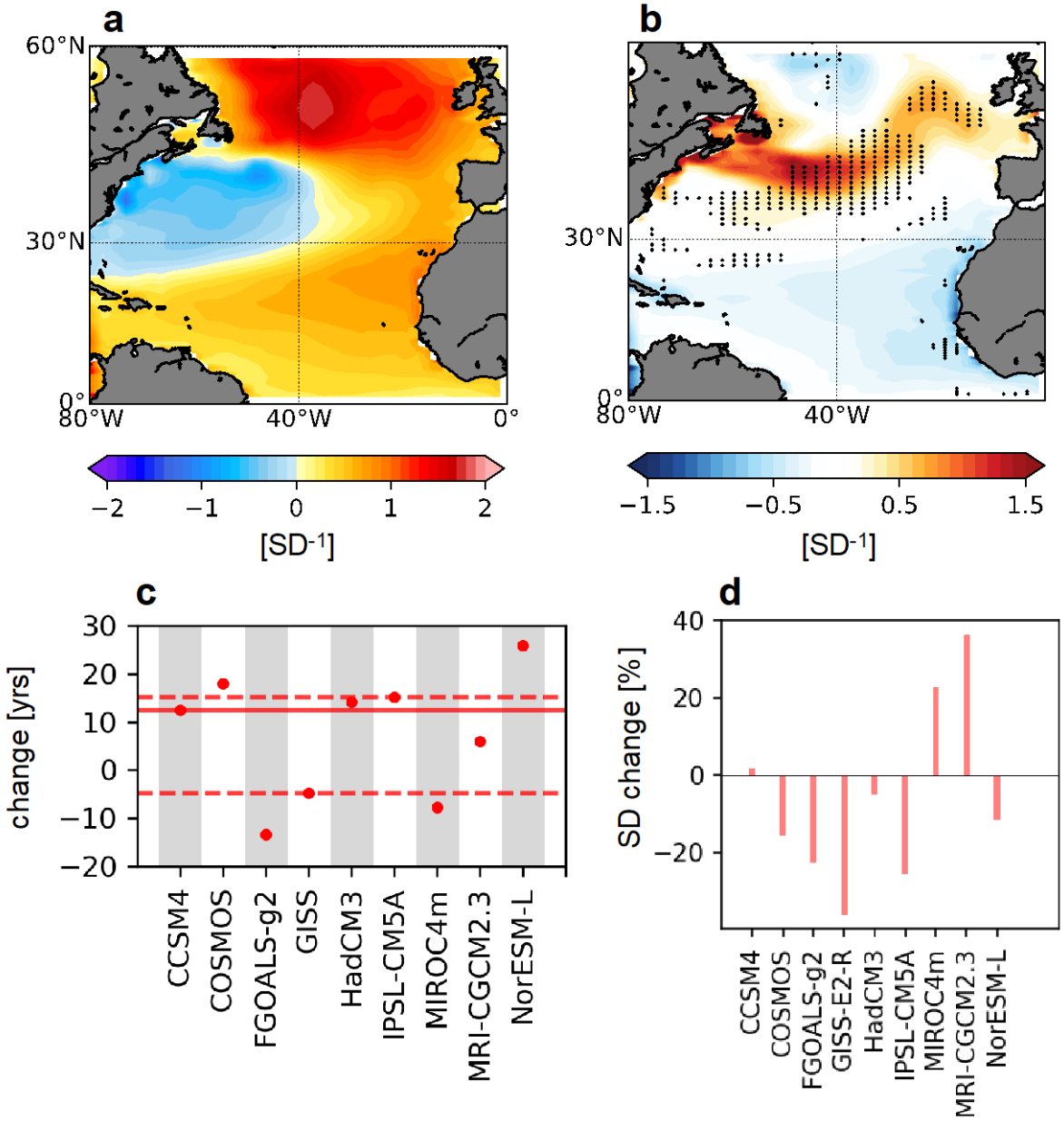


**Figure 12.** Multi-model analysis of the Atlantic Multidecadal Variability (AMV). **a** piControl MMM structure. It captures the observed HadISST structure (individual models in Appendix B). **b** Normalized MMM difference (mid-Pliocene minus piControl; units: $sd^{-1}$). Stippling indicates regions where there is a ~ 80% (at least 7 of the 9 PlioMIP models) agreement on the sign of the difference. The AMV pole has significantly expanded southwards and shifted eastwards. **c** Spectral analysis results. This panel shows the difference in the AMV power spectrum between the most energetic period for the mid-Pliocene and piControl simulation results. The power spectra for the individual models are shown in Appendix B. All but three models (FGOALS-g2, GISS, and MIROC4m) shift towards higher periods in the mid-Pliocene. **d** Difference in the time series standard deviation (mid-Pliocene minus piControl)

The AMV has an observed period of 63.3 years (Appendix B). The PlioMIP models examined here do not capture the AMV observed frequency (Appendix B). Nonetheless, 6 of the 9 models shift their respective highest power frequency towards lower frequencies from modern to mid-Pliocene conditions. It is only statistically significant at the 90% level. The MMMe change in this period is 12.5 years (from − 13.4 to 25.9 years; Figure 2d). The index-based time series does not suggest any changes in the AMV frequency with only 4 models indicating a shift towards lower frequencies (Appendix B).

The sign of the change in AMV amplitude varies across the PlioMIP models (Figure 12d). The MIROC4m and MRI-CGCM2.3 models simulate the mPWP AMV with increased variances. The CCSM4 and HadCM3 models show nearly no change. On the other hand, the simulation results from the remainder of the PlioMIP models show the AMV weakening. The changes in amplitude indicated by each model are consistent in both EOF and index-based metrics, except for MIROC4m that suggests increased amplitude in the EOF method and decreased amplitude in the index-based method (Figure 12d and Appendix B). Thus, there is no consistency about changes in the AMV amplitude. Delworth and Greatbatch (2000) reported that the presence of extratropical air-sea modes depends on the intensity at which the atmosphere responds to mid-latitude anomalies on both SST and sea ice in general circulation models. In this manner, the differing changes in AMV amplitude shown here are most likely associated with differing atmospheric responses to mPWP warmth and reduced sea ice in each model.

The structural changes in the AMV likely modify the affected continental areas. The southward and eastward expansion of the AMV pole changes heat advection to North America and Europe (Enfield et al. 2001, Sutton and Hodson 2015). The expansion of the AMV pole and the southward shift in the NAD can possibly strengthen the impact of the AMV over Europe rainfall and air temperature and amplify its impact over North America. Moreover, the

expansion of the warming region at extratropical latitudes can possibly strengthen the ITCZ northward shift response, increasing precipitation over the Sahel region and amplifying droughts over northeastern Brazil (Ting et al. 2011, Kayano et al. 2016, Villamayor et al. 2018). Further warming in the North Atlantic may also intensify moisture convergence over western Amazon (Wang et al. 2018).

#### *6.3.1.1 The role of the Atlantic Meridional Overturning Circulation*

The AMV is influenced by both large-scale ocean transports and air-sea interactions. Since the early 1990s, the AMV is considered to be a surface fingerprint of the natural oscillation of the Atlantic Meridional Overturning Circulation (AMOC) (Zhang et al. 2019; and references therein). Recently, it has also been shown that ocean-atmosphere interactions are important in reproducing the AMV pattern (Clement et al. 2015). The authors suggest that the positive (negative) AMV pattern is a result of weaker (stronger) atmospheric subtropical high and poleward (equatorward) shift of the westerly jet, which results in weaker (stronger) westerly winds in mid-latitudes that weaken (intensify) the ocean circulation and, hence, converging heat. Thus, the AMV may be triggered by increased AMOC poleward transport and/or weakened westerly winds.

Both AMV drivers, AMOC and air-sea interactions, indicate that the location of the AMV pole may depend on the position of the North Atlantic currents. Here, it is investigated whether changes in the AMV structure are related to changes in the mean state circulation in the North Atlantic. The changes in the intensity of the North Atlantic Ocean transport integrated up to 1000 m (for all models except FGOALS-g2 and IPSL-CM5A) reveal a southward shift of the North Atlantic Drift (NAD) and intensification of the subpolar gyre (Figure 13; individual models in Appendix B). The NAD delimits the northern boundary of the North Atlantic Subtropical Gyre, being responsible for heat advection from the Gulf Stream to higher latitudes across the North Atlantic (Sarmiento and Bryan 1982). There are few regions of good model

agreement in the North Atlantic transport changes (Figure 13a) as the position of the North Atlantic currents varies from model to model, especially due to the differing model resolutions (Appendix B). Nonetheless, the changes in the North Atlantic transport are consistent with changes in the AMV structure in each model (Appendix B). A given model may move its AMV pole northwards even with a southward shift of the NAD if the model also strengthens the NAD and the subpolar gyre (ex., GISS-E2-R and NorESM-L). The eastward expansion of the AMV is related to an intensification of the NAD, especially eastwards of 40° W (ex., CCSM4, GISS-E2-R, HadCM3, MRI-CGCM2.3, NorESM-L; significant at the 90% level).

These findings suggest that the location of the AMV pole depends on the dynamical setting of the North Atlantic, which includes the mean state intensity and position of the North Atlantic Ocean currents. The PlioMIP multi-model mean indicates that the NAD in the mid-Pliocene is likely to have been south of its present position (Figure 13a), as was the AMV pole. In addition, the strengthening of the NAD east of 40° W is likely responsible for enhanced variability in the northeastern North Atlantic in the PlioMIP simulations. In fact, proxy data studies have estimated a southward shift and slowdown of the NAD during the Pliocene (De Schepper et al. 2009, Friedrich et al. 2013).

The possible role of the intensity of the AMOC in driving the AMV amplitude and frequency changes is evaluated next. Firstly, it could be hypothesized that the AMV amplitude is associated with the AMOC strength. However, the changes in amplitude of the AMV across the PlioMIP models are not related to changes in the mean state of the AMOC (Figure 13a). The amplitude changes in the individual models do not follow the changes in the mean state volume and heat transport in the upper cell (< 1000 m) of the AMOC at 30° N (Figure 13a,b). In addition, Zhang et al. (2013) have shown that the full-depth AMOC mean state in the PlioMIP simulations does not differ from modern.

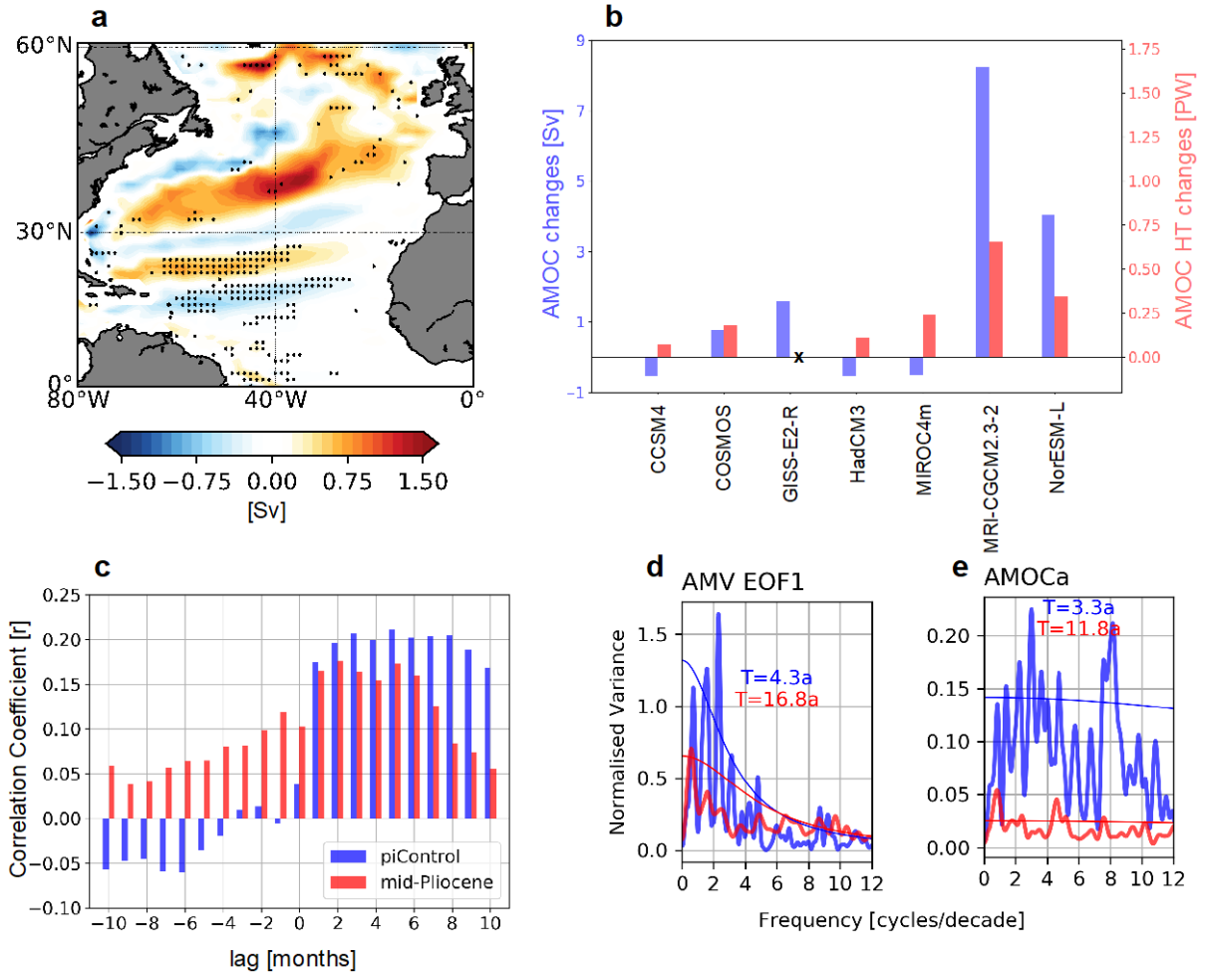


**Figure 13.** AMOC changes. **a** Multi-model mean change of the intensity of the North Atlantic transport integrated up to 1000 m. The MMM indicates an equatorward shift of the NAD and intensification of the subpolar gyre. The change for each model is shown in Figure S2. Stippling indicates a model agreement of at least 6 out of 7 models. **b** Changes in the AMOC volume transport (blue bars) and heat transport (red bars) integrated up to 1000 m at 30° N. The "x" in the position of the GISS-E2-R red bar means "no data available." **c** Cross-correlation between AMV-EOF1 time series and AMOC volume transport anomaly in the CCSM4 model. Positive time lags indicate that AMOC variability leads. **d** Power spectra of the AMV-EOF1 time series in the pre-industrial control (blue) and mid-Pliocene (red). **e** as **d** but for the AMOC volume transport anomaly. Significance lines at the 90% level based on a first-order autoregressive model are shown in **d** and **e**

Secondly, the relationship between the AMOC variability and AMV is investigated. Here, the AMOC variability is analysed through the time series of ocean volume and heat transport anomalies in the upper cell at 30° N (< 1000 m). This is examined in the simulation

results from CCSM4 which was the only model with available monthly time series of subsurface variables.

In the CCSM4 simulation results, the correlation coefficient between the AMV time series and AMOC anomaly is 0.22 ($p < 0.05$) in between a lag from 2 to 8 months in the pre-industrial control run (Figure 13c). The correlation coefficient between the AMV and AMOC ocean heat transport (OHT) anomaly is lower (0.14; $p < 0.05$; Appendix B). In the mid-Pliocene, the AMV/AMOC correlation coefficients are lower and there are positive correlations for negative lags as well, which may be associated with an increased AMV period (Figure 13c; similar results were found using the AMV index time series: Appendix B). In fact, the period with the highest power in the AMV time series (4.3 years) is similar to the period with the highest power for the AMOC transport time series (3.3 years) in the pre-industrial control (Figure 13d,e). Furthermore, both AMV and AMOC periods with the highest power shift accordingly towards higher periods in the mid-Pliocene (Figure 13d,e). The analysis in the frequency domain suggests a link between the changes in the AMV and changes in the AMOC variability.

### *6.3.2 Tropical Atlantic Modes*

Two tropical Atlantic modes of SST variability arise as the first two EOFs over the area between 20° S–20° N and 60° W–20° E (as in Deser et al. 2010). The first mode is the AEM, which is characterized by the Atlantic equatorial cold tongue. The individual PlioMIP model's representation of the Atlantic Niño differs considerably (Appendix B). The majority of the models generally have a poor representation of this variability mode, making it difficult to evaluate and interpret changes either in spatial structure or on the temporal variability. This fact may be related to westerly wind biases in the equatorial Atlantic in coupled models, which leads to deepening of the thermocline in the east and, thus, hampering the development of the cold tongue (Richter et al. 2014).

The AMM is the EOF2 spatial pattern of SST anomalies in the tropical Atlantic (Figure 14a, Deser et al. 2010). It represents an interhemispheric SST gradient that shows opposite SST anomalies on either side of the equator. This way, it can also be computed through the difference between the Tropical North Atlantic (TNA; 5° N–20° N) and the Tropical South Atlantic (15° S–5° N; Servain et al. 2000). The PlioMIP models were able to represent the AMM pattern through both EOF and index-based metrics (Appendix B). The AMM in the NorESM-L model is difficult to define as both EOFs present a dipole pattern (Appendix B). EOF2 in this mode was chosen because it has a stronger dipole structure, which is the main pattern of AMM, even though it is confined to the African coast (Appendix B). This way, here the results are discussed based on the AMM EOF metrics and the index-based results are discussed whenever appropriate.

The mid-Pliocene simulations indicate significant changes in the AMM pattern, especially in the TNA region (Figure 14a,b). The difference (mid-Pliocene minus piControl) suggests westward expansion of the northern pole (Figure 14b). The southern pole does not show large regions with significant changes. The change in the index-based spatial pattern cannot indicate structural changes as it is under the influence of amplitude changes. This analysis, instead, show reduced amplitude in the northern pole (Appendix B).

The dominant period for the twentieth-century HadISST-observed dataset is 11.6 years (Appendix B). The dominant period for the piControl MMMe is 7.7 (from 1.3 to 44.3). The extreme models are COSMOS, which simulates the AMM at a recurrence 7 times greater ($\sim 7$ cycles decade$^{-1}$), and GISS, which simulates it at multidecadal timescales ($\sim 0.23$ cycles decade$^{-1}$; Appendix B). In the mPWP simulation, the AMM power spectra show a shift in frequency towards lower values for 7 out of the 9 models. The MMMe change in period is 1.7 (from $-23.1$ to 10 years; Figure 14c). The index-based time series also indicates the prevalence of low frequencies for the AMM in 8 out of 9 models (Appendix B).

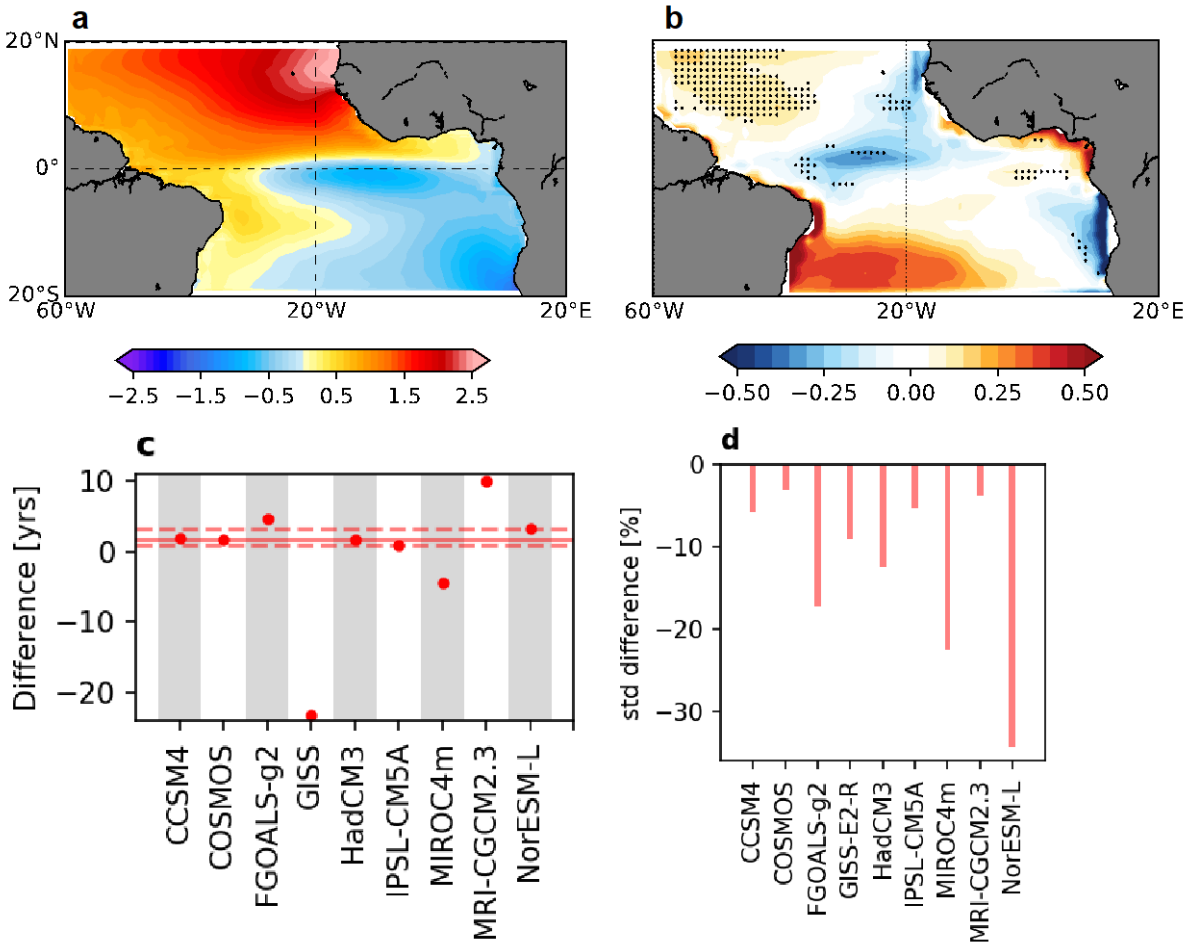


**Figure 14.** Multimodel analysis of the Atlantic Meridional Mode (AMM). **a** piControl multimodel mean. This is the regression of the normalized ATL3 index into the tropical Atlantic SST anomaly field. The spatial structure is similar to that of the observed HadISST (Appendix B). **b** Normalized multimodel mean difference (mid-Pliocene minus piControl). Stippling indicates regions where there is a ~ 80% agreement (at least 7 of the 9 models) on the sign of the difference. Westward expansion of the northern pole. **c** Spectral analysis results. This panel shows the difference in the AMM spectrum between the main period of the mid-Pliocene and piControl simulations. The power spectra of the individual models are shown in Figure S11. Seven out of 9 models shift towards higher periods in the mid-Pliocene. **d** Difference in time series standard deviation (mid-Pliocene minus piControl). All models have simulated reduced AMM amplitude in the mid-Pliocene simulation.

Both metrics, EOF and AMM index, indicates reduced AMM amplitude. All PlioMIP models show reduced amplitude in the EOF2 time series (Figure 14d), while for the AMM index, 6 out of 9 models show reduced amplitude (significant at the 90% level; Appendix B). The decreased AMM variability is consistent with changes in the AMM meridional SST gradient. The AMM SST gradient is defined as the mean SST difference between the northern

pole (5°–15° N and 20°–70° W) and the southern pole (15°–5° S and 20° W–10° E) as in (Brierley and Wainer 2018). It was found an inter-model correlation coefficient of 0.6 (significant at the 90% level), where an increase in the AMM SST gradient change is associated with a decrease in AMM amplitude (Figure 15a). This result is in agreement with Brierley and Wainer (2018), who found the same relationship for the mid-Holocene and opposite for the Last Glacial Maximum (LGM). The changes in amplitude indicated by the AMM index time series were not able to capture this relationship (Appendix B).

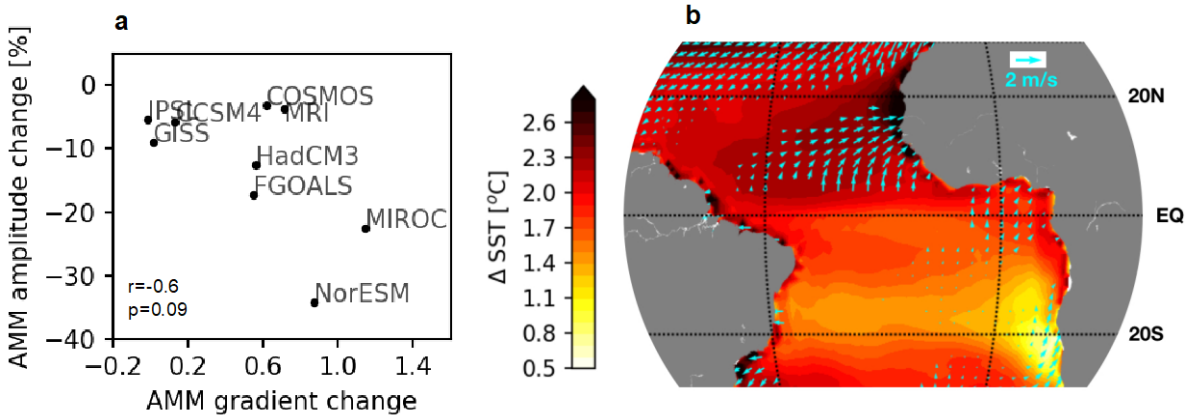


**Figure 15.** Tropical Atlantic mean state changes. **a** Relationship between AMM amplitude change and AMM SST gradient change (mPWP minus piControl). *r* indicates Pearson's correlation coefficient and *p* the two-tailed *p* value. **b** Colors: multi-model mean SST change. Vectors: multi-model mean wind change, showing regions where there is at least a 70% model agreement.

The increased AMM gradient is associated with changes in the surface winds, especially over the north tropical Atlantic (NTA; Figure 15b). Due to that, two important positive feedbacks likely play an important role. The first one is the wind-evaporation-SST (WES) feedback (Xie and Carton 2004), where the weakening of the northeast trade winds reduces the surface latent heat flux, increasing SST. This further increases the NTA SST and reinforces the AMM gradient. The second process is the feedback associated with ocean upwelling (Green et al. 2017, Mcgee et al. 2018). The weakening of the northeast trade winds dampens the upwelling of cold waters along the northwest African coast. It results in a constant

anomalous warm NTA that decreases the AMM variability. In addition, the winds over the Benguela upwelling in the south tropical Atlantic slightly intensify, contributing to increased AMM gradient in the mid-Pliocene. These results indicate that the warming in the NTA region (as in the mid-Holocene and mid-Pliocene) is associated with the decrease of the AMM amplitude.

All changes evaluated in the AMM analysis can likely modify rainfall over the tropical Atlantic. The weakening of the northeast trade winds, reduced northwest Africa upwelling, and increased AMM gradient are associated with a northward shift of the ITCZ. This way, the mid-Pliocene ITCZ-related rainfall is likely displaced into the Northern Hemisphere as it follows the warm SST anomalies, increasing rainfall over Cariaco and Sahel and reducing the rainfall over northeastern Brazil and southwestern Africa. These changes also contribute to increased North Atlantic hurricane activity in this period (Fedorov et al. 2010).

### *6.3.3 The South Atlantic Subtropical Dipole*

The SASD has a dipole structure oriented in the northeast-southwest direction. This mode corresponds to the leading EOF in the South Atlantic over the area between 50° S–0° and 60° W–20° E (Figure 16a). The SASD modifies rainfall in most of Brazil. For example, the cold pole weakens convection, decreasing moisture advection to the continent through wind changes (Wainer et al. 2014). The individual models were able to simulate a realistic SASD spatial pattern when compared to observations from the later part of the twentieth century (Appendix B).

Significant changes in the pattern of the SASD are clearly seen from the difference plot between the mid-Pliocene and piControl (Figure 16b). The southwestern pole moves towards the South American coast. This shift can potentially amplify the impact on rainfall/droughts over southeastern South America. A negative (positive) SASD pole closer to

the subtropical South American coast intensifies a cyclonic (anticyclonic) wind gyre over itself transporting humidity from the Atlantic Ocean to South America (away from the coast), increasing (decreasing) rainfall over subtropical South America (Wainer et al. 2014). In addition, the northeastern pole significantly weakens (7 out of 9 models), which, in turn, can reduce its impact in rainfall over northeastern Brazil and southwestern Africa.

The power spectrum for the SASD mode in the HadISST-observed dataset has two significant peaks (Appendix B). The major peak is at 12 years, while the second one is at ~ 5 years. The SASD highest power for the MMMe piControl is at 4.9 years (from 3.4 to 31.2 years). The extreme model is GISS-E2-R that simulates SASD at decadal timescales. The highest power for the mi-Pliocene spectra increases in 6 out of 9 models (Figure 16c). The MMMe change in the highest power is 2.82 (from − 8.2 to 79.8; Figure 16c). It should be noted that the SASD power spectrum is poorly represented among the individual PlioMIP models (Appendix B). This change indicates a shift towards higher periods, being significant at the 90%.

The majority of the models (6 out of 9) show no change in amplitude of the SASD from the mid-Pliocene with respect to piControl (change < 5%; Figure 16d). The remainders (3 of 9) show a reduction in amplitude. Thus, changes in SASD amplitude across the PlioMIP models are inconclusive.

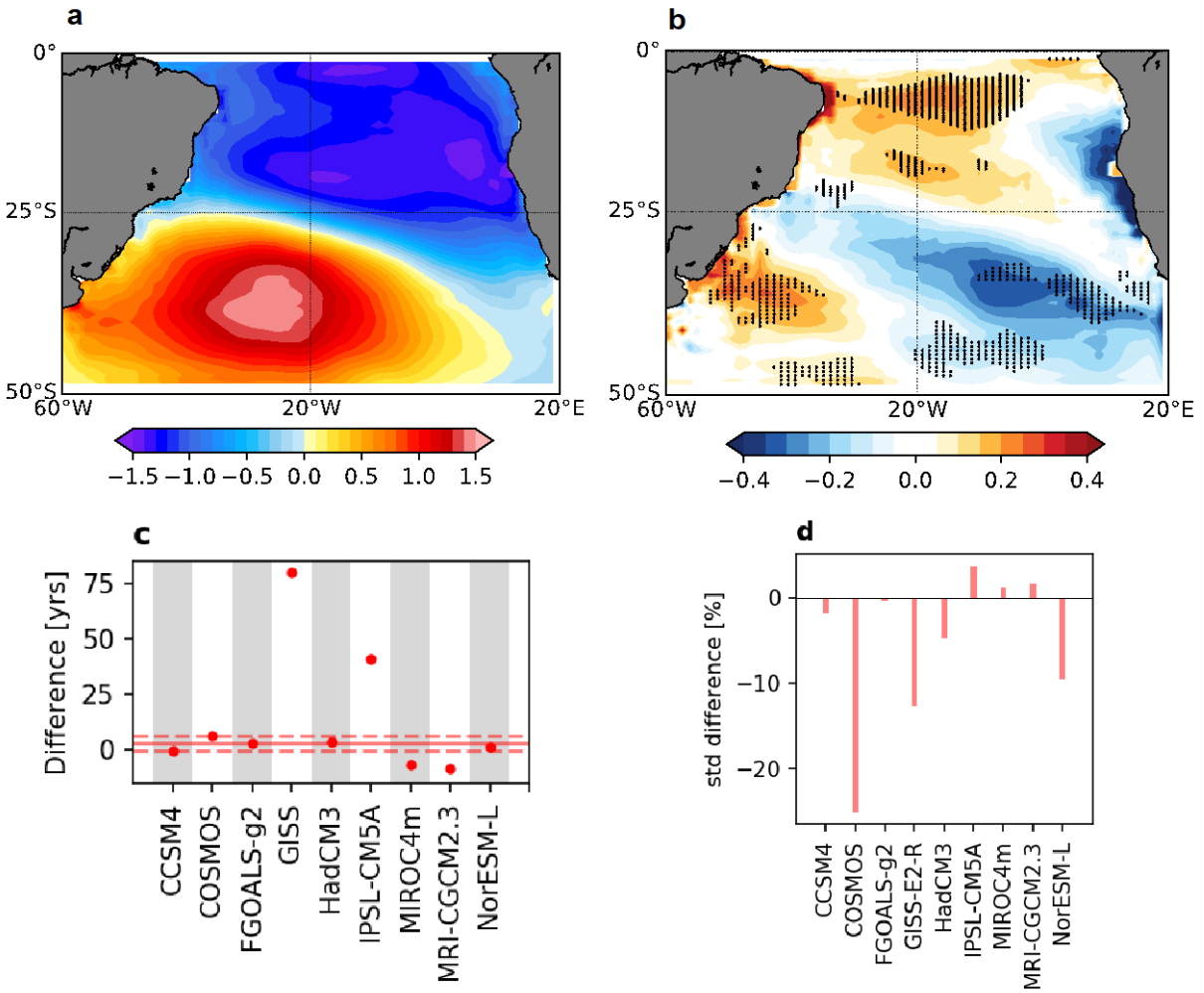


**Figure 16.** Multi-model analysis of the South Atlantic Subtropical Dipole (SASD) mode. **a** piControl MMM. It captures the observed HadISST structure reasonably well (Appendix B). **b** Normalized MMM difference (mid-Pliocene minus piControl; units: $sd^{-1}$). Stippling indicates regions where there is a ~ 80% agreement on the sign of the difference (at least 7 of the 9 PlioMIP models). Changes show overall weakening of the northeastern pole and westward shift of the southern pole. **c** Spectral analysis results. This panel shows the difference in the SASD power spectra between the main period in the mid-Pliocene and piControl simulations. The spectra for the individual models are shown in Appendix B. All but 3 models (CCSM4, MRI-CGCM2.3, and MIROC4m) shift towards higher periods in the mid-Pliocene. **d** Difference in the time series standard deviation.

### *6.3.4 Frequency*

The climate models analysed here have difficulties in reproducing the dominant frequency of the Atlantic modes of variability when compared to observations. The major difficulty is related to reproducing the multidecadal timescale of the AMV. On the other hand,

the models have a better representation of higher-frequency variability (interannual to decadal), as for AMM and SASD. This fact has also been reported in CMIP studies (Ting et al. 2011, Cheung et al. 2017). Here, possible explanations to this are related to uncertainty in the forcing represented in climate models, some inconsistencies between modelled and real-world spatial patterns of internal variability, and well-known model biases in upwelling regions (Eyring et al. 2019). However, given that the simulations (piControl and mPWP) are governed by the same model physics, the change (anomaly) in frequency provides valuable information to understand different climate scenarios.

The power spectra of the PlioMIP model results show a shift towards lower frequencies for all modes of variability analysed here. These results suggest that higher-temperature conditions may dampen higher-frequency climate variability. Draut et al. (2003) have analysed forced variability through core data indicating the prevalence of low-frequency climate variability during the Pliocene epoch. Internal variability in the mid-Pliocene has been analysed in climate models only (e.g., Brierley 2015; Tindall et al. 2016). These studies reported that the mPWP ENSO was less frequent than in pre-industrial climate. Internal variability in the last interglacial (119–116 ka BP) in the North Atlantic and was found to have a higher frequency than in the Holocene (Tzedakis et al. 2018). However, the mechanisms behind changes in frequency with respect to the internal variability of past climates remain an open question.

## 6.4 Discussion

SST variability has been investigated with the simulation results of the 9 models participating in the PlioMIP. The findings presented here indicate a decrease in tropical SST variability of around − 7% (− 27% to − 1%) and increased variability of the polar regions of both hemispheres (+ 10% [− 2% to 22%] in Southern Ocean and + 39% [11% to 122%] in the

Arctic). Here, it is suggested that SST variability is associated with meridional SST gradients, as hypothesized by Rehfeld et al. (2018). In the mid-Pliocene simulations, the reduced SST gradient between tropical and subtropical regions is accompanied by decreased variability. In polar regions, however, there is an increase in variability accompanied by an increase in the subtropical-to-polar SST gradient. In addition, ice cover could play a secondary role in regulating climate variability as they isolate property exchanges (e.g., heat) between the atmosphere and the subjacent surface (land or sea).

Climate variability in Atlantic Ocean SST modes in the PlioMIP ensemble was investigated. Each of the characteristics of the modes of variability has a different impact on the associated precipitation. The structural changes in the Atlantic SST modes of variability can modify the main pathway of heat transport into continental areas and impact land precipitation differently than they do in the modern climate. Changes in frequency and amplitude impact on duration and intensity of precipitation, respectively.

The findings presented here indicate possible changes in the rainfall associated with the Atlantic modes of variability in the mPWP as their structure changed appreciably. The AMV pole shifts equatorward and expands towards the European coast accompanying changes in the position and intensity of the North Atlantic Ocean currents. It may expand the area affected by its precipitation changes at lower latitudes and increase it impacts over Europe. The AMM's northern pole expands eastward being more effective in keeping the tropical rain belt in the Northern Hemisphere. The southern pole of the SASD in the mPWP simulation results shifts towards the South American coast. This change may intensify heat advection away (to) southeastern South America in the SASD positive (negative) phase.

Results for frequency and amplitude of the simulated Atlantic modes of variability for the mPWP indicate reduced variability. Although some models show changes in amplitude of the extratropical variability modes, these changes are not consistent across models. All models

show reduced AMM amplitude in the mPWP that are related to increased AMM SST gradient due to weaker northeast trade winds, thus inducing positive WES feedback and reduced upwelling along the northwest coast of Africa. In addition, the majority of the models show changes in the power spectrum associated with the time series of each of the modes of variability towards lower frequencies, where one can conclude that the Atlantic variability modes were less frequent in the mPWP. In this way, the Atlantic modes of variability had a weaker influence on mPWP climate than they do at present.

The uncertainty of this study is related with the ability of the climate models to reproduce the Atlantic modes of variability. Both spatial pattern and frequency could be improved. The AMV spatial pattern can be improved through a better representation of the North Atlantic Ocean circulation, which may also depend on model resolution. A good representation of the AEM and the AMM depends on the ability of the model to simulate the tropical Atlantic upwelling regions, where the models show well-known biases (Eyring et al. 2019). Finally, frequency may be better simulated once spatial pattern and forcing uncertainty are improved.

These results may have important consequences for changes in teleconnections associated with a warmer world. The majority of the SST modes of variability have weakened and/or experienced reduced frequency in the PlioMIP ensemble (i.e., ENSO (in Brierley 2015), AMV, AMM, and SASD) that can likely reduce their broader impact. In particular, all of the tropical modes of variability, ENSO, AEM, and AMM, have significantly weakened. ENSO is known to affect the north tropical Atlantic (NTA) through changes in the Walker circulation, while NTA feedbacks onto ENSO through Rossby waves generated due to a Gill-type response (Cai et al. 2019). These PlioMIP results indicate weakened ENSO-AMM teleconnections in a warmer scenario. In order to be more confident about changes in teleconnections, further analysis of temperature, precipitation, and wind variability is needed. This possible feature of

the mPWP climate needs to be further explored as it is of global interest precisely quantifying the impact of the modes of variability in warmer climates.

# 7 The El Niño-Southern Oscillation in the mPWP

In this chapter, changes and mechanisms to the El-Nino Southern Oscillation (ENSO) are investigated. The strongest mode of year-to-year variability has a significant impact over South America potentially causing extreme rainfall and droughts. Also, it is unclear how ENSO may respond to warmer scenarios and, thus, evaluating ENSO activity in the mid-Pliocene may provide important scientific advancements.

Most of the results presented in this chapter was published as a preprint in the journal Nature Geoscience and is current under review.

---

**Pontes, G. M.** et al. Northward ITCZ shift suppress ENSO activity in the mid-Pliocene Warm Period. Nature Geoscience, preprint. 2021.

---

## 7.1 Introduction

ENSO warm (El Niño) and cold (La Niña) events cause significant changes in weather patterns and ocean circulation, impacting agriculture, fisheries, coral bleaching, cyclogenesis, amongst a host of other impacts (McPhaden et al. 2006). Given its pronounced social and economic impacts and potential predictability of a few seasons in advance, ENSO has been a subject of intense investigation (Santoso et al. 2019). Whether and how ENSO changes in response to greenhouse and other external forcings may be studied by investigating past, present, and future climates with paleo-reconstructions, instrumental records, theory and numerical simulations. There is a lack of consensus among climate models in general as to how ENSO characteristics, such as amplitude and flavour, will respond to future warming (van Oldenborgh et al. 2005, Collins et al. 2010, Kim and Yu 2012, Stevenson 2012, Taschetto et al. 2014), although models that better capture ENSO nonlinearity tend to simulate enhanced ENSO sea surface temperature (SST) variability in the eastern equatorial Pacific (Cai et al. 2018) and increased frequency of events that exhibit characteristics of ENSO extremes (Santoso et al. 2013, Cai et al. 2015). These changes in ENSO properties are linked to changes in the Pacific mean state marked by a weakened Walker Circulation, increased upper-ocean stratification, and equatorially enhanced warming that causes the Intertropical Convergence Zone (ITCZ) to be displaced equatorward (Cai et al. 2014, 2015, Mamalakis et al. 2021).

Studies based on paleo-reconstructions have also suggested that ENSO activity is sensitive to the mean climate. A synthesis of mid-Holocene (~6 ka [thousand years] BP) records indicates a 33% reduction in ENSO amplitude in the eastern Pacific during this period (Emile-Geay et al. 2016). ENSO activity over the last millennium was shown to be weaker when compared to the last half-century (Grothe et al. 2020), potentially suggesting global warming related changes. Furthermore, there is evidence of significantly reduced ENSO variability during the Last Glacial Maximum (~127 ka BP; Ford et al. 2015). Proxy data for the Pliocene

(~5 to ~3 Ma [million years] BP) are controversial with regards tropical Pacific changes (Wara et al. 2005, Tierney et al. 2019, Wycech et al. 2020). A Pliocene El Niño-like mean state has been hypothesized to reduce ENSO variability (Brierley et al. 2009), although there is evidence of significant interannual variability during this period (Scroxton et al. 2011, Watanabe et al. 2011), whose magnitude could be comparable to the late Holocene (White and Ravelo 2020). As such, tropical Pacific mean state changes during the Pliocene and how they have impacted ENSO activity remain uncertain.

Here the broad PlioMIP ensemble is examined, including phases 1 and 2, to better understand how ENSO activity might change in warmer climates.

## 7.2 Methods

A total of 9 PlioMIP1 and 16 PlioMIP2 models were analysed (Table 1). The number of models used in each analysis varies according to data availability in the PlioMIP1 and PlioMIP2 databases. The last 100 years of each model's simulation is used. For completeness, observational SST and precipitation datasets are used. These were obtained from the Extended Reconstructed Sea Surface Temperature version 5 (ERSSTv5) and Global Precipitation Climatology Project (GPCP) datasets, respectively.

In this chapter, the non-parametric Spearman rank-correlation test ($r_s$) is adopted to determine if there is a monotonic relation between two variables. It worth noting that the assumption of sample independence may not be completely satisfied, given that climate models share common components and physical equations. Also, the CESM family of models may be overrepresented in the PlioMIP ensemble; however, the differing results obtained among their simulations may allow us to consider these models independent. To illustrate that, it was performed a sensitivity analysis where each model from the CESM family was considered at a

time when computing the Spearman rank correlation for the relationship shown in Figure 20a. The coefficients ranged from -0.55 (p=0.01) to -0.63 (p=3e-3).

ENSO amplitude is defined as the standard deviation of Niño3 index. The Niño3 index is calculated from SST anomalies averaged over the eastern Pacific region between 5ºN-5ºS latitude and 150º-90ºW longitude. SST anomalies were computed by removing the mean annual cycle. There are two important periods of oscillations in the equatorial Pacific: interannual and decadal (Power et al. 2021). Here, the effect of these periods is separated by defining the amplitude of low-frequency variability (>10yr) as the variance of the 11-year running mean Niño3 time series in each model. The amplitude of the interannual period is estimated as the variance of the residual time series, i.e., original Niño3 timeseries subtracted from the Niño3 decadal timeseries.

After characterizing ENSO, possible mechanisms associated with ENSO changes are investigates. First, important background features of the equatorial mean state that affect ENSO are the thermocline slope and ocean stratification. Here, the thermocline slope across the equatorial Pacific is defined as the difference between mean eastern (5ºS-5ºN; 150º-90ºW) and western Pacific thermocline depths (5ºS-5ºN; 160ºE-150ºW). The thermocline depths are computed from the mean temperature profile in each of the boxes indicated above. This is the weighted average depth, based on depths in which the temperature gradients are greater than 50% of its maximum. Equatorial Pacific Ocean stratification is computed as the difference between the mean temperature in the top 75 meters and the temperature at 100m from 150ºE to 140ºW (as indicated in Figure 18a).

To completely investigated the role of the equatorial mean state in driving ENSO changes, the Bjerknes stability index is computed (Jin et al. 2006). This framework quantifies the growth rate associated with the feedbacks that act on a developing warm SST anomaly in the eastern equatorial Pacific as formulated below:

$$2I_{BJ} = -\left(\frac{\langle\bar{u}\rangle_E}{L_x} + \frac{\langle -2y\bar{v}\rangle_E}{L_y^2} + \frac{\langle\bar{w}\rangle_E}{H_m}\right) - \alpha + \mu_a\beta_u\langle -\frac{\partial\bar{T}}{\partial x}\rangle_E + \mu_a\beta_w\langle -\frac{\partial\bar{T}}{\partial z}\rangle_E + \mu_a\beta_h\langle\frac{G(\bar{w})\bar{w}}{H_m}a_h\rangle_E \quad (5)$$

where the symbol $\langle . \rangle_E$ denotes volume average in the eastern equatorial Pacific domain taken as from 210E to 270E and 5S to 5N, where ENSO variability typically resides, and over the mixed layer thickness ($H_m$). $L_x$ and $L_y$ are the zonal and meridional extent of the eastern equatorial region. The overbar indicates the climatological mean of a given variable. The first three terms inside the large brackets accounts for the damping associated with the climatological ocean currents (zonal, meridional and vertical, respectively), which is typically negative, thus referred to as *dynamical damping*. The *thermal damping* is indicated by $\alpha$, which is the regression coefficient between SST anomalies and net surface heat flux over the eastern equatorial Pacific. The SST-wind coupling is indicated by $\mu_a$, which is the regression coefficient between SST anomalies (5S-5N; 210-270E) and zonal wind stress anomalies (5S-5N; 140-270E). This coefficient affects the growth rate of the following three positive feedbacks. The third term represents the growth rate associated with the *zonal advective feedback* which takes into account $\mu_a$, the coupling between zonal wind and zonal current (represented by $\beta_u$), and the climatological mean zonal SST gradient ($\frac{\partial\bar{T}}{\partial x}$). The fourth term accounts for the *Ekman feedback* which depends on the strength of the mean ocean stratification ($\frac{\partial\bar{T}}{\partial z}$), $\beta_w$, the regression coefficient between wind stress anomalies (5S-5N; 160-270E) and upwelling (5S-5N; 210-270E) anomalies and $\mu_a$. The final term accounts for the *thermocline feedback*, where $\beta_h$ is the regression coefficient between zonal wind stress anomalies (5S-5N; 160-270E) and thermocline slope anomalies (difference in the thermocline depth between the

eastern [5S-5N; 210-270E] and western [5S-5N; 140-210E] Pacific). The thermocline slope is the difference between the western and eastern Pacific thermocline depths. The step function $G(\overline{w})$ ensures that only upward advection is taken into account, where G=1 for upwards and G=0 for downwards vertical velocities. The regression coefficient $a_h$ represents the coupling between thermocline depth changes and subsurface temperature from the surface up to the mixed layer depth, both in the eastern (Jin et al. 2006).

Further, the extratropical influence over ENSO is analysed. Observational studies show the influence of the North and South Pacific Meridional (NPMM and SPMM, respectively) modes and the Southern Hemisphere Booster (SHB) in amplifying ENSO events. Here, the SPMM amplitude is computed as the amplitude (standard deviation) of mean SST anomalies from 15ºS to 25ºS and from 110ºW to 120ºW. The NPMM amplitude is computed as the amplitude (standard deviation) of mean SST anomalies from 20ºS to 25ºS and from 142ºW to 138ºW. Lastly, the SHB amplitude is computed as the amplitude (standard deviation) of meridional wind anomalies from 10ºS to 30ºS and from 140ºE to 170ºE.

Finally, this chapter analyses the influence of the ITCZ shift over ENSO. In this context, the CESM sensitivity experiments are used to elucidate whether the northward ITCZ shift in the Pacific Ocean is a result of the large-scale atmospheric dynamics or a result of changes in ENSO behaviour. These experiments allow us to isolate the influence of ENSO over atmospheric features, such as the ITCZ, as the atmospheric model component is forced with climatological SSTs, which does not allow SST variability. It is worth noting that the climatological SST may still be affected by ENSO nonlinearities. To check this, the multi-model mean mPWP warming during all years is compared with the resultant warming accounting non-ENSO years only. Differences in the tropical Pacific were approximately two orders of magnitude (<0.05 K) lower than the mean tropical Pacific warming (~2 K).

## 7.3 Results

### *7.3.1 Reduced ENSO amplitude*

The PlioMIP ensemble simulates a significant reduction in the amplitude of SST variability across most of the global tropics (Figure 17a; see Appendix C for PlioMIP1). In the Indian Ocean, there is a robust weakening in the western sector while no significant changes in the eastern sector (Figure 17a). The tropical Atlantic shows reduced SST variability in both sides of the equator likely indicating reduced variability of the Atlantic Meridional Mode (Pontes et al. 2020a; Figure 17a). The most pronounced weakening of tropical variability occurs in the equatorial Pacific (Figure 17a). The reduced amplitude in SST variability in the eastern equatorial Pacific (Niño 3 region; 5ºN-5ºS; 150º-90ºW) is simulated by 21 out of 23 PlioMIP models (including phases 1 and 2 of PlioMIP). Considering PlioMIP2 models only, there is a multi-model mean amplitude reduction of 25% (±16% standard deviation; Figure 17b).

Separating the Niño3 variability change into interannual (<10yr) and longer timescales (>10 yrs) shows that all but one model simulate reduced amplitude in the interannual band (Appendix C), a timescale that is dominated by ENSO. Additionally, 75% (17 out of 23) of the models indicate a shift towards lower frequencies as indicated by either an increased amplitude at low-frequency (>10 yr) or a more pronounced weakening at interannual than on longer time scales (Appendix C). However, changes in decadal or longer periods must be further evaluated using longer timeseries data. Here due to data availability, the analyses are performed on the last 100 years of each model's simulation, making decadal analysis more uncertain.

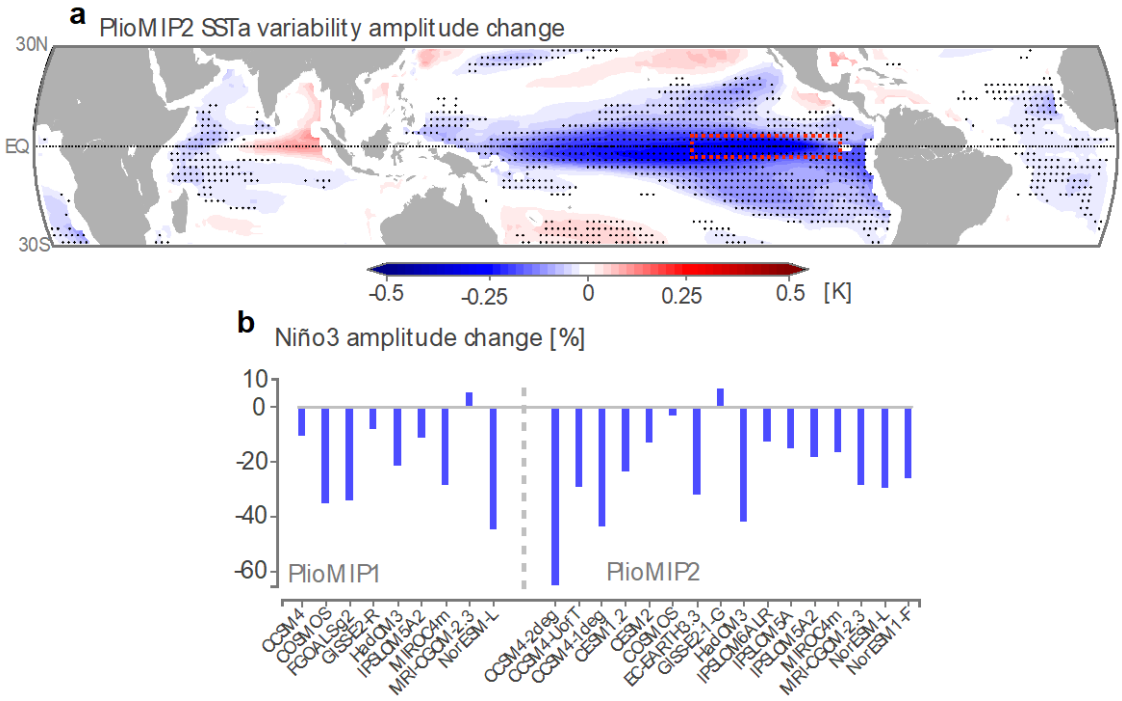


**Figure 17. Simulated mPWP tropical variability changes. a** multi-model mean change in the amplitude (standard deviation) of SST anomaly variability in the PlioMIP2 models (see Extended Data Fig. 1 for PlioMIP1 models). SST anomaly is obtained through removing the mean seasonal cycle. Stippling indicates locations where there is a significant model agreement (at least 70%) in the sign of the change. **b** Change in the amplitude (standard deviation) of the Niño3 time series in each PlioMIP model. Red box in the eastern Pacific in panel 'a' indicates the Niño3 region.

### *7.3.2 Role of equatorial Pacific Ocean changes*

ENSO dynamics is dominated by equatorial processes, which are influenced by the background state (Jin et al. 2006). Although the PlioMIP models simulate an amplified eastern Pacific warming (Figure 18a), there are large inter-model differences in this pattern, as indicated by not consistent changes in the zonal SST difference[28] (Appendix C). Of particular importance for ENSO dynamics are changes in equatorial thermal gradients in the mixed-layer[5,6,29].

Firstly, changes in the thermocline slope are evaluated, which plays an important role in ENSO dynamics. Strong (weak) westward equatorial currents drive increased (decreased) east-west thermocline slope, as it shoals (deepens) the eastern thermocline while deepening (shoaling) its western sector (Santoso et al. 2013). The thermocline slope better represents the resultant effect

of changes in zonal equatorial ocean dynamics than the zonal SST gradient in the PlioMIP models, as reflected in a higher inter-model correlation with ENSO amplitude change (Figure 18b; Appendix C). Models with a steeper mean thermocline in the mPWP are typically associated with larger ENSO amplitude reductions, while a flatter mean thermocline is associated with either a slight increase or a weak decrease in ENSO variability ($r_s$=-0.43; Figure 2b). This indicates that an equatorial Pacific mean state with a steeper thermocline, which is associated with intensified trades and westward surface currents, is less favourable for strong ENSO variability. Under such a "La Niña-like" mean state, stronger initial anomalies are required to weaken the normal climatological conditions sufficiently for El Niño development (Santoso et al. 2013).

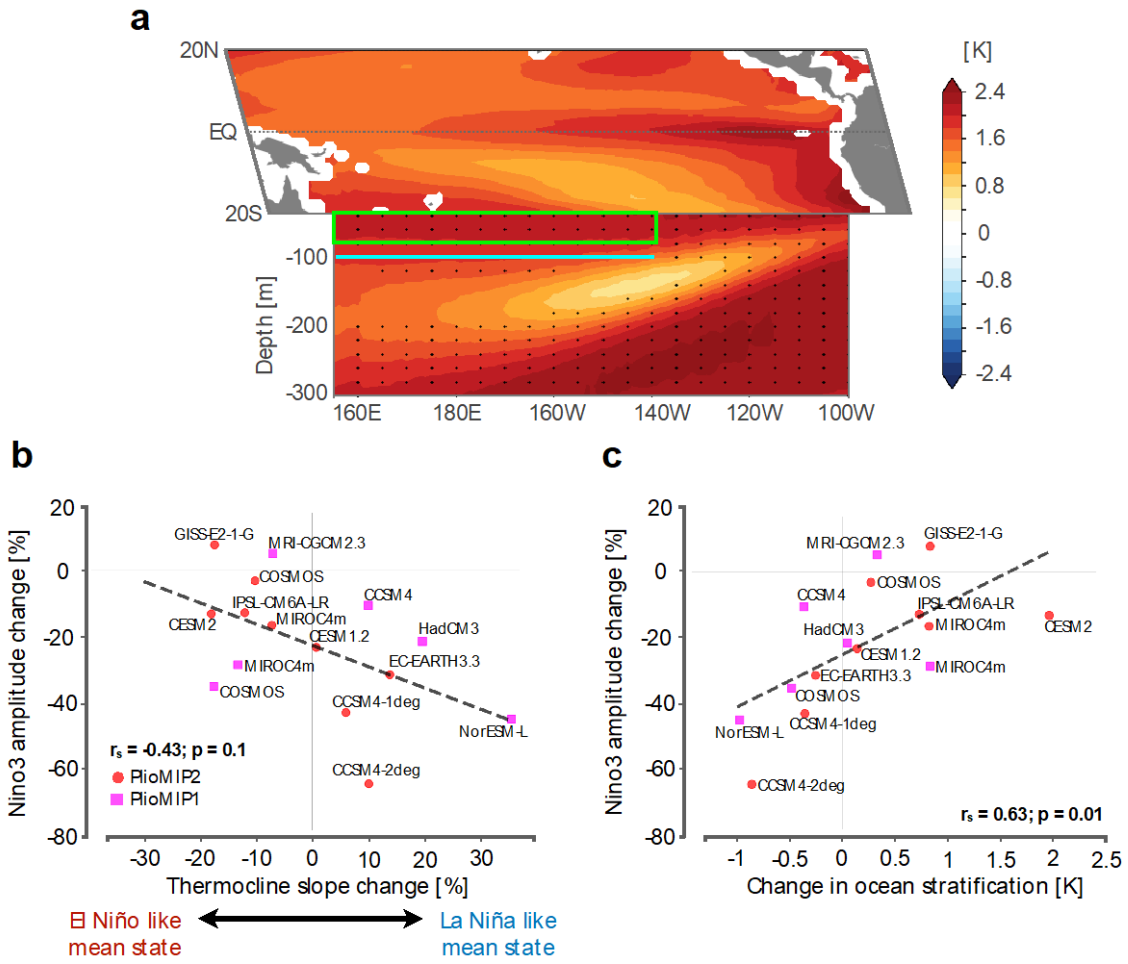


**Figure 18. Equatorial Pacific Ocean changes. a** PlioMIP2 multi-model mean change in surface tropical and sub-surface equatorial Pacific temperatures. The vertical profile is averaged between 5ºS and 5ºN. Stippling indicates significant change at the 95% level (in the SST panel the entire basin-wide warming is significant at the 95% level). **b** inter-model relationship between the change in the thermocline slope between the eastern and western Pacific (see Methods) and the change in the Niño3 amplitude. **c** inter-model relationship between the change in ocean stratification and in the Niño3 amplitude. Ocean stratification was measured as the difference between the average temperature in the top 75m (green box, panel **a)** and at 100m (blue line), between 150ºE-140ºE.

Another mean-state factor that can affect ENSO development is the equatorial upper-ocean stratification (Cai et al. 2018). In particular, western-central equatorial Pacific stratification influences the variability of strong ENSO events, through changes in the dynamical coupling between the ocean and the atmosphere. As such, we evaluate ocean stratification in the central-western Pacific, a region of maximum wind variability, where wind anomalies trigger oceanic Kelvin and Rossby waves which influence ENSO genesis[30]. Models

with decreased ocean stratification are typically associated with larger ENSO reductions, while weaker reductions occur in models where ocean stratification increases (Figure 2c). Given that over half of the models show increased stratification, this relationship cannot explain the consistent decrease in ENSO across the ensemble. Similarly, the fact that many models show a decrease in thermocline slope indicates that this is not the underlying cause for ENSO amplitude reduction. In summary, while changes in the thermocline and stratification help explain inter-model differences in ENSO amplitude changes, it appears that other processes that apply across models are required for the overall weakening of ENSO variability.

### *7.3.3 Increased ENSO stability*

The consistency in the ENSO change across models suggest that a common mechanism might be responsible for the simulated difference between piControl and mid-Pliocene. Although this is not related to changes in the equatorial mean state, it can possibly still be explained by changes in equatorial ENSO feedbacks. To test this, it is examined the air-sea coupled feedback processes governing ENSO that make up the Bjerknes feedback across models that have the required model output available, through the Bjerknes (BJ) stability index framework (Jin et al. 2006; c.f. Methods) which formulates the growth rate of SSTs in the eastern equatorial Pacific in terms of the governing air-sea coupled feedbacks and mean states. The air-sea coupling consists of two negative and three positive feedback terms. The negative feedback involves 1) a *dynamical damping* that represents the effectiveness of the mean equatorial currents in damping the initial SST anomalies, and 2) a *thermal damping* that represents the effectiveness in which the surface ocean transfers heat to the atmosphere to limit the growth of SST anomalies. The positive feedbacks consist of 1) *Ekman pumping feedback* that is a function of wind-upwelling coupling and the mean vertical temperature gradient in the mixed layer; 2) *zonal advective feedback* as a function of sensitivity of zonal currents to zonal wind anomalies and mean zonal SST gradient; and 3) *thermocline feedback* that represents the

effectiveness of the thermocline or subsurface temperature anomalies respond to wind anomalies in the backdrop of mean upwelling. The total BJ index in the pre-industrial simulations is dominated by the *thermal damping* term in all models, consistent with the historical period (Lübbecke and McPhaden 2014) (Figure 3a). The growth of eastern equatorial Pacific SST anomalies is mostly due to the *thermocline feedback*, followed by the positive effects of *zonal advective* anomalies and *Ekman pumping*, respectively (Figure 19a).

All six models indicate increased ENSO stability (i.e., the total BJ index becomes more negative), in agreement with reduced ENSO variability in the mid-Pliocene (Figure 19b). However, the governing feedback processes are not necessarily consistent among all the models (Figure 19b). The largest contribution to the increased stability is either through the *thermal damping* (CESM1.2, CESM2, IPSL-CM6A-LR, MIROC4m) or thermocline feedback (CCSM4-PlioMIP1, CCSM4-1deg); changes in Ekman pumping and zonal advective feedbacks are overall small and inconsistent (Figure 19b). All four models however agree on an enhanced dynamical damping mainly due to a weaker positive effect of the zonal currents (Figure 19b). It should be noted that the Dynamical Damping term has a relatively minor contribution to the overall BJ index (Figure 19b).

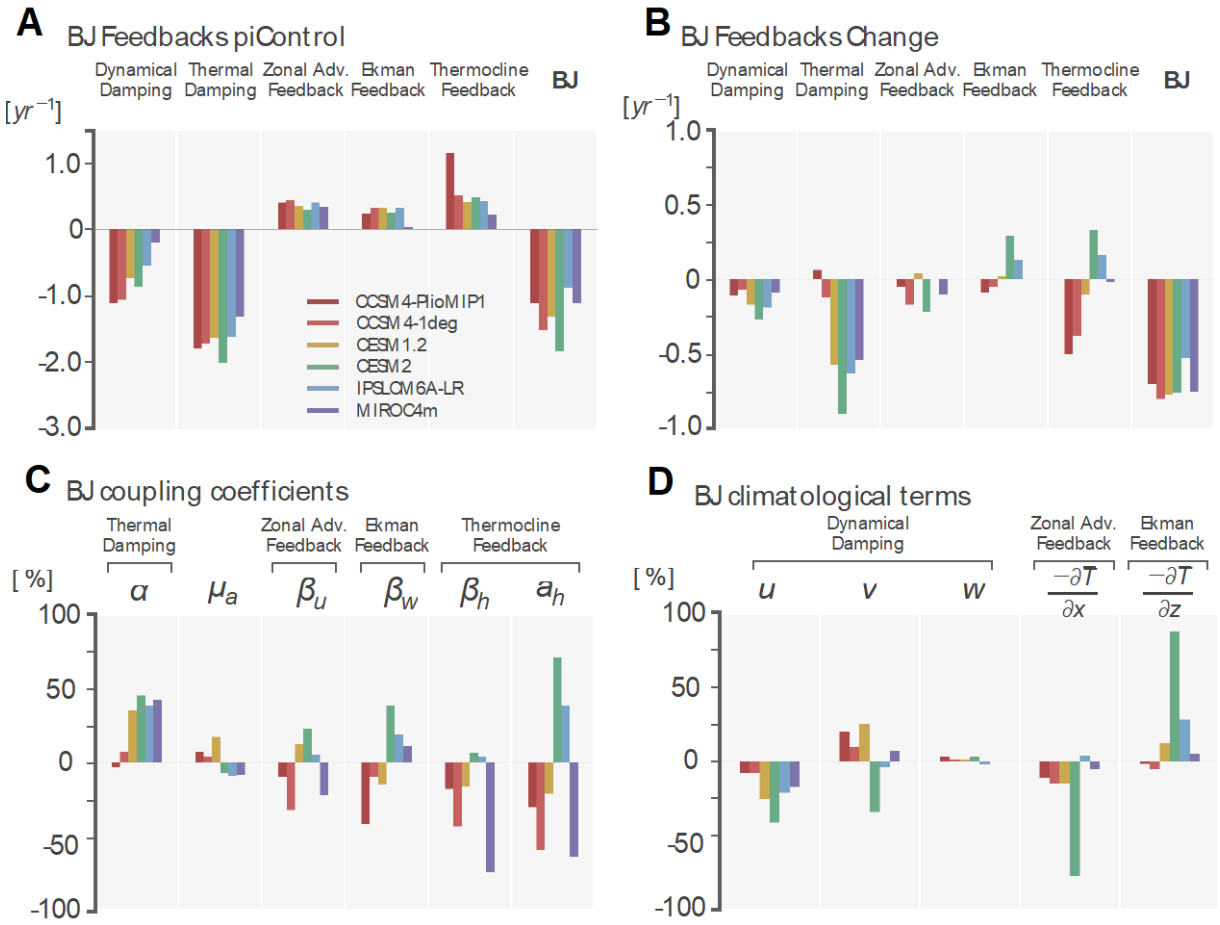


**Figure 19.** Increased ENSO stability. a) Bjerknes stability index terms in the pre-industrial simulations of each model. The last column (BJ) indicates the total BJ stability index. b) change (mid-Pliocene minus piControl) in each term of the BJ stability index. All models agree in an increased stability as indicated by a more negative total BJ index in the mid-Pliocene than in the piControl simulations. c) change in the mean-state components of the BJ stability index. d) change in the coupling coefficients of the BJ stability index. Bars in 'c' and 'd' indicate relative change (%) in the mid-Pliocene with respect to the piControl simulation. The coupling coefficient $\mu_a$ affects all three feedback terms (zonal advective, Ekman and thermocline).

Changes in the equatorial Pacific surface wind are responsible for the response in *thermocline feedback* and *thermal damping* that differs among models. The reduced positive *thermocline feedback* (in CCSM4-PlioMIP1 and CCSM4-1deg; Figure 19b) is caused by a decrease in wind-thermocline coupling ($\beta_h$; Figure 19c), despite an enhanced mean upwelling that is favourable for the *thermocline feedback* (Figure 19d; c.f. Equation 5 in Methods). This indicates that for the CCSM4 the wind anomalies do not effectively produce changes in the thermocline slope that allow for a rigorous Bjerknes feedback. In these simulations, the

climatological winds increase across the basin in the mid-Pliocene (Appendix C), confining the western Pacific warm pool further west and enhancing the mean thermocline slope (Appendix C; see Methods). The results show that an increased climatological thermocline slope weakens the thermocline feedback (Appendix C). Such stronger mean state weakens the response of the thermocline to wind anomalies, and vice-versa, and is thus favourable for increased ENSO stability.

In the case of the other four models (CESM1.2, CESM2, IPSL-CM6A-LR and MIROC4m), the climatological winds in the eastern Pacific weaken (Appendix C). The weakened Pacific trades can amplify the background surface warming through Wind-Evaporation-SST feedback (Bordbar et al. 2019), which in turn leads to enhanced *thermal damping* via a higher sensitivity between SST and air-sea heat fluxes anomalies ($\alpha$, Appendix C). It is worth noting that weakened Pacific trades tend to lead to a decreased thermocline slope, which favours the *thermocline feedback* (Appendix C), and thus reduced ENSO stability (i.e. the BJ index). This occurs in CESM2 and IPSL-CM6A-LR, although it is counteracted by increased *thermal damping* (Figure 19b). CESM1.2 and MIROC4m show minor changes in the eastern Pacific trades and climatological thermocline slope (Appendix C). Thus, the results of the equatorial pacific dynamics presented until now demonstrate that the equatorial dynamics alone cannot fully explain ENSO changes across the PlioMIP models.

### *7.3.4 Role of off-equatorial Pacific changes*

Whilst ENSO development is closely related to the zonal equatorial dynamics (Jin et al. 2006), ENSO events are also affected by a variety of other large-scale processes beyond the equatorial Pacific (Larson and Kirtman 2013, Hong et al. 2014, Cai et al. 2015). For instance, changes to the mean meridional SST gradient or processes in the extratropics can play an important role in triggering ENSO events. In particular, all PlioMIP models simulate a weaker

equator-to-pole temperature gradient associated with polar amplified warming (Haywood et al. 2020).

To investigate processes outside the equatorial Pacific, it is first evaluated the role of meridional SST gradients through possible displacements of the ITCZ in the mPWP. Southward (northward) ITCZ displacements, due to changes in off-equatorial SST gradients, have been shown to affect ENSO activity through increased (reduced) probability of occurrences of deep convection in the central-eastern Pacific (Cai et al. 2014). Here, a mean northward ITCZ shift during austral spring-summer, i.e., during developing and mature ENSO phases, is strongly related to the ENSO weakening across models ($r_s$=-0.64; Figure 20a). This scenario increases convergence throughout the tropical North Pacific that suppresses anomalous convergence feedback at the equator (Extended Data Fig. 4). To further illustrate this effect, it is evaluated models' performance in simulating the non-linear relationship between SST anomalies and precipitation events in the eastern Pacific (Appendix C). Six models correctly simulate this characteristic and indicate that the further north the mean ITCZ migrates the less probable are occurrences of deep convection events in the eastern Pacific associated with ENSO SST anomalies (Figure 20). The ITCZ shift can fully explain ENSO weakening across these 6 models ($r_s$=0.94; Appendix C).

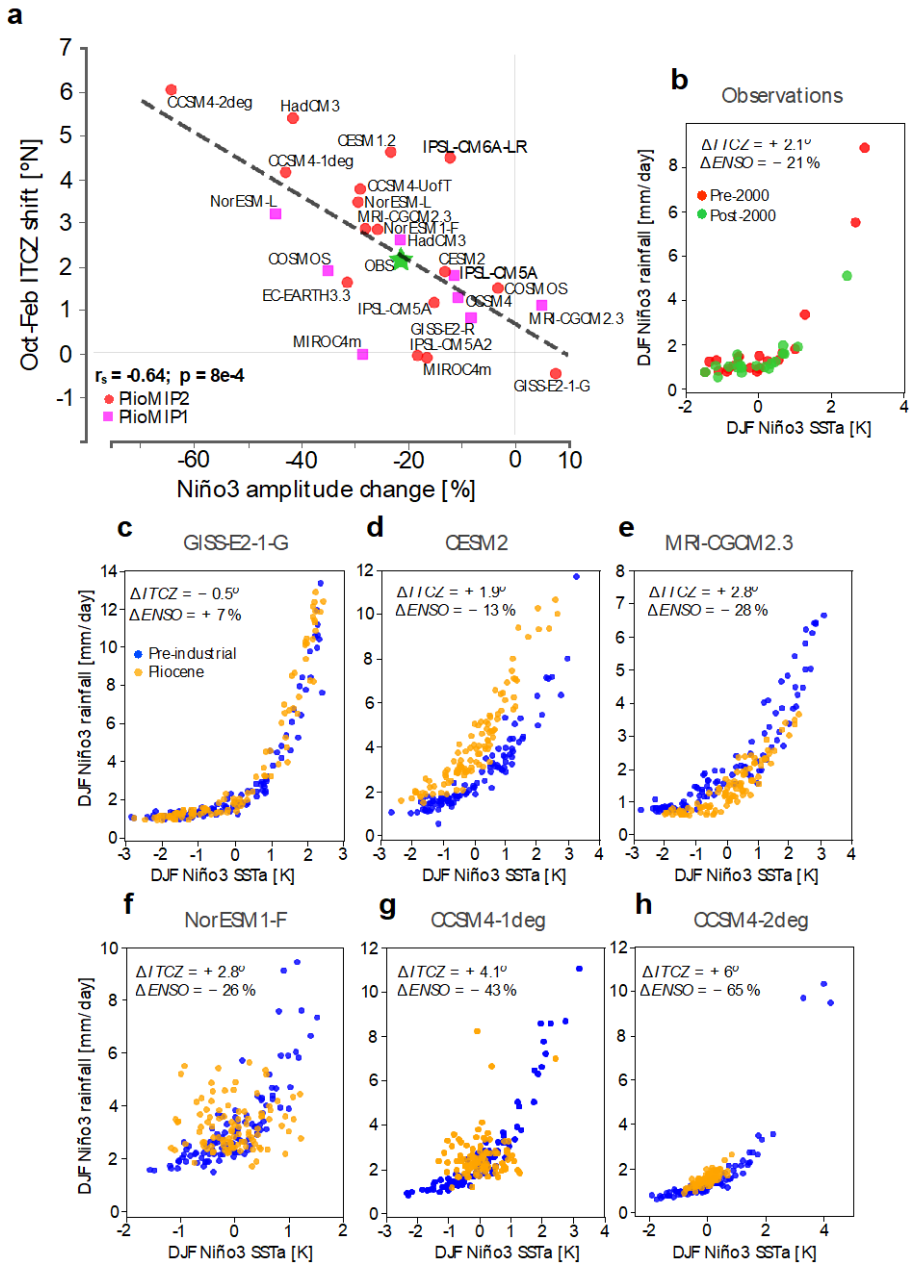


**Figure 20. ITCZ–ENSO relationship. a** PlioMIP2 inter-model relationship between the change in the Niño3 amplitude and mean ITCZ shift from October to February. Green star indicates values obtained from observations by comparing periods 1979-1999 and 2000-2020. The correlation coefficient was evaluated considering PlioMIP models only. **b** relationship between DJF Niño3 SST anomalies and DJF Niño3 rainfall for the period pre-2000 (red) and and post-2000 (green). **c** to **h** as in panel '**b**' but for selected PlioMIP models that correctly simulate non-linear ENSO characteristics (See Methods), pre-industrial simulation in blue and Pliocene in yellow.

This PlioMIP result is analogous to the reduced ENSO activity in the past two decades, which corresponded with a more northward position of the ITCZ (Figure 20a; (Hu and Fedorov 2018). The multi-decadal period pre-2000 was marked by enhanced ENSO variability, while after 2000 it has been reduced by 21% (Lübbecke and McPhaden 2014, Zhao and Fedorov 2020), resulting in weaker rainfall events in the eastern Pacific (Figure 20b). This reduction has been attributed to enhanced trade winds and surface ocean currents, due to a negative phase of the Interdecadal Pacific Oscillation (England et al. 2014), and reduced positive ENSO feedbacks (Lübbecke and McPhaden 2014). Consistently, the PlioMIP models indicate a larger reduction in ENSO activity when shifted towards a mean state that is more La Niña-like (Figure 18b).

Also, possible changes to the other processes that are known to initiate ENSO events are evaluated (Figure 21). Firstly, the reversal of the circulation of easterly trade winds in the western Pacific is known to initiate ENSO development (Timmermann et al. 2018). In the PlioMIP models, the annual mean intensification of the western Pacific trade winds corresponds with weaker wind variability over this region (Figure 21a). Climatologically stronger easterly trades tend to inhibit: 1) the stochastic forcing of westerly wind bursts in the western Pacific (Chen et al. 2015) that triggers the positive thermocline feedback; 2) southward shifts of the ITCZ through positive Wind-Evaporation-SST feedback which cools the equatorial Pacific Ocean, thereby increasing the meridional SST gradient; and 3) eastward displacements of the Walker circulation.

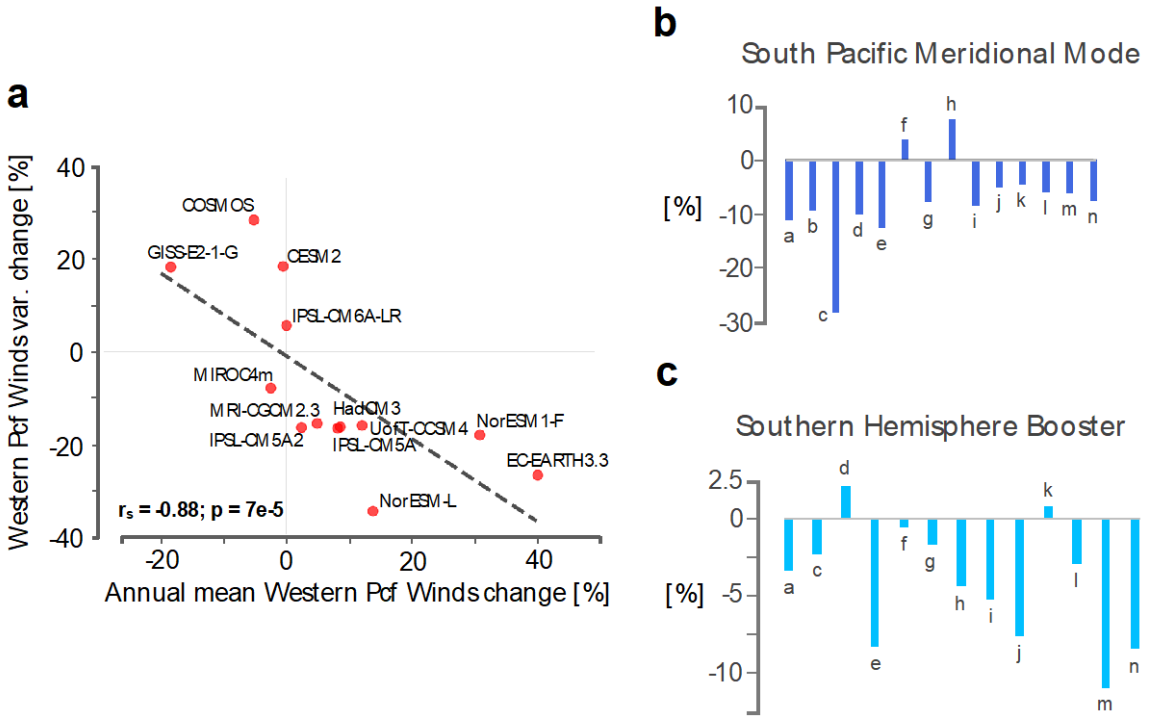


**Figure 21. Changes to potential ENSO triggers. a** inter-model relationship between the change in the intensity of the western Pacific trade winds (10ºS-10ºN; 160ºE-150ºW) and the amplitude (standard deviation) of its monthly variability. To ideally examine changes in the western wind bursts we would need high frequency output, which is not available for the PlioMIP models. **b** Change in the amplitude (standard deviation) of the South Pacific Meridional mode time series, defined as the mean SST anomaly between 15ºS-25ºS and 110ºW-120WºE. **c** Change in the amplitude (standard deviation) of the meridional wind variability over the Southern Hemisphere Booster region (10ºS-30ºS; 140º-170ºE). PlioMIP2 models in panels **b** and **c**: a – CCSM4-UofT; b – CCSM4-2deg; c – CESM2; d – COSMOS; e – EC-EARTH3.3; f – GISS-E2-1-G; g – HadCM3; h – IPSL-CM6A-LR; i – IPSL-CM5A; j – IPSL-CM5A2; k – MIROC4m; l – MRI-CGCM2.3; m – NorESM-L; n – NorESM1-F.

Further, patterns of variability that promote wind anomalies in the western Pacific are analysed, these contribute to the development of El Niño events. Firstly, the South Pacific Meridional Mode (SPMM), analogue to the North Pacific Meridional Mode (NPMM), is initiated by the weakening of off-equatorial southeast trade winds in the eastern Pacific. This alters the latent heat flux, triggering a wind-evaporation-SST feedback that propagates wind anomalies into the tropics (Zhang et al. 2014). All but two PlioMIP2 models simulate decreased SPMM variability in the mPWP (Figure 21b). Equivalent changes in the NPMM are not consistent across models and do not help explain ENSO changes (Appendix C).

Finally, extreme El Niño events are amplified by an anomalous zonal pressure dipole in the Southern Hemisphere (Hong et al. 2014). In such condition, an anomalous high pressure over Australia facilitates cold surges through the Coral Sea (the Southern Hemisphere Booster, SHB)[31], that promote westerly wind bursts in the western Pacific conducive for El Niño development. This meridional wind variability in the SHB region also decreases in 10 out of 12 PlioMIP2 models (Figure 21c). All these aforementioned changes are associated with reduced probability of El Niño initiation, which results in weaker ENSO activity.

### *7.3.5 Large-scale forcing*

The Pacific ITCZ-ENSO relationship demonstrated in the previous section can either be a result of a large-scale global ITCZ shift modulating ENSO or a local response of the Pacific ITCZ to changes in ENSO activity. The PlioMIP models indicate that the northward ITCZ shift during the mPWP occurs in all basins, as indicated by an anomalous meridional dipole in rainfall across the global tropics (Figure 22a; see Appendix C for PlioMIP1). Additionally, the PlioMIP models systematically simulate polar amplified warming in both hemispheres (Figure 22b), which can give rise to large-scale changes in the meridional temperature gradient and affect the ITCZ position through changes in atmospheric heat fluxes (Schneider et al. 2014).

It is important noting that increased rainfall south of equator in the eastern Pacific may be a result of double-ITCZ bias in the PlioMIP models (Tian and Dong 2020, Mamalakis et al. 2021). A more consistent northward ITCZ shift across the tropical North Pacific is evident through increased low-level wind convergence (Appendix C), which indicates that the increased precipitation in the eastern Pacific is likely a result of the thermodynamic effect over the double-ITCZ region (Held and Soden 2006).

To further evaluate the cause of the ITCZ shift, sensitivity experiments using an Atmospheric General Circulation Model are performed (AGCM; the NCAR Community Atmospheric Model version 4 [CAM4]). Here the AGCM is forced with PlioMIP mean SSTs,

which allow us to isolate changes in atmospheric circulation from changes in ocean-atmosphere variability, such as ENSO. It is worth noting the mPWP climatological-mean warming pattern, used to force the atmospheric model, may still contain some non-linear influence of ENSO changes, but this effect is negligible (see Methods).

In the present climate, during austral summer, increased insolation in the Southern Hemisphere results in intensification of the Northern Hemisphere Hadley circulation, northward energy flux across the equator, and southward ITCZ shift (Schneider et al. 2014). In the mPWP, the AGCM simulates a decreased northward heat transport across the equator during the austral summer (Figure 22c). Due to the mutual relationship between changes in the energy flux across the equator and ITCZ position, a decreased northward energy flux at the equator is accompanied by a northward ITCZ shift. Higher rates of warming in the Northern Hemisphere drive an intensification and northward expansion of the Southern Hemisphere Hadley cell and weaker circulation in the Northern counterpart (Figure 22d; see Appendix C for PlioMIP1), which reduces the atmospheric energy input from the Southern to the Northern Hemisphere during the austral summer.

The AGCM experiments suggest that the meridional displacement of the ITCZ is a global feature of the PlioMIP simulations and occurs due to the mean mPWP warming. One of the most robust features of the mPWP simulations is the polar amplified warming, especially in the Northern Hemisphere which increases the inter-hemispheric temperature gradient (Figure 22b). However, whether the mPWP ITCZ shift is a response to tropical or extratropical warming is still an open question. For instance, our AGCM experiments indicate an overall decrease in the northward atmospheric heat transport in the Northern Hemisphere and a slight increase in the southward heat transport in the Southern Hemisphere (Figure 22c), which initially points to changes in pole-to-pole temperature gradient.

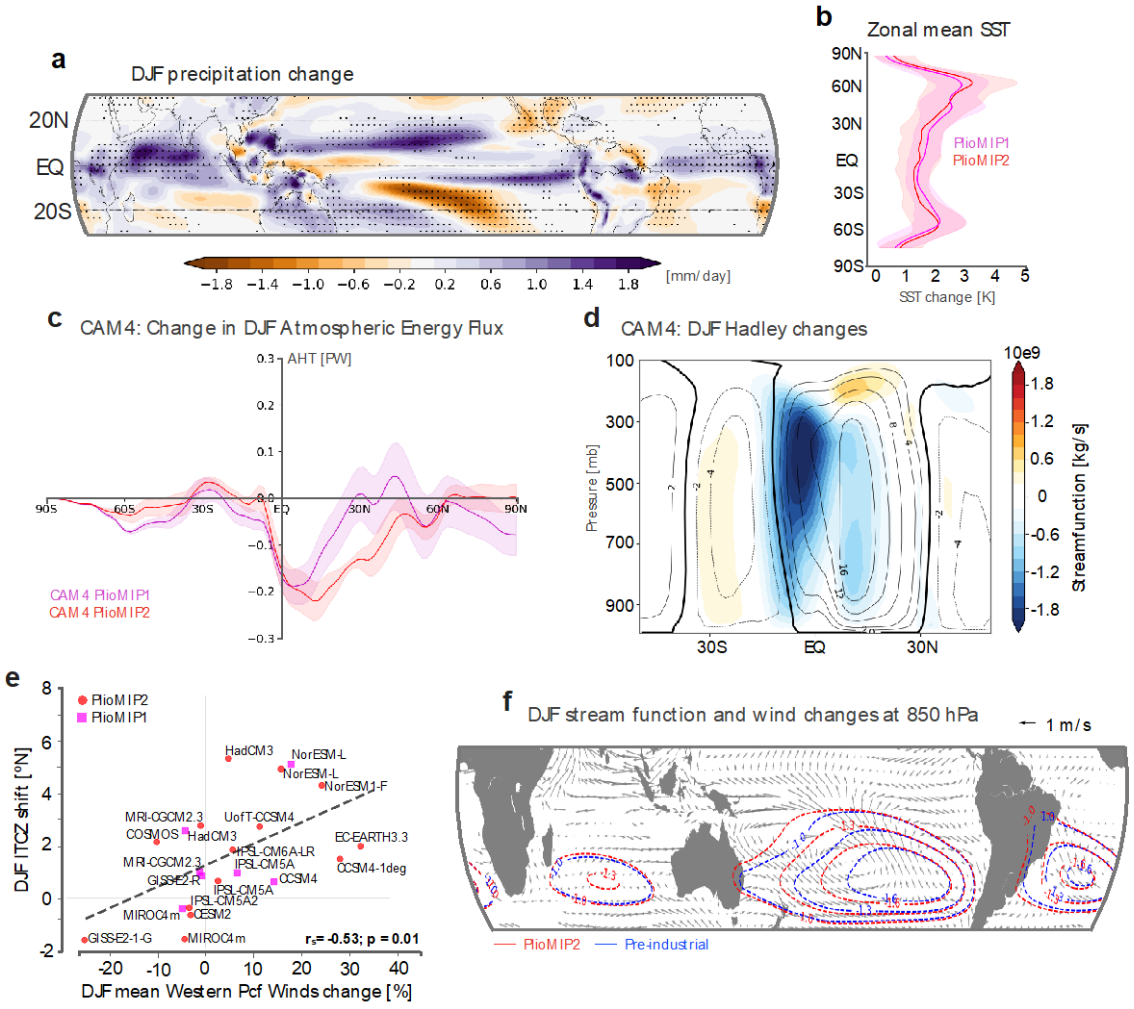


**Figure 22. Energetic constraints for the ITCZ position. a** DJF precipitation change in the PlioMIP2 models (mPWP minus pre-industrial). Stippling indicates where the change is significant at the 95% level. **b** multi-model mean change zonally averaged SST for PlioMIP1 (magenta) and PlioMIP2 (red). Banding indicates standard deviation range. **c** Changes in DJF atmospheric energy flux, computed as the residual between the total top-of-the-atmosphere and surface energy fluxes, in the AGCM experiments forced with PlioMIP1 and 2 climatological SST and sea-ice (see Methods). Banding indicates standard deviation range of a 5-member ensemble. Negative anomalies in the Northern Hemisphere indicate weakening of the northward heat transport, while negative anomalies in the Southern Hemisphere indicate intensification of the southward heat transport. **d** Changes in the meridional streamfunction in the AGCM experiment forced with PlioMIP2 SST and sea-ice. Contours indicate pre-industrial streamfunction (zero contour in bold). Colours indicate change. **e** Inter-model relationship between changes in the intensity of the zonal western Pacific trades and ITCZ shift during austral summer. **f** Changes in low-level (850 hPa) winds and streamfunction in the PlioMIP2 models. Wind changes are only shown where changes are significant at the 95% level.

The large-scale changes in the meridional circulation likely induce changes in horizontal circulation. In the Pacific Ocean, the PlioMIP models indicate that a northward ITCZ shift is significantly related to intensified western Pacific trades (Figure 22d), which is

analogous to synchronized shifts of the Walker and Hadley circulations during different ENSO phases (Yun et al. 2021). An analysis of the low-level circulation indicates that the anomalously stronger western trades in the mPWP are sourced at the subtropical South Pacific due to an intensified circulation of the South Pacific Subtropical High system (Figure 22e,f; see Appendix C for PlioMIP1). These changes are not exclusive to the South Pacific but occur in all ocean basins (Figure 22f). The synchronized changes in the meridional and zonal atmospheric circulation are likely a result of global changes in atmospheric heat fluxes during the warmer mPWP. This illustrates a possible influence of changes in global atmospheric dynamics on ENSO in a warmer climate.

## 7.4 Discussion

The results presented here suggest a link between reduced ENSO amplitude and the northward shift of the ITCZ in the mPWP, associated with stronger climatological circulation in the Southern Hemisphere (Figure 23). The northward shift of the ITCZ reduces the probability of ENSO-related rainfall events in the eastern Pacific. Northward ITCZ shift and intensified Southern Hemisphere Hadley and subtropical circulations are a response to enhanced Northern Hemisphere warming via energetic constraints for the ITCZ position (Figure 23). This intensified Southern Hemisphere circulation reduces wind variability in the western Pacific, may suppress zonal sea-level pressure anomalies imposed by the South Pacific Meridional Mode and the Southern Hemisphere Booster and weakens and shifts the South Pacific Convergence Zone polewards, reducing its interaction with equatorial processes (Figure 23). As such, the climatological stability imposed by intensified tropical Southern Hemisphere circulation acts to increase ENSO stability, as ENSO, by definition, is a deviation from the mean climate, and thus stronger climatological circulations can be viewed as unfavourable to ENSO-induced changes.

In addition to the reduced ENSO amplitude, SST variability in other tropical basins also decreases (Figure 1a). This may also contribute to weakened ENSO variability via pan-tropical teleconnections related to a delayed and weaker negative feedback (Cai et al. 2019), although reduced variability in other tropical basins itself might also be a consequence of reduced ENSO variability. Pontes et al. (2020) reported that all PlioMIP1 models simulate reduced tropical North Atlantic variability associated with a warming of this basin and a northward Atlantic ITCZ shift. Taken together, these results suggest that a northward shift of the global ITCZ may mute tropical Pacific and Atlantic SST variability.

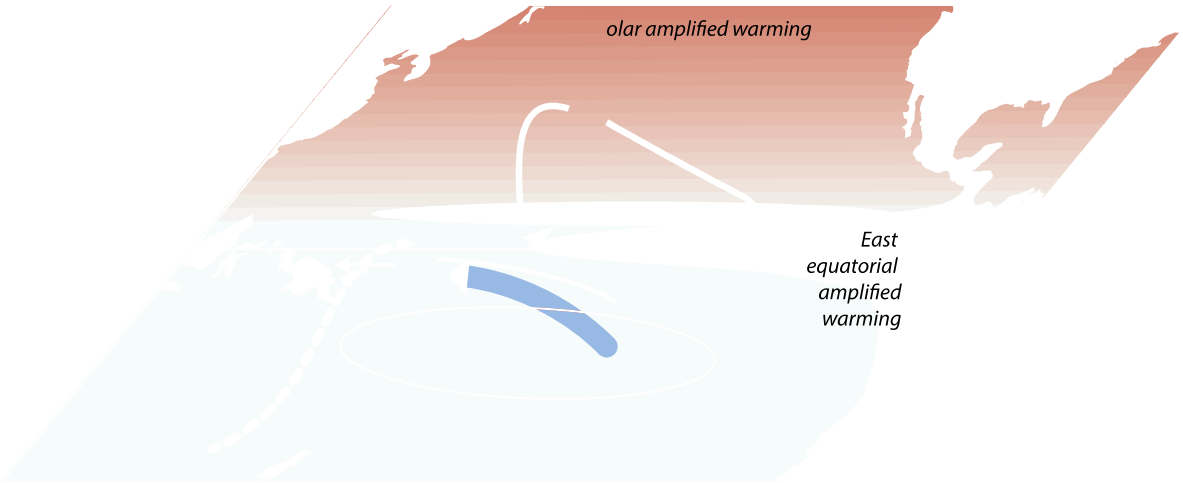


**Figure 23.** Schematic of the drivers of suppressed ENSO activity in the mPWP. A northward ITCZ shift reduces the probability of occurrence of deep convection in the central-eastern Pacific. Energetic constrains for the ITCZ position indicates that higher rates of warming in Northern Hemisphere drive a northward ITCZ shift and intensified enhanced Southern Hemisphere Hadley circulation. These changes are also associated with enhanced subtropical high and intensified western Pacific trades. Enhanced trade winds suppress wind variability in the western Pacific, which are important for El Niño initiation. An intensified subtropical high is thought to impede zonal pressure anomalies across the tropical South Pacific and, thus, suppress the activity of the South Pacific Meridional Mode (SPMM) and Southern Hemisphere Booster that are important for the development of strong El Niño events. Image credits: Professor Alex Sen Gupta (UNSW).

The results presented in this chapter are subject to a number of uncertainties in the simulations tied to sparse and limited proxy data, which are used to constrain the PlioMIP experiments, and systematic climate model biases (Fedorov et al. 2013). Changes in the inter-hemispheric SST gradient for example could be affected by uncertainties in the extension of the mPWP ice sheets (Koenig et al. 2015), poor representation of certain polar feedbacks (i.e. interactive land-ice; Fischer et al. 2018), climate sensitivity (Zhu et al. 2020), and biases in tropical convection and SST of the climate models, such as double-ITCZs (Tian and Dong 2020) and an overly strong cold tongue. Despite different model biases, we show that the current generation of climate models simulate consistent changes to ENSO related to shifts in the ITCZ position in the mPWP.

Paleoclimate states have particular relevance as analogues for future warming. the findings presented here indicate that, although the mPWP warming is comparable to that projected for the end of 21$^{st}$ century under a 'business as usual' scenario (~3K) (Burke et al. 2018), the mPWP ENSO response is the opposite to that projected (Cai et al. 2014). It is worth noting the mPWP exemplifies an equilibrium climate with similar $CO_2$ levels as today, indicating we could end-up in a Pliocene-like climate if present-day $CO_2$ concentrations were to be maintained constant and a steady-state is reached. However, the current rate of atmospheric $CO_2$ rise is unprecedented in Earth's history, causing current climate warming trends to differ regarding how Earth has warmed in the past. Thus, relating past and future warmings is not straightforward. Here evaluating the empirically based mPWP warming we find that a northward ITCZ shift supresses ENSO activity. If this mechanism can be applied to the 21$^{st}$ century projections where a southward shift of the Pacific ITCZ is projected (Mamalakis et al. 2021), then an increase in ENSO variability (Cai et al. 2018) in the coming decades appears to be a potential outcome.

# 8 Conclusion

## 8.1 Scientific Progress

The present thesis has provided significant advancements to the current understanding of the climate system by evaluating how Earth has responded to the mid-Pliocene global warming. First, Chapter 5 complements the 'wet-wetter' theory (Held and Soden 2006) by showing that dynamical processes can overwhelm the importance of thermodynamical ones in a warmer atmosphere, depending on changes in the inter-hemispheric energy imbalance. The evaluation of the mid-Pliocene indicates that this is the case for the tropical and subtropical Southern Hemisphere (Figure 24). Furthermore, it highlights key dynamical atmospheric features that modulate rainfall in South America. Chapter 6 indicates that the global latitudinal pattern of SST variability may be driven by the intensity of meridional SST gradients. It also shows that the activity of the Atlantic Meridional Mode is tightly linked to mean meridional SST gradient within the tropical Atlantic and, thus, its amplitude is driven by the mean position of the ITCZ (Figure 24). Lastly, Chapter 7 shows, for the first-time, that changes in off-equatorial atmospheric features are the most important factors in explaining the ENSO response to a differing background state, overwhelming changes in equatorial dynamics (Figure 24). It adds important information to the current understanding of ENSO and to the complexity of this climate phenomenon, providing insights into how ENSO is affected by global warming.

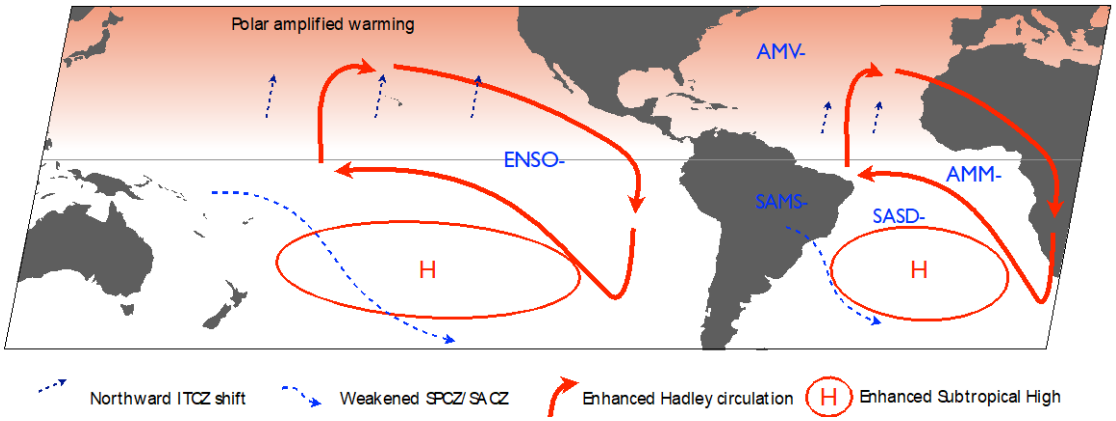


**Figure 24. Schematic of the drivers of the changes in ocean-atmosphere processes in the mid-Pliocene.** Higher rates of warming in the Northern Hemisphere reorganizes the large-scale atmospheric circulation in order to export out the excess heat towards the Southern Hemisphere. These include: northward expansion and intensified Southern Hemisphere Hadley circulation, northward ITCZ shift and intensified and expanded Southern Hemisphere Subtropical High pressure system. These changes weaken tropical ocean-atmosphere modes of variability (ENSO and AMM), the Subtropical Convergence Zones (namely SPCZ and SACZ) and the South American Monsoon System (SAMS).

## 8.2 Concluding remarks

Climate models simulate a mean mid-Pliocene warming of ~3 ºC, which is similar to the projected warming for the end-of-century climate (Burke et al. 2018). However, both warmer scenarios differ considerably. The mid-Pliocene climate analysed in this thesis represents an equilibrium climate that took thousands of years to be established (Haywood et al. 2016a). In fact, it is a climate optimum scenario that occurred during the geological scale cooling trend between 4.5Ma BP and 2.8Ma BP (Figure 2). During this geological period, $CO_2$ concentrations were as high as ~450 ppm at 5 Ma and declined to ~250 ppm at the Northern Hemisphere glaciation (~2.8 Ma BP), with a slight increase during the mid-Pliocene (~3.2 Ma BP; Seki et al. 2010). This shows a slow variation along ~2.5 Ma interval, indicating that climate feedbacks acted on increasing Earth's temperature up until it reached +3 ºC, especially on polar regions (Haywood et al., 2020).

Very different from the mid-Pliocene context is the ongoing global warming, marked by an unprecedented $CO_2$ forcing during a couple of centuries, which modifies how regional

climates respond to the large-scale warming. For example, the current global warming shows significant warming at equatorial regions that is not seen in the mid-Pliocene. Additionally, the collapse of the Greenland and Western Antarctic ice sheets are unlikely to happen before the end of the century, indicating that the magnitude of the polar amplification will not reach similar values relative to those estimated for the mid-Pliocene.

Therefore, the mid-Pliocene climate cannot be considered a perfect analogue to the ongoing warming. The present work shows that differing rates of warming between hemispheres drive tropical and subtropical climate changes. In the mid-Pliocene, the Northern Hemisphere experienced higher rates of warming than the Southern counterpart, likely due to stronger polar feedbacks caused by the greatly reduced sea-ice area (Hill et al. 2014). This caused high latitudes in the North Atlantic to show the most significant warming. Inter-hemispheric differences drove changes in atmospheric heat fluxes that are associated with a northward ITCZ shift and intensified Southern Hemisphere Hadley and subtropical circulations. The results presented here show that these changes are linearly related to weakened South American Monsoon System (SAMS), weakened Atlantic Meridional Mode (AMM) and reduced activity of the El Niño Southern Oscillation in the mid-Pliocene. On the other hand, in the current $CO_2$-induced warming of the Atlantic and Pacific ITCZs are expected to srink towards the equator due to enhanced equatorial warming (Mamalakis et al. 2021). Although the mid-Pliocene warming differs from the projected warming, its evaluation can possibly constrain physical mechanisms associated with global warming. If the mechanisms here proposed for mid-Pliocene climate changes can be applied to the 21$^{st}$ century warming, then an intensification of the AMM and ENSO and a weakening of the SAMS seems to be a potential outcome.

Thus, this thesis indicates that the mid-Pliocene is not an analogue to the ongoing global warming. Nonetheless, the evaluation of the physical processes that are important to the

South American climate in the warmer mid-Pliocene may sheds light on climatic changes of the upcoming decades.

# REFERENCES

**De Almeida et al.** (**2007**) R. A. F. De Almeida et al. Negative ocean-atmosphere feedback in the South Atlantic Convergence Zone. *Geophysical Research Letters*. 34, 18 (Sep.-2007), L18809. doi: 10.1029/2007GL030401.

**Bakker and Prange** (**2018**) Pepijn Bakker and Matthias Prange. Response of the Intertropical Convergence Zone to Antarctic Ice Sheet Melt. *Geophysical Research Letters*. 45, 16 (Aug.-2018), 8673–8680. doi: 10.1029/2018GL078659.

**Bischoff and Schneider** (**2014**) Tobias Bischoff and Tapio Schneider. Energetic Constraints on the Position of the Intertropical Convergence Zone. *Journal of Climate*. 27, 13 (Jul.-2014), 4937–4951. doi: 10.1175/JCLI-D-13-00650.1.

**Bordbar et al.** (**2019**) Mohammad Hadi Bordbar et al. Uncertainty in near-term global surface warming linked to tropical Pacific climate variability. *Nature Communications*. 10, 1 (Dec.-2019), 1–10. doi: 10.1038/s41467-019-09761-2.

**Bragg et al.** (**2012**) F. J. Bragg et al. Mid-Pliocene climate modelled using the UK Hadley Centre Model: PlioMIP Experiments 1 and 2. *Geoscientific Model Development*. 5, 5 (2012), 1109–1125. doi: 10.5194/gmd-5-1109-2012.

**Brierley et al.** (**2009**) C. M. Brierley et al. Greatly Expanded Tropical Warm Pool and Waekened Hadley Circulation in the Early Pliocene. *Science*. 323, March (2009), 1714–1718. doi: 10.1126/science.1167625.

**Brierley** (**2015**) C. M. Brierley. Interannual climate variability seen in the Pliocene Model Intercomparison Project. *Climate of the Past*. 11, 3 (2015), 605–618. doi: 10.5194/cp-11-605-2015.

**Brierley and Wainer** (**2018**) Chris Brierley and Ilana Wainer. Inter-annual variability in the tropical Atlantic from the Last Glacial Maximum into future climate projections simulated by CMIP5/PMIP3. *Clim. Past*. 14, (2018), 1377–1390. doi: 10.5194/cp-14-1377-2018.

**Burke et al.** (**2018**) K. D. Burke et al. Pliocene and Eocene provide best analogs for near-future climates. *Proceedings of the National Academy of Sciences of the United States of America*. 115, 52 (Dec.-2018), 13288–13293. doi: 10.1073/pnas.1809600115.

**Cai et al.** (**2014**) Wenju Cai et al. Increasing frequency of extreme El Niño events due to greenhouse warming. *Nature Climate Change*. 4, 2 (Feb.-2014), 111–116. doi: 10.1038/nclimate2100.

**Cai et al.** (**2015**) Wenju Cai et al. ENSO and greenhouse warming. *Nature Climate Change*. Nature Publishing Group. doi: 10.1038/nclimate2743.

**Cai et al.** (**2018**) Wenju Cai et al. Increased variability of eastern Pacific El Niño under greenhouse warming. *Nature*. 564, 7735 (Dec.-2018), 201–206. doi: 10.1038/s41586-018-0776-9.

**Cai et al.** (**2019**) Wenju Cai et al. Pantropical climate interactions. *Science (New York, N.Y.)*. 363, 6430 (Mar.-2019), eaav4236. doi: 10.1126/science.aav4236.

**Carvalho et al.** (**2002**) Leila M. V. Carvalho et al. Extreme Precipitation Events in Southeastern South America and Large-Scale Convective Patterns in the South Atlantic Convergence Zone. *Journal of Climate*. 15, 17 (Sep.-2002), 2377–2394. doi: 10.1175/1520-0442(2002)015<2377:EPEISS>2.0.CO;2.

**Carvalho et al.** (**2004**) Leila M. V. Carvalho et al. The South Atlantic Convergence Zone: Intensity, Form, Persistence, and Relationships with Intraseasonal to Interannual Activity and Extreme Rainfall. *Journal of Climate*. 17, 1 (Jan.-2004), 88–108. doi: 10.1175/1520-0442(2004)017<0088:TSACZI>2.0.CO;2.

**Carvalho et al.** (**2011**) Leila M. V. Carvalho et al. Moisture transport and intraseasonal variability in the South America monsoon system. *Climate Dynamics*. 36, 9–10 (May.-2011), 1865–1880. doi: 10.1007/s00382-010-0806-2.

**Chan et al.** (**2011**) W. L. Chan et al. Simulating the mid-Pliocene climate with the MIROC general circulation model: experimental design and initial results. *Geoscientific Model Development*. 4, 4 (2011), 1035–1049. doi: 10.5194/gmd-4-1035-2011.

**Chan and Abe-Ouchi** (**2020**) Wing Le Chan and Ayako Abe-Ouchi. Pliocene Model Intercomparison Project (PlioMIP2) simulations using the Model for Interdisciplinary Research on Climate (MIROC4m). *Climate of the Past*. 16, 4 (Aug.-2020), 1523–1545. doi: 10.5194/cp-16-1523-2020.

**Chandan and Peltier** (**2017**) Deepak Chandan and W. Richard Peltier. Regional and global climate for the mid-Pliocene using the University of Toronto version of CCSM4 and PlioMIP2 boundary conditions. *Climate of the Past*. 13, (2017), 919–942. doi: https://doi.org/10.5194/cp-13-919-2017.

**Chandler et al.** (**2013**) M. A. Chandler et al. Simulations of the mid-Pliocene Warm Period using two versions of the NASA/GISS ModelE2-R Coupled Model. *Geoscientific Model Development*. 6, (2013), 517–531. doi: 10.5194/gmdd-5-2811-2012.

**Chaves** (**2004**) Rosane Rodrigues Chaves. Interactions between sea surface temperature over the South Atlantic Ocean and the South Atlantic Convergence Zone. *Geophysical Research Letters*. 31, 3 (2004), L03204. doi: 10.1029/2003GL018647.

**Chen et al.** (**2015**) Dake Chen et al. Strong influence of westerly wind bursts on El Niño diversity. *Nature Geoscience*. Nature Publishing Group. doi: 10.1038/ngeo2399.

**Cheung et al.** (**2017**) Anson H. Cheung et al. Comparison of Low-Frequency Internal Climate Variability in CMIP5 Models and Observations. *Journal of Climate*. 30, 12 (Jun.-2017), 4763–4776. doi: 10.1175/JCLI-D-16-0712.1.

**Chiang and Friedman** (**2012**) John C. H. Chiang and Andrew R. Friedman. Extratropical Cooling, Interhemispheric Thermal Gradients, and Tropical Climate Change. *Annual Review of Earth and Planetary Sciences*. 40, (2012), 383–412. doi: 10.1146/annurev-earth-042711-105545.

**Clement et al.** (**2015**) Amy Clement et al. The Atlantic Multidecadal Oscillation without a role for ocean circulation. *Science*. 350, 320 (2015), 324. doi: 10.1126/science.aad1886.

**Collins et al.** (**2010**) Mat Collins et al. The impact of global warming on the tropical Pacific Ocean and El Niño. *Nature Geoscience*. 3, 6 (Jun.-2010), 391–397. doi: 10.1038/ngeo868.

**Contoux et al.** (**2012**) C. Contoux et al. Modelling the mid-pliocene warm period climate with the IPSL coupled model and its atmospheric component LMDZ5A. *Geoscientific Model Development*. 5, 3 (2012), 903–917. doi: 10.5194/gmd-5-903-2012.

**Delworth and Greatbatch** (**2000**) Thomas L. Delworth and Richard J. Greatbatch. Multidecadal Thermohaline Circulation Variability Driven by Atmospheric Surface Flux Forcing. (2000). Retrieved 22-May.-2018, from https://journals.ametsoc.org/doi/pdf/10.1175/1520-

0442%282000%29013%3C1481%3AMTCVDB%3E2.0.CO%3B2.

**Deser et al.** (**2010**) Clara Deser et al. Sea Surface Temperature Variability: Patterns and Mechanisms. *Annu. Rev. Mar. Sci*. 2, (2010), 115–43. doi: 10.1146/annurev-marine-120408-151453.

**Dowsett et al.** (**2010**) H. Dowsett et al. The PRISM3D paleoenvironmental reconstruction. *Stratigraphy*. 7, 2–3 (2010), 123–139.

**Dowsett et al.** (**2009**) H. J. Dowsett et al. Pliocene three-dimensional global ocean temperature reconstruction. *Climate of the Past*. 5, 4 (2009), 769–783. doi: 10.5194/cp-5-769-2009.

**Dowsett et al.** (**1996**) Harry Dowsett et al. Middle Pliocene sea surface temperatures : a global reconstruction. *Marine Micropaleontology*. 27, 1991 (1996), 13–25.

**Dowsett et al.** (**2016**) Harry Dowsett et al. The PRISM4 (mid-Piacenzian) paleoenvironmental reconstruction. *Climate of the Past*. 12, (2016), 1519–1538. doi: 10.5194/cp-12-1519-2016.

**Dowsett et al.** (**2005**) Harry J. Dowsett et al. Middle Pliocene sea surface temperature variability. *Paleoceanography*. 20, 2 (Jun.-2005), 1–8. doi: 10.1029/2005PA001133.

**Draut et al.** (**2003**) Amy E. Draut et al. Climate stability during the Pliocene warm period. *Paleoceanography*. 18, 4 (2003), 1–12. doi: 10.1029/2003PA000889.

**Emile-Geay et al.** (**2016**) J. Emile-Geay et al. Links between tropical Pacific seasonal, interannual and orbital variability during the Holocene. *Nature Geoscience*. Nature Publishing Group. doi: 10.1038/ngeo2608.

**Enfield et al.** (**2001**) David B. Enfield et al. The Atlantic multidecadal oscillation and its relation to rainfall and river flow in the continental US. *Geophysical Research Letters*. 28, 10 (2001), 2077–2080.

**England et al.** (**2014**) Matthew H. England et al. Recent intensification of wind-driven circulation in the Pacific and the ongoing warming hiatus. *Nature Climate Change*. 4, 3 (Feb.-2014), 222–227. doi: 10.1038/nclimate2106.

**Et al.** (**2009**) T. Naish Et al. Obliquity-paced Pliocene West Antarctic ice sheet oscillations. *Nature*. 458, 2009 (2009), 322–329. doi: 10.1038/nature07867.

**Eyring et al.** (**2019**) Veronika Eyring et al. Taking climate model evaluation to the next level. *Nature Climate Change*. 9, 2 (Feb.-2019), 102–110. doi: 10.1038/s41558-018-0355-y.

**Fedorov et al.** (**2013**) A. V. Fedorov et al. Patterns and mechanisms of early Pliocene warmth. *Nature*. 496, 7443 (Apr.-2013), 43–49. doi: 10.1038/nature12003.

**Fedorov et al.** (**2010**) Alexey V Fedorov et al. Tropical cyclones and permanent El Niño in the early Pliocene epoch. *Nature*. 463, February (2010), 1066–1071. doi: 10.1038/nature08831.

**Feng et al.** (**2020**) Ran Feng et al. Increased Climate Response and Earth System Sensitivity From CCSM4 to CESM2 in Mid-Pliocene Simulations. *Journal of Advances in Modeling Earth Systems*. 12, 8 (Aug.-2020), e2019MS002033. doi: 10.1029/2019MS002033.

**Fischer et al.** (**2018**) Hubertus Fischer et al. Palaeoclimate constraints on the impact of 2 °c anthropogenic warming and beyond. *Nature Geoscience*. Nature Publishing Group. doi: 10.1038/s41561-018-0146-0.

**Ford et al.** (**2015**) Heather L. Ford et al. Reduced El Niño-Southern Oscillation during the

last glacial maximum. *Science*. 347, 6219 (Jan.-2015), 255–258. doi: 10.1126/science.1258437.

**Friedrich et al.** (**2013**) Oliver Friedrich et al. Late Pliocene to early Pleistocene changes in the North Atlantic Current and suborbital-scale sea-surface temperature variability. *Paleoceanography*. 28, 2 (Jun.-2013), 274–282. doi: 10.1002/palo.20029.

**Giannini et al.** (**2003**) A. Giannini et al. Oceanic Forcing of Sahel Rainfall on Interannual to Interdecadal Time Scales. *Science*. 302, 5647 (Nov.-2003), 1027–1030. doi: 10.1126/science.1089357.

**Green et al.** (**2017**) Brian Green et al. Twentieth century correlations between extratropical SST variability and ITCZ shifts. *Geophysical Research Letters*. 44, 17 (2017), 9039–9047. doi: 10.1002/2017GL075044.

**Grothe et al.** (**2020**) Pamela R. Grothe et al. Enhanced El Niño–Southern Oscillation Variability in Recent Decades. *Geophysical Research Letters*. 47, 7 (Apr.-2020). doi: 10.1029/2019GL083906.

**Haywood et al.** (**2011**) A. M. Haywood et al. Pliocene Model Intercomparison Project ( PlioMIP ): experimental design and boundary conditions ( Experiment 2 ). *Geoscientific Model Development*. 4, (2011), 571–577. doi: 10.5194/gmd-4-571-2011.

**Haywood et al.** (**2007**) Alan M. Haywood et al. A permanent El Niño-like state during the Pliocene? *Paleoceanography*. 22, 1 (2007), 1–21. doi: 10.1029/2006PA001323.

**Haywood et al.** (**2016a**) Alan M. Haywood et al. Intregation geological archives and climate models for the mid-Pliocene warm period. *Nature Communications*. 6, May 2015 (2016), 1–14. doi: 10.1038/ncomms10646.

**Haywood et al.** (**2016b**) Alan M. Haywood et al. The Pliocene Model Intercomparison Project ( PlioMIP ) Phase 2 : scientific objectives and experimental design. *Climate of the Past*. 12, (2016), 663–675. doi: 10.5194/cp-12-663-2016.

**Haywood et al.** (**2020**) Alan M. Haywood et al. The Pliocene Model Intercomparison Project Phase 2: large-scale climate features and climate sensitivity. *Climate of the Past*. 16, 6 (Nov.-2020), 2095–2123. doi: 10.5194/cp-16-2095-2020.

**Held and Soden** (**2006**) Isaac M. Held and Brian J. Soden. Robust Responses of the Hydrological Cycle to Global Warming. *Journal of Climate*. 19, 21 (Nov.-2006), 5686–5699. doi: 10.1175/JCLI3990.1.

**Hill et al.** (**2014**) D. J. Hill et al. Evaluating the dominant components of warming in Pliocene climate simulations. *Climate of the Past*. 10, (2014), 79–90. doi: 10.5194/cp-10-79-2014.

**Hoffman et al.** (**1998**) Paul F. Hoffman et al. A neoproterozoic snowball earth. *Science*. 281, 5381 (Aug.-1998), 1342–1346. doi: 10.1126/science.281.5381.1342.

**Hong et al.** (**2014**) Li-Ciao Hong et al. A Southern Hemisphere booster of super El Niño. *Geophysical Research Letters*. 41, 6 (Mar.-2014), 2142–2149. doi: 10.1002/2014GL059370.

**Hu and Fedorov** (**2018**) Shineng Hu and Alexey V. Fedorov. Cross-equatorial winds control El Niño diversity and change. *Nature Climate Change*. Nature Publishing Group. doi: 10.1038/s41558-018-0248-0.

**Hunter et al.** (**2019**) Stephen J. Hunter et al. The HadCM3 contribution to PlioMIP phase 2. *Climate of the Past*. 15, 5 (Sep.-2019), 1691–1713. doi: 10.5194/cp-15-1691-2019.

**IPCC** (**2007**) IPCC. *The Physical Science Basis: Working Group I Contribution to the Fourth Assessment Report of the IPCC*.

**Jansen et al.** (**2007**) E. Jansen et al. Paleoclimate IPCC AR4. *Climate Change 2007: The Physical Science Basis. Contribution of Working Group I to the Fourth Assessment Report of the Intergovernmental Panel on Climate Change*. (2007), 433–497. doi: 10.2753/JES1097-203X330403.

**Jin et al.** (**2006**) Fei Fei Jin et al. A coupled-stability index for ENSO. *Geophysical Research Letters*. 33, 23 (Dec.-2006), L23708. doi: 10.1029/2006GL027221.

**Johnson and Xie** (**2010**) Nathaniel C. Johnson and Shang Ping Xie. Changes in the sea surface temperature threshold for tropical convection. *Nature Geoscience*. 3, 12 (Dec.-2010), 842–845. doi: 10.1038/ngeo1008.

**Jones and Carvalho** (**2002**) Charles Jones and Leila M. V Carvalho. Active and Break Phases in the South American Monsoon System. *Journal of Climate*. April, (2002), 905–914. Retrieved from https://journals.ametsoc.org/doi/pdf/10.1175/1520-0442%282002%29015%3C0905%3AABPIT%3E2.0.CO%3B2.

**Jouzel et al.** (**1987**) J. Jouzel et al. Vostok ice core: A continuous isotope temperature record over the last climatic cycle (160,000 years). *Nature*. 329, 6138 (1987), 403–408. doi: 10.1038/329403a0.

**Kamae and Ueda** (**2012**) Y. Kamae and H. Ueda. Mid-Pliocene global climate simulation with MRI-CGCM2.3: Set-up and initial results of PlioMIP Experiments 1 and 2. *Geoscientific Model Development*. 5, 3 (2012), 793–808. doi: 10.5194/gmd-5-793-2012.

**Kamae et al.** (**2016**) Youichi Kamae et al. Sensitivity of Pliocene climate simulations in MRI-CGCM2.3 to respective boundary conditions. *Climate of the Past*. 12, 8 (Aug.-2016), 1619–1634. doi: 10.5194/cp-12-1619-2016.

**Kang et al.** (**2009**) Sarah M. Kang et al. The Tropical Response to Extratropical Thermal Forcing in an Idealized GCM: The Importance of Radiative Feedbacks and Convective Parameterization. *journal of Atmospheric Sciences*. 66, (2009), 2812–2827. doi: 10.1175/2009JAS2924.1.

**Kayano et al.** (**2016**) M. Kayano et al. A further analysis of the tropical Atlantic SST modes and their relations to north-eastern Brazil rainfall during different phases of Atlantic Multidecadal Oscillation. *International Journal of Climatology*. 32, 12 (2016), 4006–4018.

**Kennett and Stott** (**1991**) J. P. Kennett and L. D. Stott. Abrupt deep-sea warming, palaeoceanographic changes and benthic extinctions at the end of the Palaeocene. *Nature*. 353, 6341 (1991), 225–229. doi: 10.1038/353225a0.

**Kiladis et al.** (**1989**) George N. Kiladis et al. Origin of the South Pacific Convergence Zone. *Journal of Climate*. 2, 10 (Oct.-1989), 1185–1195. doi: 10.1175/1520-0442(1989)002<1185:ootspc>2.0.co;2.

**Kim and Yu** (**2012**) Seon Tae Kim and Jin-Yi Yu. The two types of ENSO in CMIP5 models. *Geophysical Research Letters*. 39, 11 (Jun.-2012). doi: 10.1029/2012GL052006@10.1002/(ISSN)1944-8007.GRLCMIP5.

**Kodama** (**1993**) Yasu Masa Kodama. Large-scale common features of sub-tropical convergence zones (The baiu frontal zone, the SPCZ, and the SACZ) part II: Conditions of the circulations for generating the STCZs. *Journal of the Meteorological Society of Japan*. 71, 5 (1993), 581–610. doi: 10.2151/jmsj1965.71.5_581.

**Kodama** (**1992**) Yasumasa Kodama. Large-scale common features of subtropical precipitation zones (the Baiu frontal zone, the SPCZ, and the SACZ) part I: Characteristics of subtropical frontal zones. *Journal of the Meteorological Society of Japan*. 70, 4 (1992), 813–836. doi: 10.2151/jmsj1965.70.4_813.

**Koenig et al.** (**2015**) S. J. Koenig et al. Ice sheet model dependency of the simulated Greenland Ice Sheet in the mid-Pliocene. *Climate of the Past*. 11, 3 (Mar.-2015), 369–381. doi: 10.5194/cp-11-369-2015.

**Larson and Kirtman** (**2013**) Sarah Larson and Ben Kirtman. The Pacific Meridional Mode as a trigger for ENSO in a high-resolution coupled model. *Geophysical Research Letters*. 40, 12 (Jun.-2013), 3189–3194. doi: 10.1002/grl.50571.

**Li et al.** (**2018**) Xiangyu Li et al. Mid-Pliocene global land monsoon from PlioMIP1 simulations. *Palaeogeography, Palaeoclimatology, Palaeoecology*. 512, (Dec.-2018), 56–70. doi: 10.1016/J.PALAEO.2018.06.027.

**Li et al.** (**2020**) Xiangyu Li et al. PlioMIP2 simulations with NorESM-L and NorESM1-F. *Climate of the Past*. 16, 1 (Jan.-2020), 183–197. doi: 10.5194/cp-16-183-2020.

**Liebmann et al.** (**1999**) Brant Liebmann et al. Submonthly Convective Variability over South America and the South Atlantic Convergence Zone. *Journal of Climate*. 12, 7 (Jul.-1999), 1877–1891. doi: 10.1175/1520-0442(1999)012<1877:SCVOSA>2.0.CO;2.

**Lisiecki and Raymo** (**2005**) Lorraine E. Lisiecki and Maureen E. Raymo. A Pliocene-Pleistocene stack of 57 globally distributed benthic ?? 18O records. *Paleoceanography*. 20, 1 (2005), 1–17. doi: 10.1029/2004PA001071.

**Lübbecke and McPhaden** (**2014**) Joke F. Lübbecke and Michael J. McPhaden. Assessing the Twenty-First-Century Shift in ENSO Variability in Terms of the Bjerknes Stability Index. *Journal of Climate*. 27, 7 (Apr.-2014), 2577–2587. doi: 10.1175/JCLI-D-13-00438.1.

**Lunt et al.** (**2012**) Daniel J. Lunt et al. On the causes of mid-Pliocene warmth and polar amplification. *Earth and Planetary Science Letters*. 321–322, (2012), 128–138. doi: 10.1016/j.epsl.2011.12.042.

**Lurton et al.** (**2020**) Thibaut Lurton et al. Implementation of the CMIP6 Forcing Data in the IPSL-CM6A-LR Model. *Journal of Advances in Modeling Earth Systems*. 12, 4 (Apr.-2020), e2019MS001940. doi: 10.1029/2019MS001940.

**Mamalakis et al.** (**2021**) Antonios Mamalakis et al. Zonally contrasting shifts of the tropical rain belt in response to climate change. *Nature Climate Change*. (Jan.-2021), 1–9. doi: 10.1038/s41558-020-00963-x.

**Mann et al.** (**2021**) Michael E. Mann et al. Multidecadal climate oscillations during the past millennium driven by volcanic forcing. *Science*. 371, 6533 (Mar.-2021), 1014–1019. doi: 10.1126/science.abc5810.

**Marshall et al.** (**2014**) J. Marshall et al. The ocean's role in setting the mean position of the Inter-Tropical Convergence Zone. *Climate Dynamics*. 42, (2014), 1967–1979. doi: 10.1007/s00382-013-1767-z.

**Mcgee et al.** (**2018**) David Mcgee et al. Hemispherically asymmetric trade wind changes as signatures of past ITCZ shifts. *Quaternary Science Reviews*. 180, (2018), 214–228. doi: 10.1016/j.quascirev.2017.11.020.

**McGee et al.** (**2014**) David McGee et al. Changes in ITCZ location and cross-equatorial heat

transport at the Last Glacial Maximum, Heinrich Stadial 1, and the mid-Holocene. *Earth and Planetary Science Letters*. 390, (2014), 69–79. doi: 10.1016/j.epsl.2013.12.043.

**McPhaden et al.** (**2006**) Michael J. McPhaden et al. ENSO as an integrating concept in earth science. *Science*. American Association for the Advancement of Science. doi: 10.1126/science.1132588.

**Morioka et al.** (**2011**) Yushi Morioka et al. On the Growth and Decay of the Subtropical Dipole Mode in the South Atlantic. *Journal of Climate*. 24, 21 (Nov.-2011), 5538–5554. doi: 10.1175/2011JCLI4010.1.

**Mudelsee** (**2014**) Manfred Mudelsee. Spectral Analysis. 169–215. doi: 10.1007/978-3-319-04450-7_5.

**Neelin et al.** (**1987**) J. David Neelin et al. Modeling Tropical Convergence Based on the Moist Static Energy Budget. *Monthly Weather Review*. 115, 1 (Jan.-1987), 3–12. doi: 10.1175/1520-0493(1987)115<0003:MTCBOT>2.0.CO;2.

**Nicholson** (**2000**) S. E. Nicholson. The nature of rainfall variability over Africa on time scales of decades to millenia. *Global and Planetary Change*. 26, 1–3 (2000), 137–158. doi: 10.1016/S0921-8181(00)00040-0.

**van Oldenborgh et al.** (**2005**) G. J. van Oldenborgh et al. El Niño in a changing climate: a multi-model study. *Ocean Science*. 1, 2 (Oct.-2005), 81–95. doi: 10.5194/os-1-81-2005.

**Paolo et al.** (**2015**) Fernando S. Paolo et al. Volume loss from Antarctic ice shelves is accelerating. *Science*. 348, 6232 (Apr.-2015), 327–331. doi: 10.1126/science.aaa0940.

**Pausata et al.** (**2017**) Francesco S. R. Pausata et al. Tropical cyclone activity enhanced by Sahara greening and reduced dust emissions during the African Humid Period. *Proceedings of the National Academy of Sciences of the United States of America*. 114, 24 (Jun.-2017), 6221–6226. doi: 10.1073/pnas.1619111114.

**Pausata et al.** (**2020**) Francesco S. R. Pausata et al. The Greening of the Sahara: Past Changes and Future Implications. *One Earth*. 2, 3 (Mar.-2020), 235–250. doi: 10.1016/j.oneear.2020.03.002.

**Pontes et al.** (**2020**) G. M. Pontes et al. Reduced Atlantic variability in the mid-Pliocene. *Climatic Change*. 160, 3 (Jun.-2020), 445–461. doi: 10.1007/s10584-020-02675-9.

**Power et al.** (**2021**) Scott Power et al. Decadal climate variability in the tropical Pacific: Characteristics, causes, predictability, and prospects. *Science*. 374, 6563 (Oct.-2021). doi: 10.1126/SCIENCE.AAY9165.

**Power et al.** (**2012**) Scott B. Power et al. Consensus on Twenty-First-Century Rainfall Projections in Climate Models More Widespread than Previously Thought. *Journal of Climate*. 25, 11 (Jun.-2012), 3792–3809. doi: 10.1175/JCLI-D-11-00354.1.

**Reboita et al.** (**2019**) Michelle Simões Reboita et al. The South Atlantic Subtropical Anticyclone: Present and Future Climate. *Frontiers in Earth Science*. 7, (Feb.-2019), 8. doi: 10.3389/feart.2019.00008.

**Rehfeld et al.** (**2018**) Kira Rehfeld et al. Global patterns of declining temperature variability from the Last Glacial Maximum to the Holocene. *Nature*. 554, (2018), 356–359. doi: 10.1038/nature25454.

**Richter et al.** (**2014**) Ingo Richter et al. Equatorial Atlantic variability and its relation to mean state biases in CMIP5. *Climate Dynamics*. 42, (2014), 171–188. doi: 10.1007/s00382-012-1624-5.

**Rosenbloom et al.** (**2013**) N. a. Rosenbloom et al. Simulating the mid-Pliocene Warm Period with the CCSM4 model. *Geoscientific Model Development*. 6, 2 (2013), 549–561. doi: 10.5194/gmd-6-549-2013.

**RUBEY** (**1951**) WILLIAM W. RUBEY. GEOLOGIC HISTORY OF SEA WATERAN ATTEMPT TO STATE THE PROBLEM. *GSA Bulletin*. 62, 9 (Sep.-1951), 1111–1148. doi: 10.1130/0016-7606(1951)62[1111:GHOSW]2.0.CO;2.

**Salzmann et al.** (**2008**) U. Salzmann et al. A new global biome reconstruction and data-model comparison for the Middle Pliocene. *Global Ecology and Biogeography*. 17, 3 (May.-2008), 432–447. doi: 10.1111/j.1466-8238.2008.00381.x.

**Santoso et al.** (**2013**) Agus Santoso et al. Late-twentieth-century emergence of the El Niño propagation asymmetry and future projections. *Nature*. 504, 7478 (Nov.-2013), 126–130. doi: 10.1038/nature12683.

**Santoso et al.** (**2017**) Agus Santoso et al. The Defining Characteristics of ENSO Extremes and the Strong 2015/2016 El Niño. *Reviews of Geophysics*. Blackwell Publishing Ltd. doi: 10.1002/2017RG000560.

**Santoso et al.** (**2019**) Agus Santoso et al. Dynamics and predictability of El Niño-Southern oscillation: An Australian perspective on progress and challenges. *Bulletin of the American Meteorological Society*. 100, 3 (Mar.-2019), 403–420. doi: 10.1175/BAMS-D-18-0057.1.

**Sarmiento and Bryan** (**1982**) J. L. Sarmiento and K. Bryan. An ocean transport model for the North Atlantic. *Journal of Geophysical Research*. 87, C1 (1982), 394. doi: 10.1029/JC087iC01p00394.

**De Schepper et al.** (**2009**) Stijn De Schepper et al. North Atlantic Current variability through marine isotope stage M2 (circa 3.3 Ma) during the mid-Pliocene. *Paleoceanography*. 24, 4 (Dec.-2009). doi: 10.1029/2008PA001725.

**De Schepper et al.** (**2013**) Stijn De Schepper et al. Northern Hemisphere Glaciation during the globally warm early late Pliocene. *PLoS ONE*. 8, 12 (2013). doi: 10.1371/journal.pone.0081508.

**Schneider et al.** (**2014**) Tapio Schneider et al. Migrations and dynamics of the intertropical convergence zone. *Nature*. 513, 7516 (2014), 45–53. doi: 10.1038/nature13636.

**Schneider** (**2017**) Tapio Schneider. Feedback of Atmosphere-Ocean Coupling on Shifts of the Intertropical Convergence Zone. *Geophysical Research Letters*. 44, 22 (Nov.-2017), 11,644-11,653. doi: 10.1002/2017GL075817.

**Scroxton et al.** (**2011**) N. Scroxton et al. Persistent El Niño-Southern Oscillation variation during the Pliocene Epoch. *Paleoceanography*. 26, 2 (2011), 1–13. doi: 10.1029/2010PA002097.

**Seki et al.** (**2010**) Osamu Seki et al. Alkenone and boron-based Pliocene pCO2 records. *Earth and Planetary Science Letters*. 292, 1–2 (2010), 201–211. doi: 10.1016/j.epsl.2010.01.037.

**Servain et al.** (**2000**) Jacques Servain et al. The Relationship Between the Simulation Climatic Variability Modes of the Tropical Atlantic. *International Journal of Climatology*. 20, March 2014 (2000), 939–953. doi: 10.1002/1097-0088(200007)20.

**Stellema et al.** (**2019**) Annette Stellema et al. Projected slow down of South Indian Ocean circulation. *Scientific Reports*. 9, 1 (Dec.-2019), 17705. doi: 10.1038/s41598-019-54092-

3.

**Stepanek and Lohmann** (**2012**) C. Stepanek and G. Lohmann. Modelling mid-pliocene climate with COSMOS. *Geoscientific Model Development*. 5, 5 (2012), 1221–1243. doi: 10.5194/gmd-5-1221-2012.

**Stepanek et al.** (**2020**) Christian Stepanek et al. Contribution of the coupled atmosphere-ocean-sea ice-vegetation model COSMOS to the PlioMIP2. *Climate of the Past*. 16, 6 (Nov.-2020), 2275–2323. doi: 10.5194/cp-16-2275-2020.

**Stevenson** (**2012**) S. L. Stevenson. Significant changes to ENSO strength and impacts in the twenty-first century: Results from CMIP5. *Geophysical Research Letters*. 39, 17 (Sep.-2012). doi: 10.1029/2012GL052759.

**Stroeve et al.** (**2007**) Julienne Stroeve et al. Arctic sea ice decline: Faster than forecast. *Geophysical Research Letters*. 34, 9 (May.-2007). doi: 10.1029/2007GL029703.

**Sun et al.** (**2016**) Yong Sun et al. Drivers and mechanisms for enhanced summer monsoon precipitation over East Asia during the mid-Pliocene in the IPSL-CM5A. *Climate Dynamics*. 46, 5–6 (Mar.-2016), 1437–1457. doi: 10.1007/s00382-015-2656-4.

**Sutton and Hodson** (**2015**) Rowan T. Sutton and Daniel L. R. Hodson. Atlantic Ocean Forcing of North American and European Summer Climate. *Science (New York, N.Y.)*. 309, 5731 (2015), 115–118.

**Tan et al.** (**2020**) Ning Tan et al. Modeling a modern-like *p*CO2 warm period (Marine Isotope Stage KM5c) with two versions of an Institut Pierre Simon Laplace atmosphere-ocean coupled general circulation model. *Climate of the Past*. 16, 1 (Jan.-2020), 1–16. doi: 10.5194/cp-16-1-2020.

**Taschetto et al.** (**2014**) Andréa S. Taschetto et al. Cold Tongue and Warm Pool ENSO Events in CMIP5: Mean State and Future Projections. *Journal of Climate*. 27, (2014), 2861–2885. doi: 10.1175/JCLI-D-13-00437.1.

**Tian and Dong** (**2020**) Baijun Tian and Xinyu Dong. The Double-ITCZ Bias in CMIP3, CMIP5 and CMIP6 Models Based on Annual Mean Precipitation. *Geophysical Research Letters*. (Mar.-2020), e2020GL087232. doi: 10.1029/2020GL087232.

**Tierney et al.** (**2019**) Jessica E. Tierney et al. Pliocene Warmth Consistent With Greenhouse Gas Forcing. *Geophysical Research Letters*. 46, 15 (Aug.-2019), 9136–9144. doi: 10.1029/2019GL083802.

**Timmermann et al.** (**2018**) Axel Timmermann et al. El Niño–Southern Oscillation complexity. *Nature*. Nature Publishing Group. doi: 10.1038/s41586-018-0252-6.

**Tindall et al.** (**2016**) Julia C. Tindall et al. Accounting for centennial-scale variability when detecting changes in ENSO: A study of the Pliocene. *Paleoceanography*. 31, 10 (2016), 1330–1349. doi: 10.1002/2016PA002951.

**Ting et al.** (**2011**) Mingfang Ting et al. Robust features of Atlantic multi-decadal variability and its climate impacts. *Geophysical Research Letters*. 38, LI7705 (2011), 1–6. doi: 10.1029/2011GL048712.

**Trenberth and Shea** (**2006**) Kevin E. Trenberth and Dennis J. Shea. Atlantic hurricanes and natural variability in 2005. *Geophysical Research Letters*. 33, 12 (2006), 1–4. doi: 10.1029/2006GL026894.

**Trewartha** (**1968**) G. T. Trewartha. *An introduction to climate*. McGraw-Hill Book Co.

**Tzedakis et al.** (**2018**) P. C. Tzedakis et al. Enhanced climate instability in the North Atlantic and southern Europe during the Last Interglacial. *Nature Communications*. 9, 4235 (2018), 1–14. doi: 10.1038/s41467-018-06683-3.

**Utida et al.** (**2019**) Giselle Utida et al. Tropical South Atlantic influence on Northeastern Brazil precipitation and ITCZ displacement during the past 2300 years. *Scientific Reports*. 9, 1 (Dec.-2019), 1–8. doi: 10.1038/s41598-018-38003-6.

**Vera et al.** (**2006**) C. Vera et al. Toward a Unified View of the American Monsoon Systems. *Journal of Climate*. 19, (2006), 4977–5000. Retrieved 4-Feb.-2019, from https://journals.ametsoc.org/doi/pdf/10.1175/JCLI3896.1.

**Villamayor et al.** (**2018**) J. Villamayor et al. Influence of decadal sea surface temperature variability on northern Brazil rainfall in CMIP5 simulations. *Climate Dynamics*. 51, 1–2 (2018), 563–579.

**Vimont et al.** (**2001**) Daniel J. Vimont et al. Footprinting: A seasonal connection between the tropics and mid-latitudes. *Geophysical Research Letters*. 28, 20 (Oct.-2001), 3923–3926. doi: 10.1029/2001GL013435.

**Vincent** (**1994**) D. G. Vincent. The South Pacific convergence zone (SPCZ): a review. *Monthly Weather Review*. 122, 9 (1994), 1949–1970. doi: 10.1175/1520-0493(1994)122<1949:TSPCZA>2.0.CO;2.

**Wainer et al.** (**2014**) Ilana Wainer et al. Reconstruction of the South Atlantic Subtropical Dipole index for the past 12,000 years from surface temperature proxy. *Scientific reports*. 4, 5291 (2014), 1–8. doi: 10.1038/srep05291.

**Wainer and Soares** (**1997**) Ilana Wainer and Jacyra Soares. North northeast Brazil rainfall and its decadal-scale relationship to wind stress and sea surface temperature. *Geophysical Research Letters*. 24, 3 (Feb.-1997), 277–280. doi: 10.1029/96GL03970.

**Wang et al.** (**2018**) Xin-Yue Wang et al. The strengthening of Amazonian precipitation during the wet season driven by tropical sea surface temperature forcing. *Environmental Research Letters*. (2018). doi: 10.1088/1748-9326/aadbb9.

**Wara et al.** (**2005**) Michael W. Wara et al. Permanent El Niño-like Conditions during the Pliocene Warm Period. *Source: Science, New Series*. 309, 5735 (2005), 758–761. doi: 10.1126/science.1112596.

**Watanabe et al.** (**2011**) Tsuyoshi Watanabe et al. Permanent El Niño during the Pliocene warm period not supported by coral evidence. *Nature*. 471, (2011), 209–211. doi: 10.1038/nature09777.

**White and Ravelo** (**2020**) S. M. White and A. C. Ravelo. Dampened El Niño in the Early Pliocene Warm Period. *Geophysical Research Letters*. 47, 4 (Feb.-2020), e2019GL085504. doi: 10.1029/2019GL085504.

**Widlansky et al.** (**2011**) Matthew J. Widlansky et al. On the location and orientation of the South Pacific Convergence Zone. *Climate Dynamics*. 36, 3 (Feb.-2011), 561–578. doi: 10.1007/s00382-010-0871-6.

**van der Wiel et al.** (**2015**) Karin van der Wiel et al. A dynamical framework for the origin of the diagonal South Pacific and South Atlantic Convergence Zones. *Quarterly Journal of the Royal Meteorological Society*. 141, 691 (Jul.-2015), 1997–2010. doi: 10.1002/qj.2508.

**Wycech et al.** (**2020**) J. Wycech et al. Reconstructing Pliocene west Pacific warm pool

hydroclimate using *in situ* microanalyses on fossil planktic foraminifer shells. *Paleoceanography and Paleoclimatology*. (May.-2020). doi: 10.1029/2019PA003772.

**Xie et al.** (**2010**) Shang-Ping Xie et al. Global Warming Pattern Formation: Sea Surface Temperature and Rainfall. *Journal of Climate*. 23, 4 (Feb.-2010), 966–986. doi: 10.1175/2009JCLI3329.1.

**Xie and Carton** (**2004**) Shang Ping Xie and James A. Carton. Tropical atlantic variability: Patterns, mechanisms, and impacts. *Geophysical Monograph Series*. 147, (2004), 121–142. doi: 10.1029/147GM07.

**Yun et al.** (**2021**) Kyung Sook Yun et al. Synchronized spatial shifts of Hadley and Walker circulations. *Earth System Dynamics*. 12, 1 (Feb.-2021), 121–132. doi: 10.5194/esd-12-121-2021.

**Zhang et al.** (**2014**) Honghai Zhang et al. The south pacific meridional mode: A mechanism for ENSO-like variability. *Journal of Climate*. 27, 2 (Jan.-2014), 769–783. doi: 10.1175/JCLI-D-13-00082.1.

**Zhang** (**2005**) Jinlun Zhang. Warming of the arctic ice-ocean system is faster than the global average since the 1960s. *Geophysical Research Letters*. 32, 19 (Oct.-2005), n/a-n/a. doi: 10.1029/2005GL024216.

**Zhang et al.** (**2013**) R. Zhang et al. Mid-Pliocene East Asian monsoon climate simulated in the PlioMIP. *Climate of the Past*. 9, 5 (2013), 2085–2099. doi: 10.5194/cp-9-2085-2013.

**Zhang et al.** (**2015**) Ran Zhang et al. Causes of mid-Pliocene strengthened summer and weakened winter monsoons over East Asia. *Advances in Atmospheric Sciences*. 32, 7 (Jul.-2015), 1016–1026. doi: 10.1007/s00376-014-4183-3.

**Zhang et al.** (**2019**) Rong Zhang et al. A Review of the Role of the Atlantic Meridional Overturning Circulation in Atlantic Multidecadal Variability and Associated Climate Impacts. *Reviews of Geophysics*. 57, 2 (Jun.-2019), 316–375. doi: 10.1029/2019RG000644.

**Zhang et al.** (**2012**) Z. Zhang et al. Pre-industrial and mid-Pliocene simulations with NorESM-L. *Geoscientific Model Development*. 5, (2012), 523–533. doi: 10.5194/gmd-5-523-2012.

**Zhao and Fedorov** (**2020**) Bowen Zhao and Alexey Fedorov. The effects of background zonal and meridional winds on ENSO in a coupled GCM. *Journal of Climate*. 33, 6 (Mar.-2020), 2075–2091. doi: 10.1175/JCLI-D-18-0822.1.

**Zheng et al.** (**2019**) Jianqiu Zheng et al. Contribution of sea ice albedo and insulation effects to Arctic amplification in the EC-Earth Pliocene simulation. *Climate of the Past*. 15, 1 (Feb.-2019), 291–305. doi: 10.5194/cp-15-291-2019.

**Zheng et al.** (**2013**) W. Zheng et al. The mid-Pliocene climate simulated by FGOALS-g2. *Geoscientific Model Development*. 6, (2013), 1127–1135. doi: 10.5194/gmd-6-1127-2013.

**Zhu et al.** (**2020**) Jiang Zhu et al. High climate sensitivity in CMIP6 model not supported by paleoclimate. *Nature Climate Change*. Nature Research. doi: 10.1038/s41558-020-0764-6.

**Zilli et al.** (**2019**) Marcia T. Zilli et al. The poleward shift of South Atlantic Convergence Zone in recent decades. *Climate Dynamics*. 52, 5–6 (Mar.-2019), 2545–2563. doi: 10.1007/s00382-018-4277-1.

# APPENDIX A – Supplementary Information for Chapter 5

This section provides additional information for the following analysis: (1) Position of the Subtropical Convergence Zones (STCZ) in each PlioMIP1 (Figure S1) and PlioMIP2 model (Figure S2); (2) Rainfall climatology of the STCZs (Figure S3); (3) comparison of the PlioMIPs multi-model means rainfall changes and the rainfall changes simulated with the CAM4 model (Figure S4). In addition, table S1 lists the PlioMIP models used in this study as well as their respective variables. Table S2 specifies the boundary conditions used by PlioMIP1 and PlioMIP2 models. Finally, all results computed in this study are presented in Table S3.

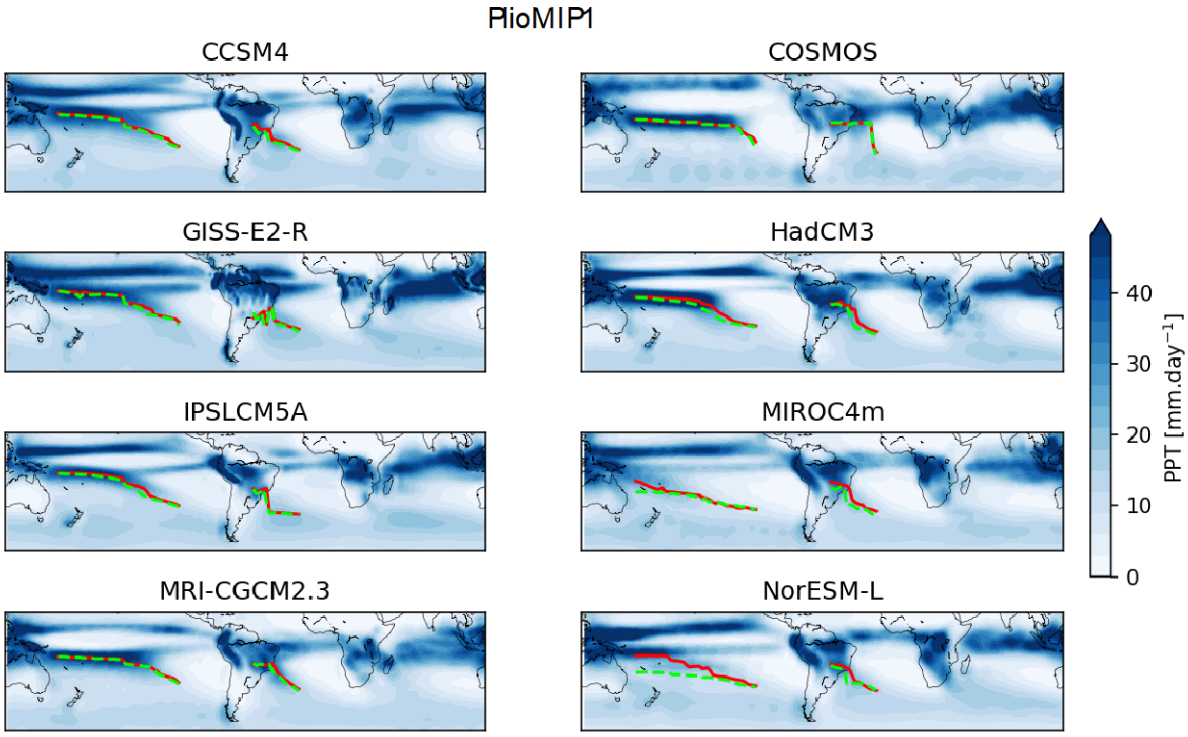


**Figure A1.** Position of the STCZs as simulated by each individual model participant of the PlioMIP1. Red: position in the pre-industrial control simulation; Green: position in the mid-Pliocene simulation.

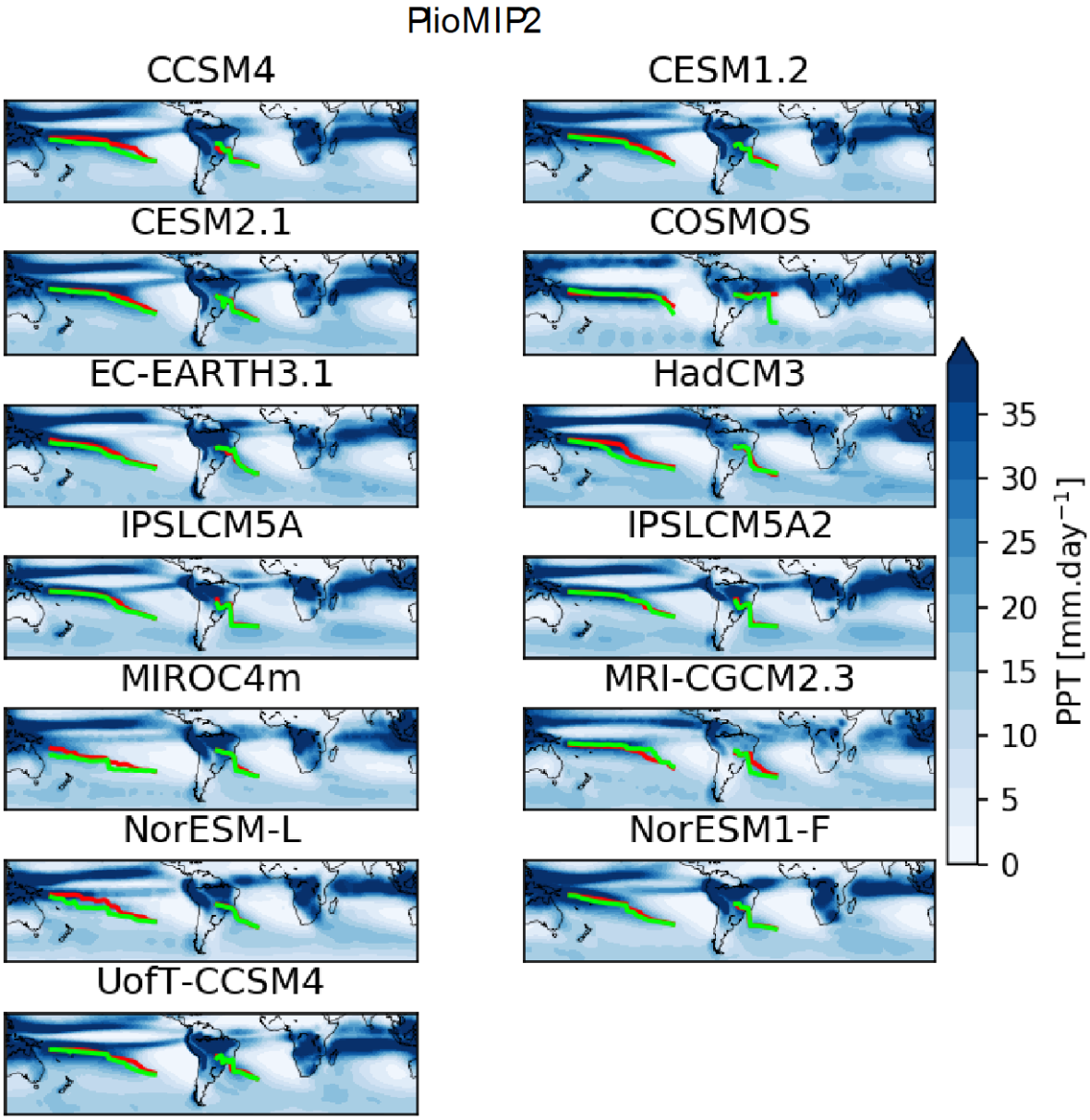


**Figure A2.** As per "Figure S1" but for PlioMIP2.

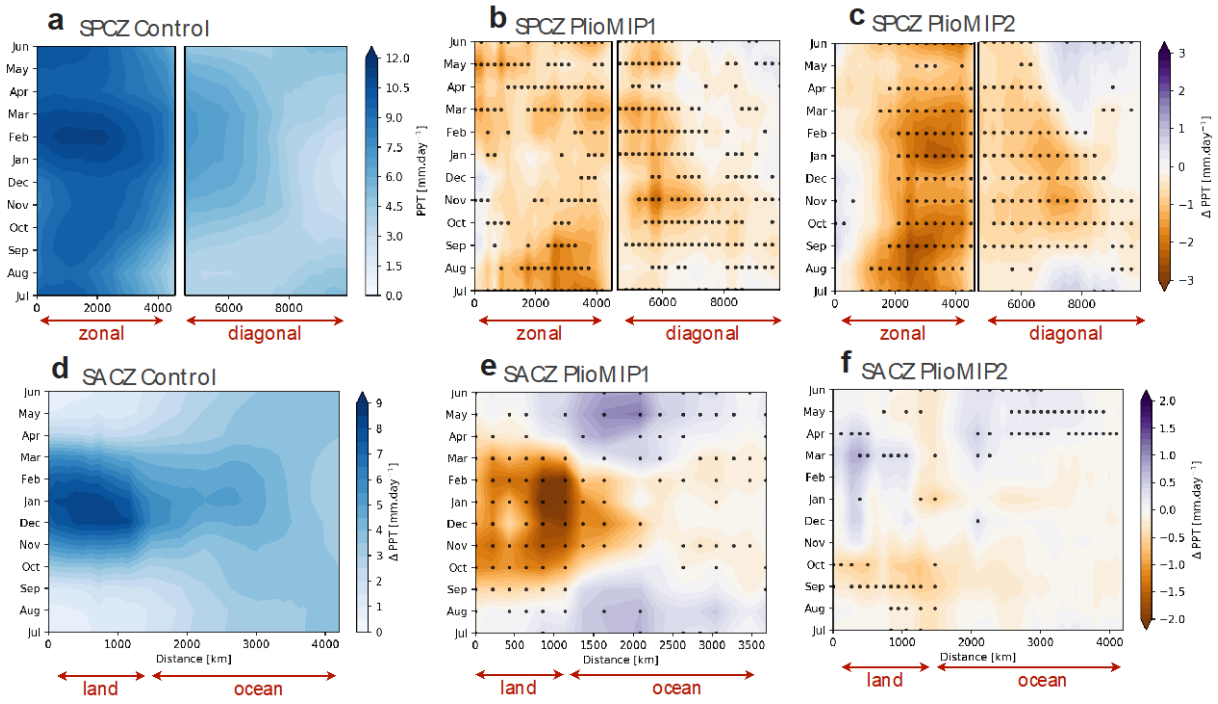


**Figure A3.** STCZs rainfall climatology. **a)** MMM rainfall climatology along the SPCZ length in the PlioMIP2 pre-industrial control simulation. **b)** MMM change (mid-Pliocene minus piControl) in the PlioMIP1 SPCZ climatology. **c)** as per 'b' but for PlioMIP2. 'd', 'e', and 'f' as per 'a', 'b' and 'c', respectively, but for SACZ. Stippling indicates 70% model agreement in the sign of the change.

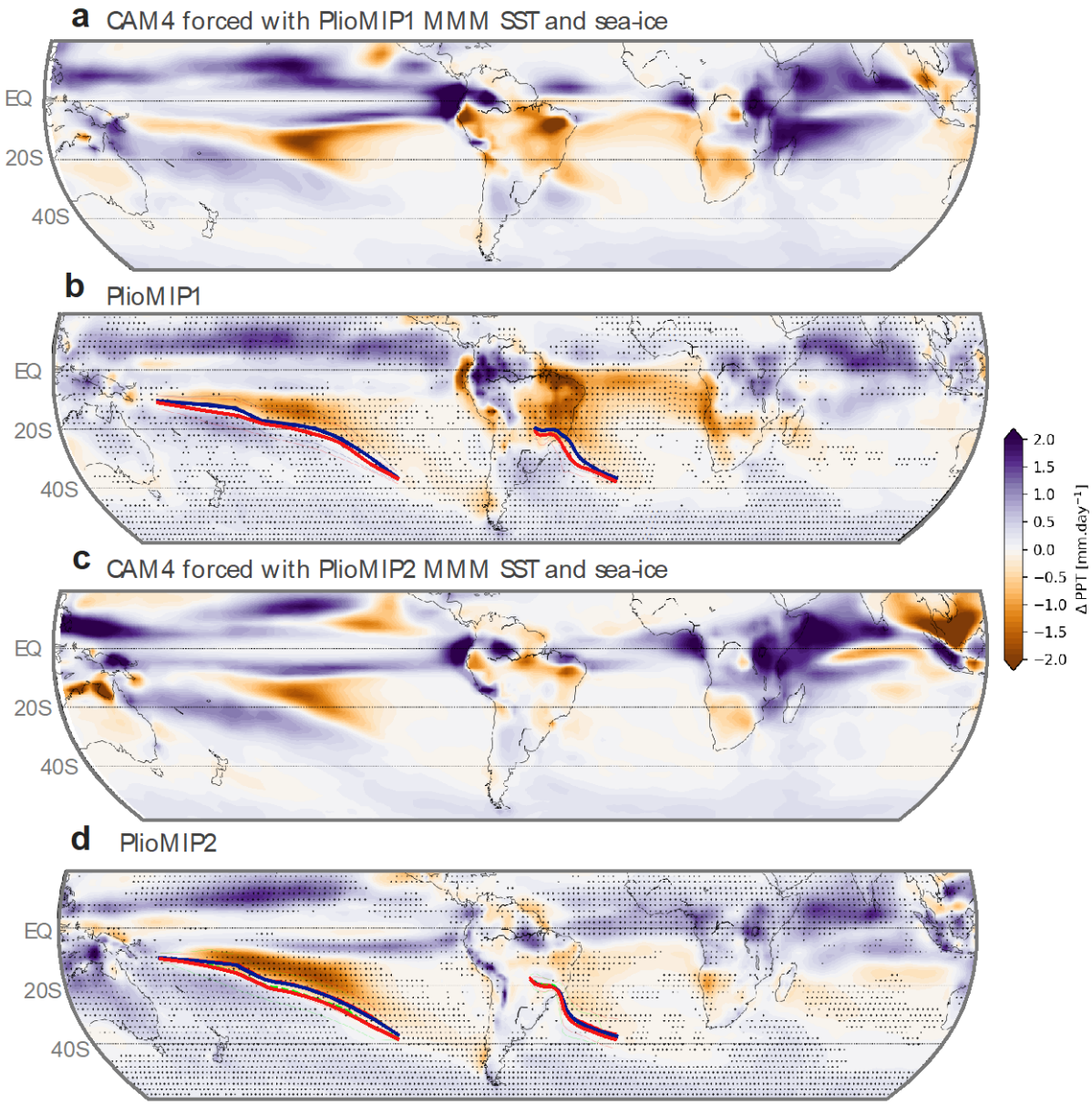


**Figure A4.** comparative of mean November-to-March rainfall changes simulated by the CAM4 model forced with PlioMIP multi-model mean SST and sea-ice with the rainfall changes simulated by the fully coupled PlioMIP models. a) 5-member ensemble mean rainfall change of the CAM4 model forced with PlioMIP1 multi-model mean and sea-ice. b) multi-model mean PlioMIP November-to-March rainfall change. c) as per 'a' but CAM4 forced with multi-model mean PlioMIP2 SST and sea-ice. d) as per 'b' but for PlioMIP2.

# APPENDIX B – Supplementary Information for Chapter 6

This section provides the individual results of each PlioMIP for the following analysis: (1) spatial representation of the Atlantic Multidecadal variability by the EOF analysis; (2) spatial representation of the Atlantic Multidecadal variability by the AMV-index metrics; (3) AMV-EOF1 spectrum; (4) AMV-index spectrum; (5) AMV-index amplitude change; (6) North Atlantic ocean transport; (7) AMV/AMOC correlations; (8) spatial representation of the AEM through the EOF analysis; (9) spatial representation of the AMM through the EOF analysis; (10) spatial representation of the AMM through the index-based metrics; (11) AMM EOF2 spectrum; (12) AMM-index spectrum; (13) AMM-index amplitude change; (14) AMM-index vs AMM gradient change; (15) spatial representation of the SASD; (16) SASD spectrum.

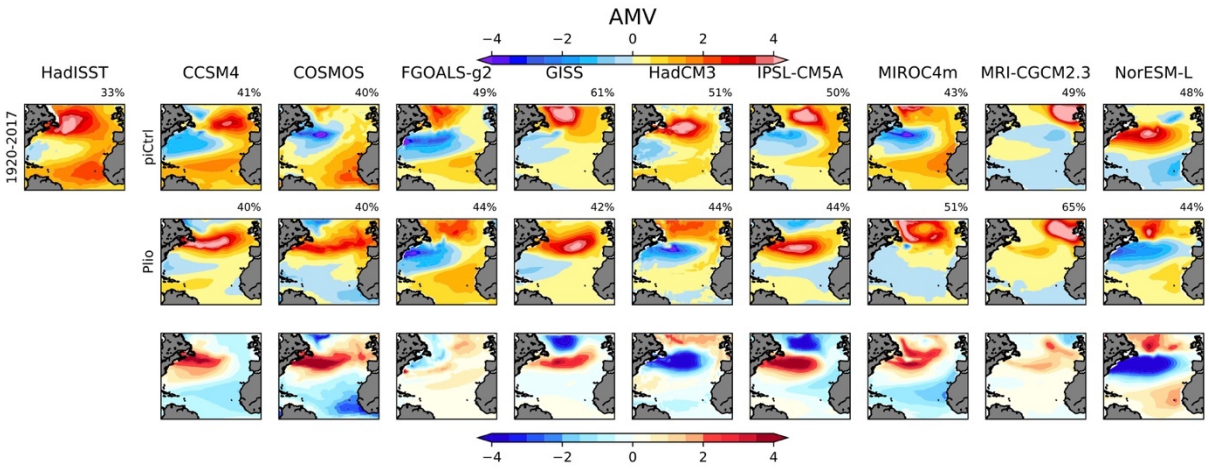


**Figure B1.** Atlantic multi-decadal variability on each PlioMIP model through the EOF method. Upper panel: HadISST AMV pattern between 1920-1950. First line: piControl AMVpattern on each PLioMIP model. Second line: mPWP pattern. Third line: difference (mPWP minus piControl).

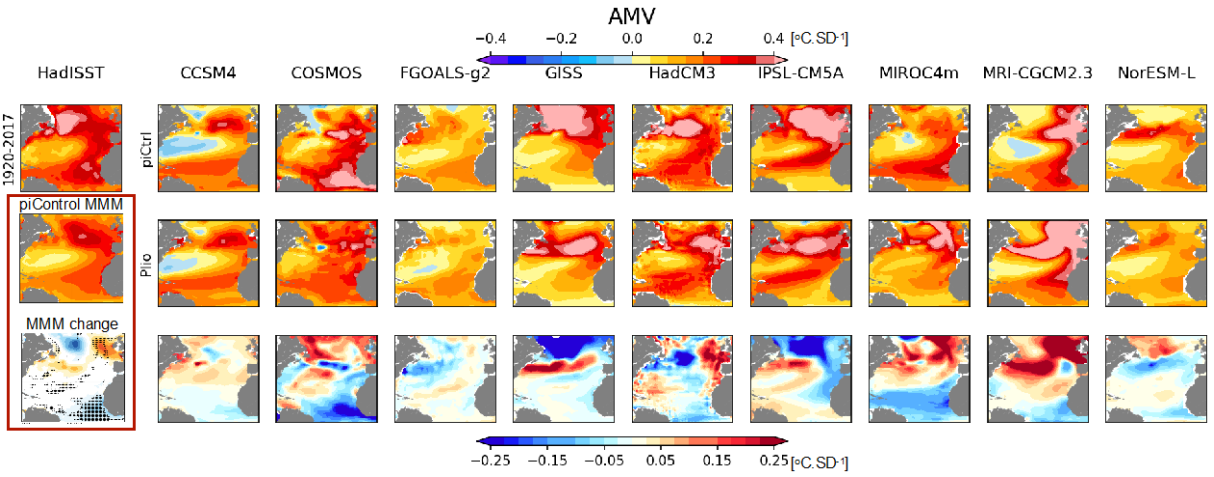


**Figure B2.** As per Figure B1 but computed through the index method.

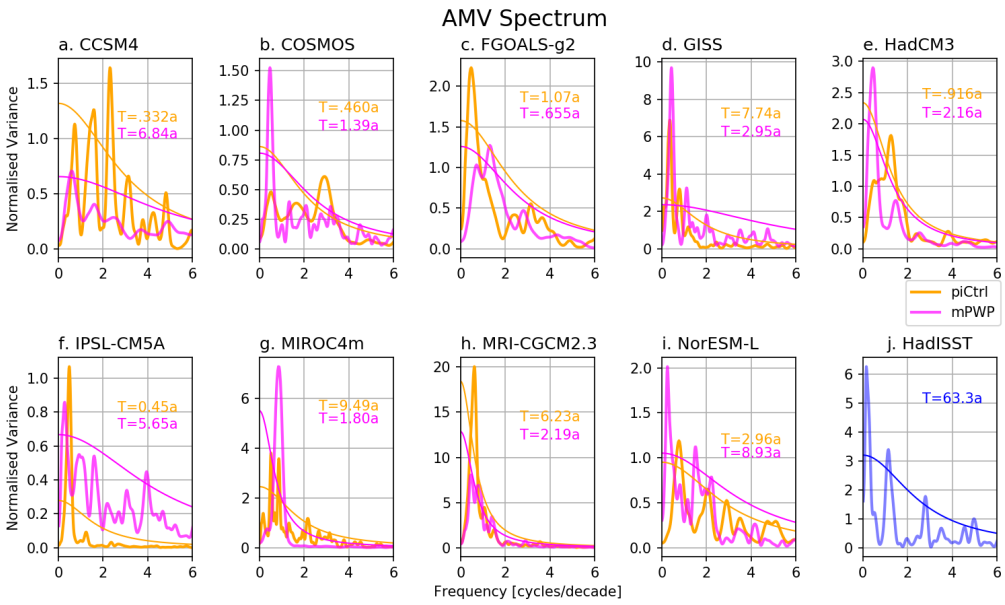


**Figure B3.** AMV spectral analysis for each PlioMIP model in the EOF method time series. Orange line: piCtrl spectrum. Magenta line: mPWP spectrum. All models, except FGOALS-g2, GISS, and MIROC4m, shifts towards lower frequencies in the mPWP. 'T' indicates the period with highest power in the spectrum for each simulation: piControl in orange and mPWP in magenta. Red noise lines are plotted at the 90% level. The "j" panel refers to HadISST observational dataset. Note: The y-axis range is different on each panel.

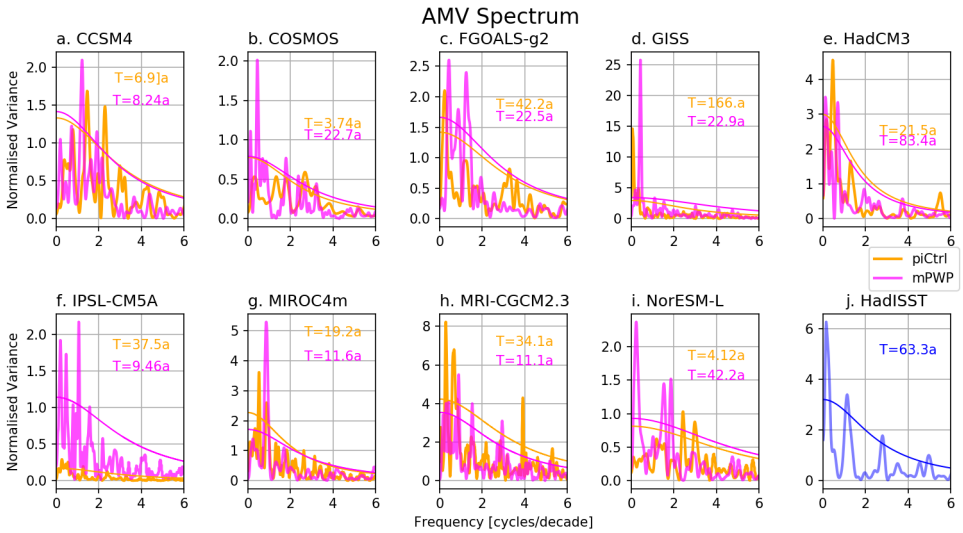


**Figure B4.** As per Figure B3 but for the index-based metrics time series.

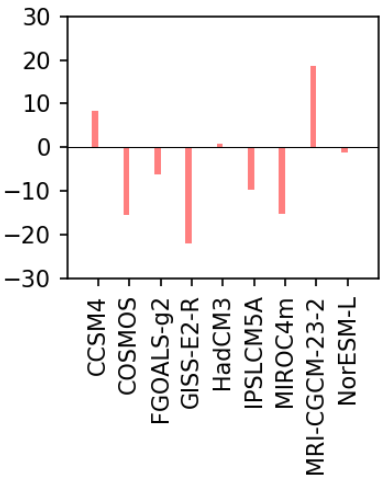


**Figure B5.** Amplitude change of the AMV index-based time series (units; %).

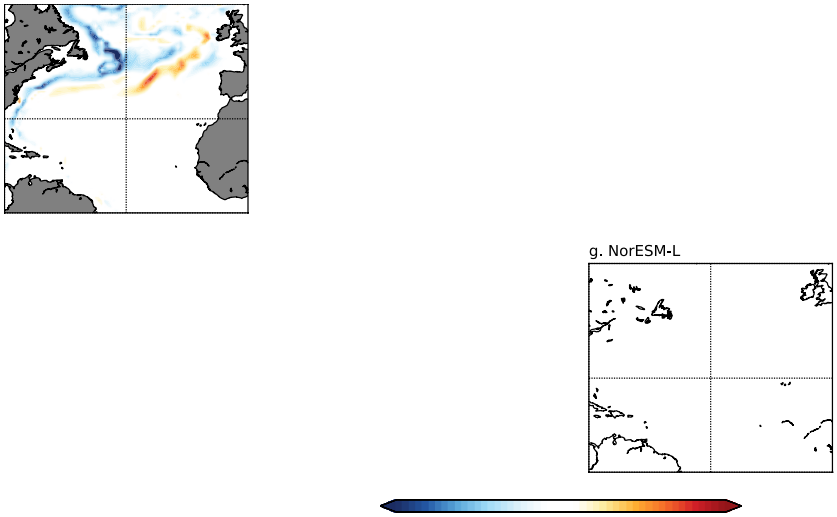


**Figure B6.** North Atlantic transport changes integrated up to 1000m. Colors show change in intensity for each PlioMIP model. Units: Sverdrup [Sv].

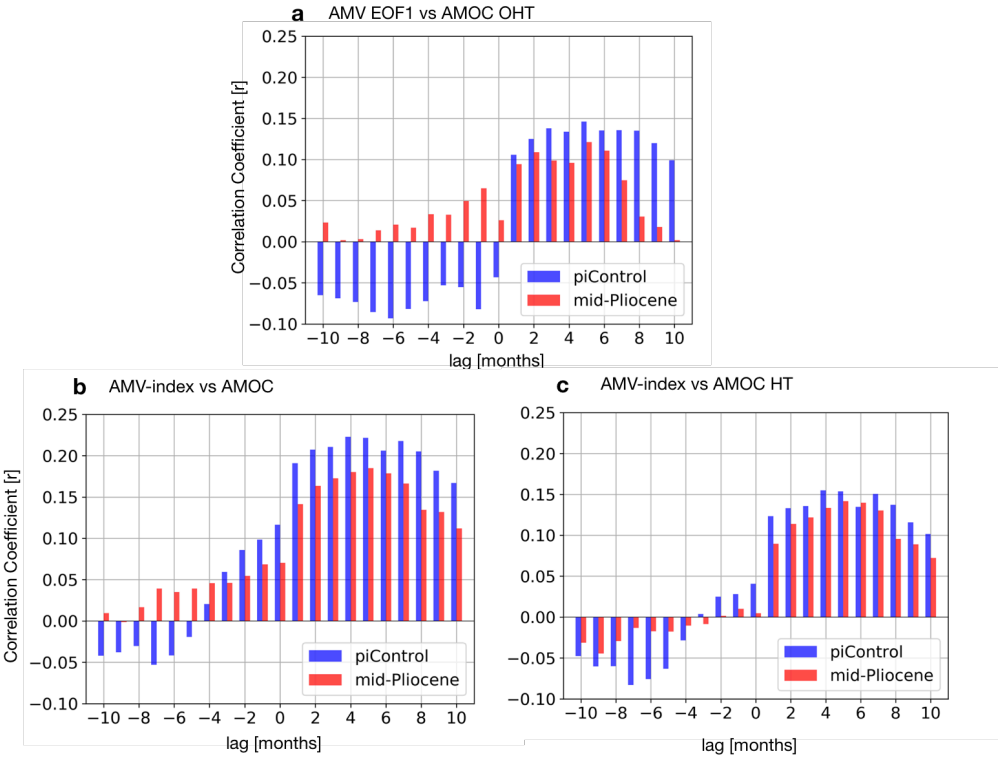


**Figure B7.** Cross correlations between a) AMV EOF1 time series and AMOC OHT anomalies, b) AMV-index time series and AMOC volume transport anomalies, and c) AMV-index time series and AMOC heat transport anomalies.


**Figure B8.** As per Figure B1 but for the EOF1 in the Tropical Atlantic (units $SD^{-1}$).

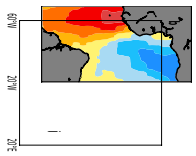

**Figure B9.** As pwe Figure B1 but for the EOF2 in the Tropical Atlantic (units: $SD^{-1}$).

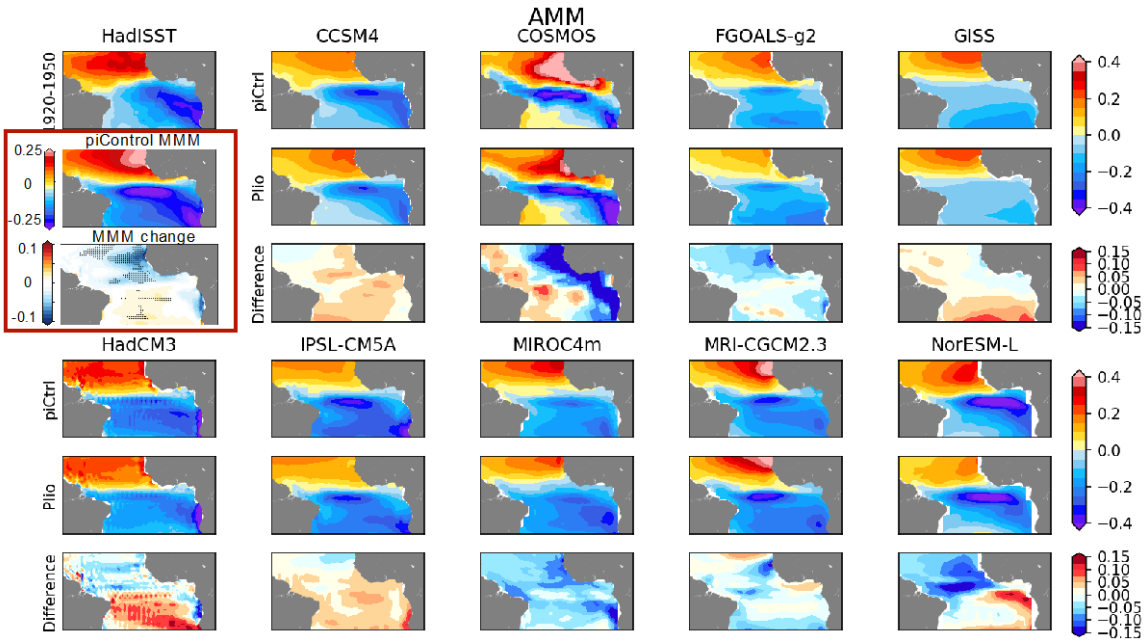


**Figure B10.** As per Figure B1 but for the AMM index (units: ºC.SD$^{-1}$).

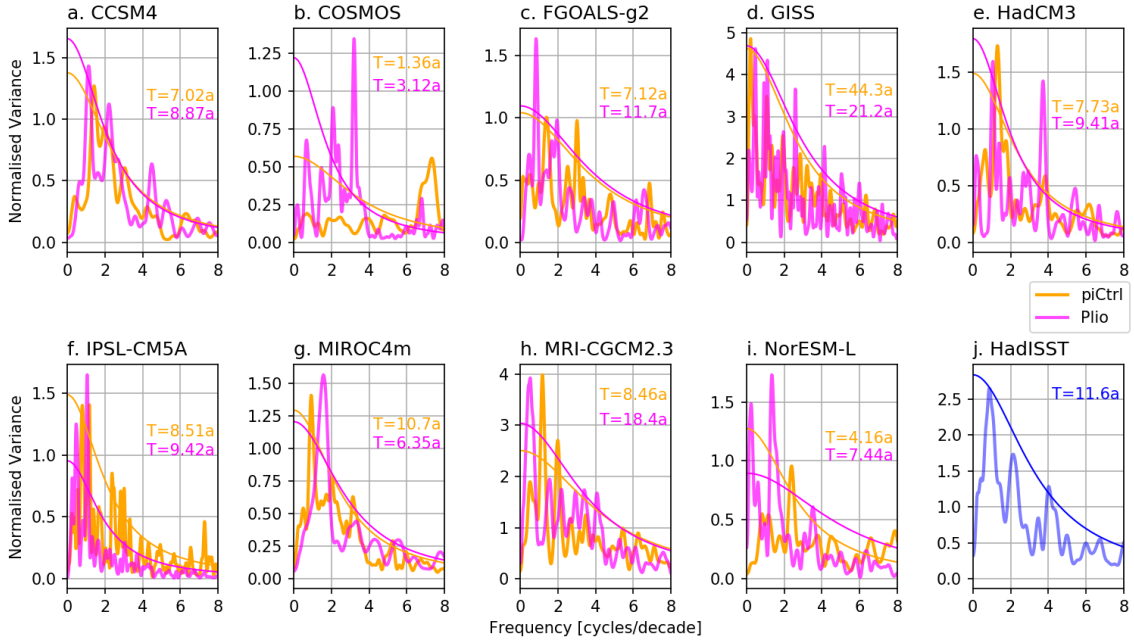


**Figure B11.** As per Figure B3 but for the EOF2 time series in the Tropical Atlantic.

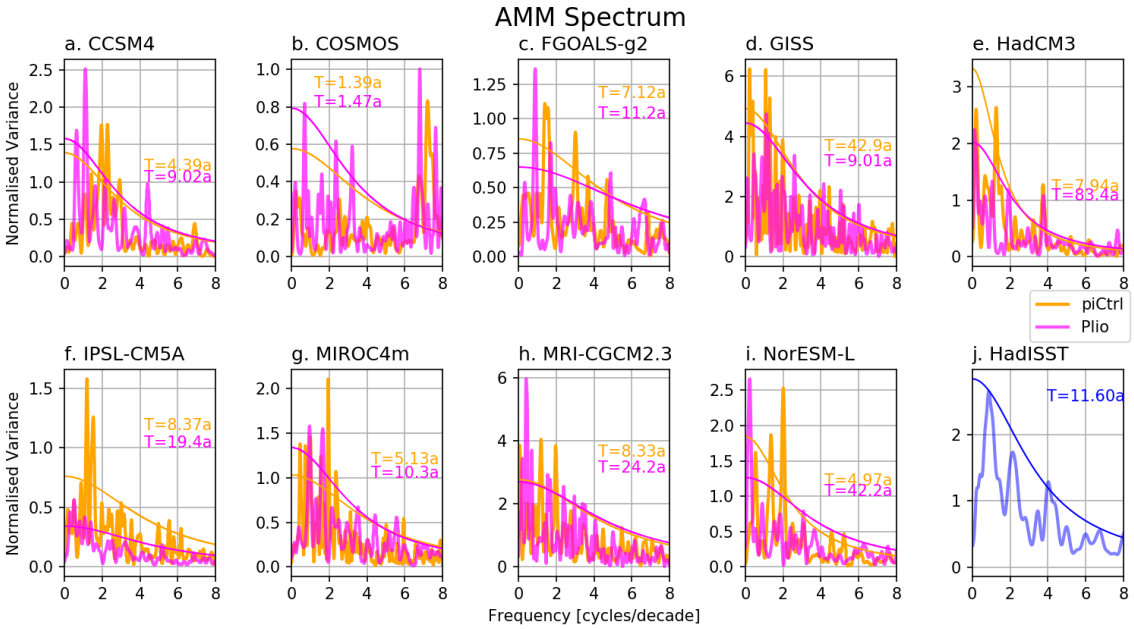


**Figure B12.** As per Figure B3 but for the AMM index time series.

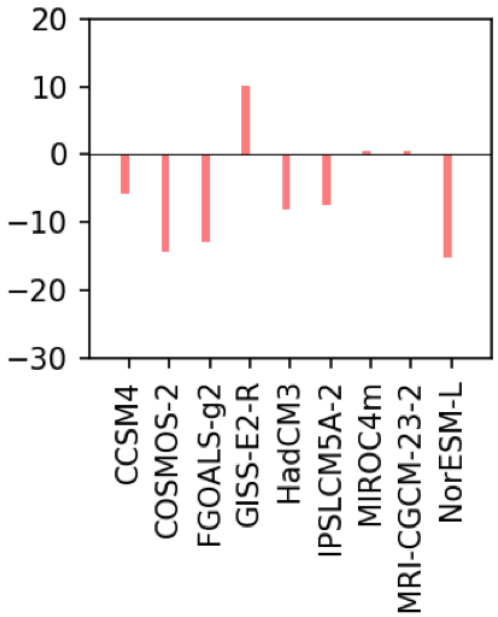


**Figure B13.** AMM-index amplitude change (units: %).

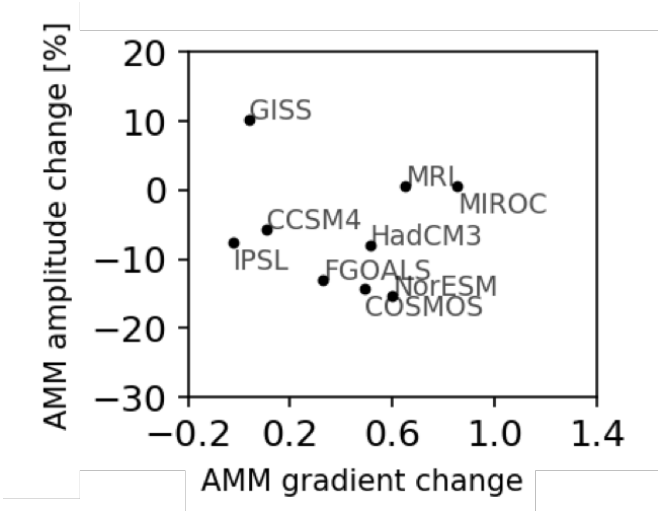


**Figure B14.** Relationship between the amplitude change in the AMM-index time series and the AMM gradient change.

**Figure B15.** As per Figure B1 but for the South Atlantic Subtropical Dipole mode (SASD; units: $SD^{-1}$).

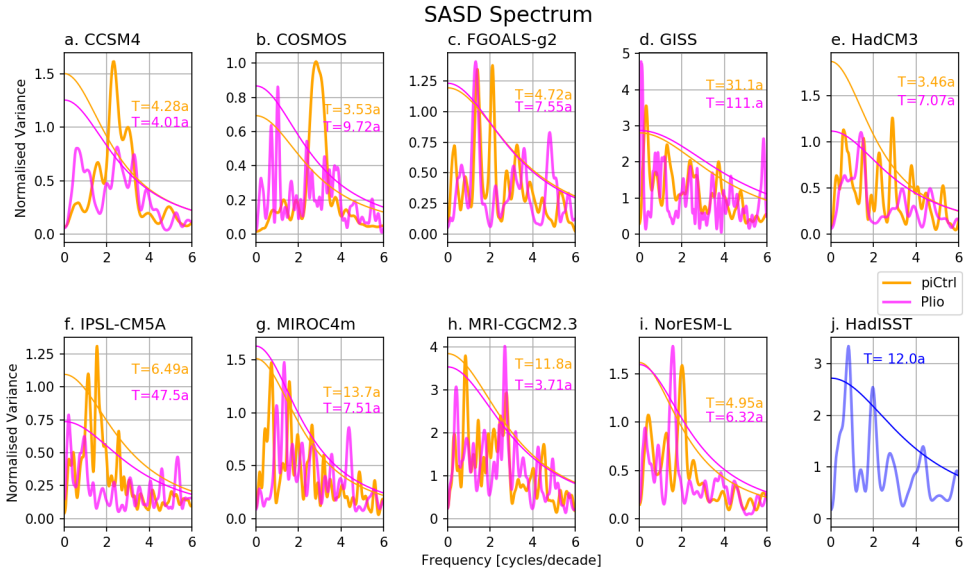


**Figure B16.** As per Figure B3 but for SASD.

# APPENDIX C – Supplementary Information for Chapter 7

This section provides additional information for the following analysis: (1) Change in the amplitude of SST variability in the PlioMIP1 models; (2) Separation of the Niño 3 amplitude change into interannual and decadal or lower periods; (3) Relationship between ENSO amplitude change and zonal SST difference; (4) Changes in low-level wind divergence; (5) Correlations between Bj index coefficients and mean state changes; (6) Evaluation of simulated ENSO non-linear characteristics for each PlioMIP2 model; (7) ITCZ-ENSO relationship for selected models (8) NPMM amplitude change; and (9) atmospheric circulation changes for PlioMIP1.

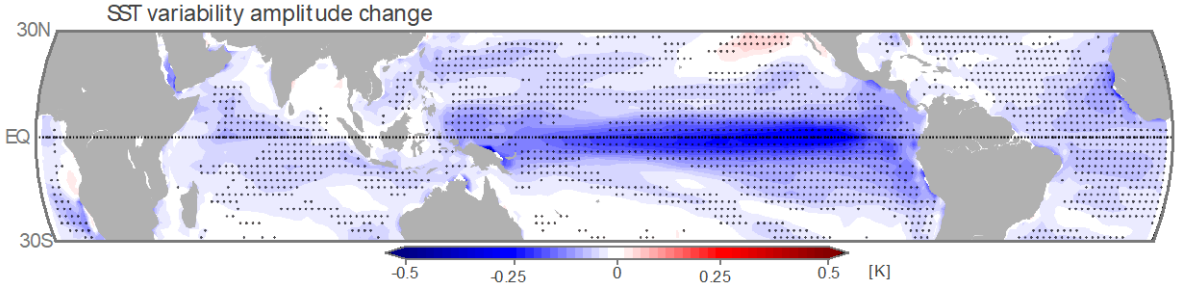


**Figure C1.** Change in amplitude of SST anomalies in the PlioMIP1 models. Stippling indicates where the change is significant at the 95% level.

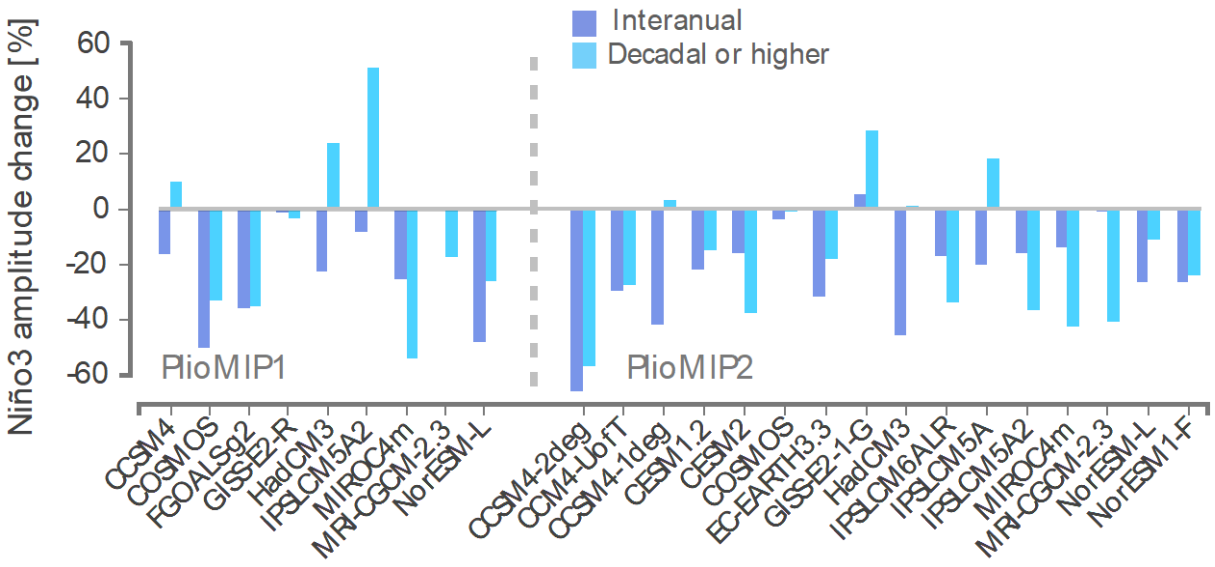


**Figure C2.** mPWP changes in eastern Pacific SST variability by frequency bands. Percentage change in Niño3 (5ºN-5ºS; 150º-90ºW) standard deviation separated by interannual (dark blue) and decadal/multi-decadal (light blue) variability. The amplitude of decadal or higher periods is evaluated through the variance of the 11-year running mean Niño3 time series in each model. The amplitude of the interannual period is estimated as the variance of the residual time series, i.e. original Niño3 timeseries subtracted from the Niño3 decadal timeseries.

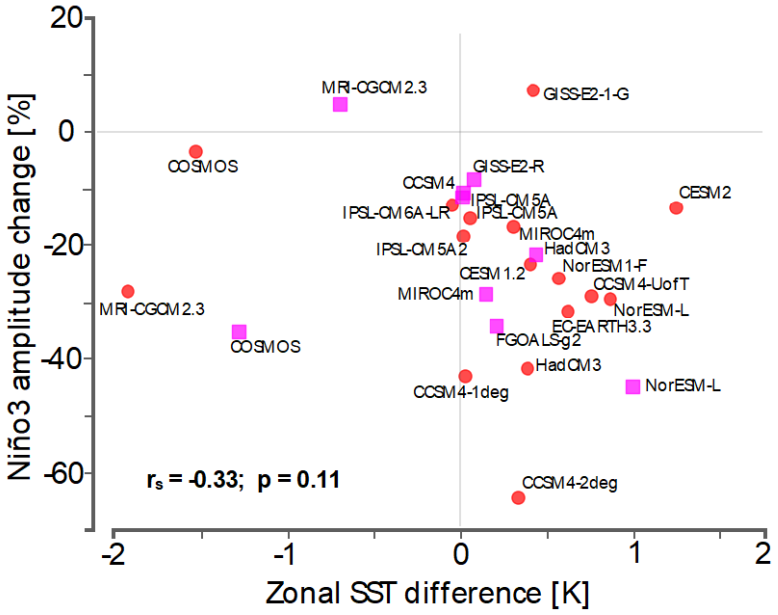


**Figure C3. Relationship between ENSO amplitude change and zonal SST difference.** Zonal SST change evaluated as the difference between the cold tongue (5ºS-5ºN; 120ºW-100ºW) and warm pool regions (5ºS-5ºN; 150ºE-170ºE) in the equatorial Pacific. PlioMIP1 models are represented by magenta squares while PlioMIP2 models are represented by red circles.

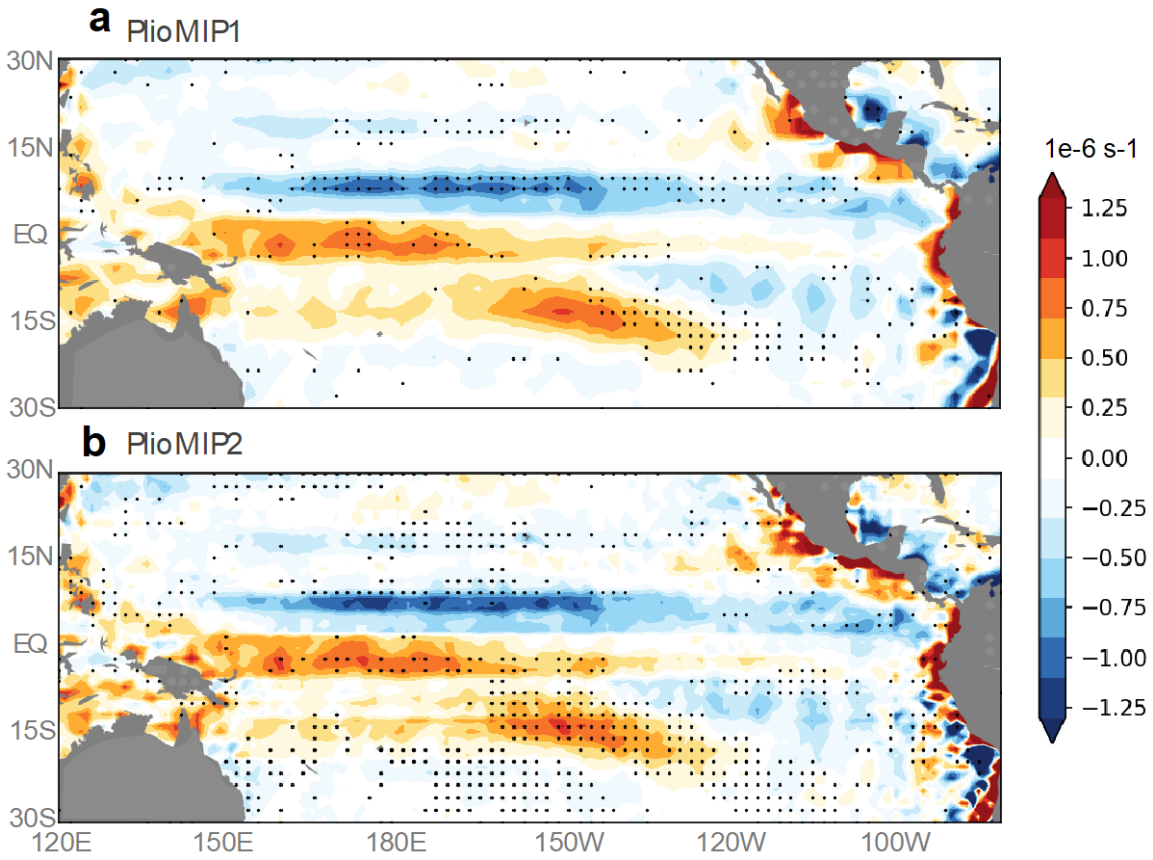


**Figure C4. Changes in the low-level wind (850hPa) divergence. a** PlioMIP1 and **b** PlioMIP2 from preindustrial. Stippling indicates where changes are significant at the 95% level. A consistent increased convergence in the tropical North Pacific indicates a northward ITCZ shift across the Pacific Ocean.

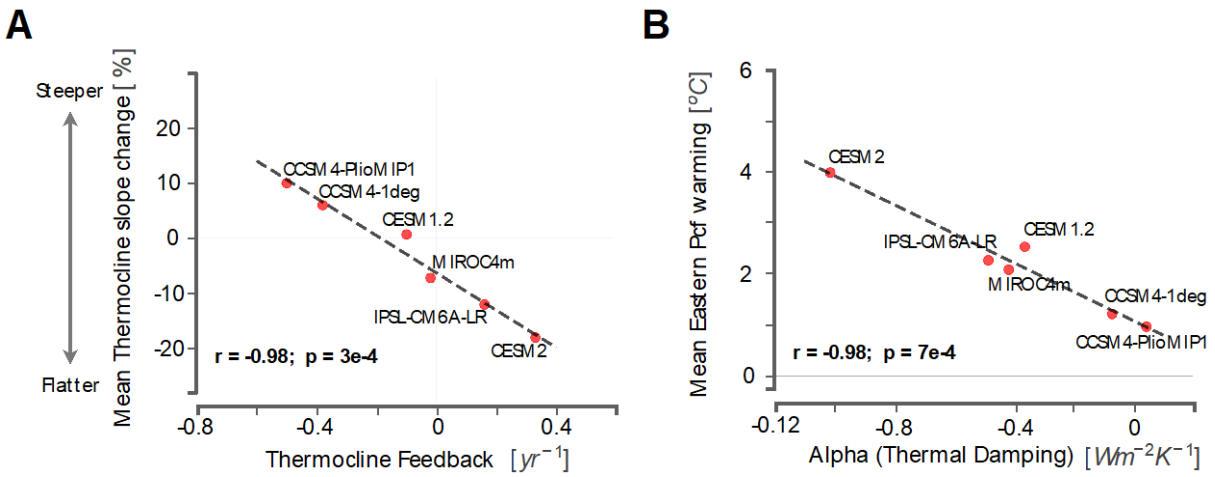


**Figure C6.** a) relationship between the change in the Thermocline Feedback and the change in the climatological thermocline slope. The thermocline slope is calculated as the difference between the mean thermocline depth in the eastern Pacific (5S-5N; 210-270E) minus that in the western Pacific (5S-5N) divided by the zonal distance between the centre of the two boxes. b) relationship between the change in the SST-heat flux coupling coefficient ($\alpha$) and the change in the mean eastern Pacific (5S-5N; 210-270E) warming.

**Criteria for model selection.** Models were selected according to their ability to simulate ENSO non-linear characteristics. Models were required to be able to simulate DJF Niño3 precipitation greater than 5 mm per day, and Niño3 precipitation skewness greater than 1 in the pre-industrial control run. These criteria underscore the essential definition of an extreme El Niño (Cai et al. 2014) which is fundamental to the ENSO system in observations (Santoso et al. 2017). Out of 14 PlioMIP2 models, six models met these criteria (Appendix C). The skewness criterion filters out models that systematically simulate overly wet and dry conditions in the eastern equatorial Pacific. Such biases tend to reduce rainfall skewness in the models as they simulate SSTs well below or above the convective threshold of 26-28ºC (Johnson and Xie 2010), affecting Niño3 precipitation variability.

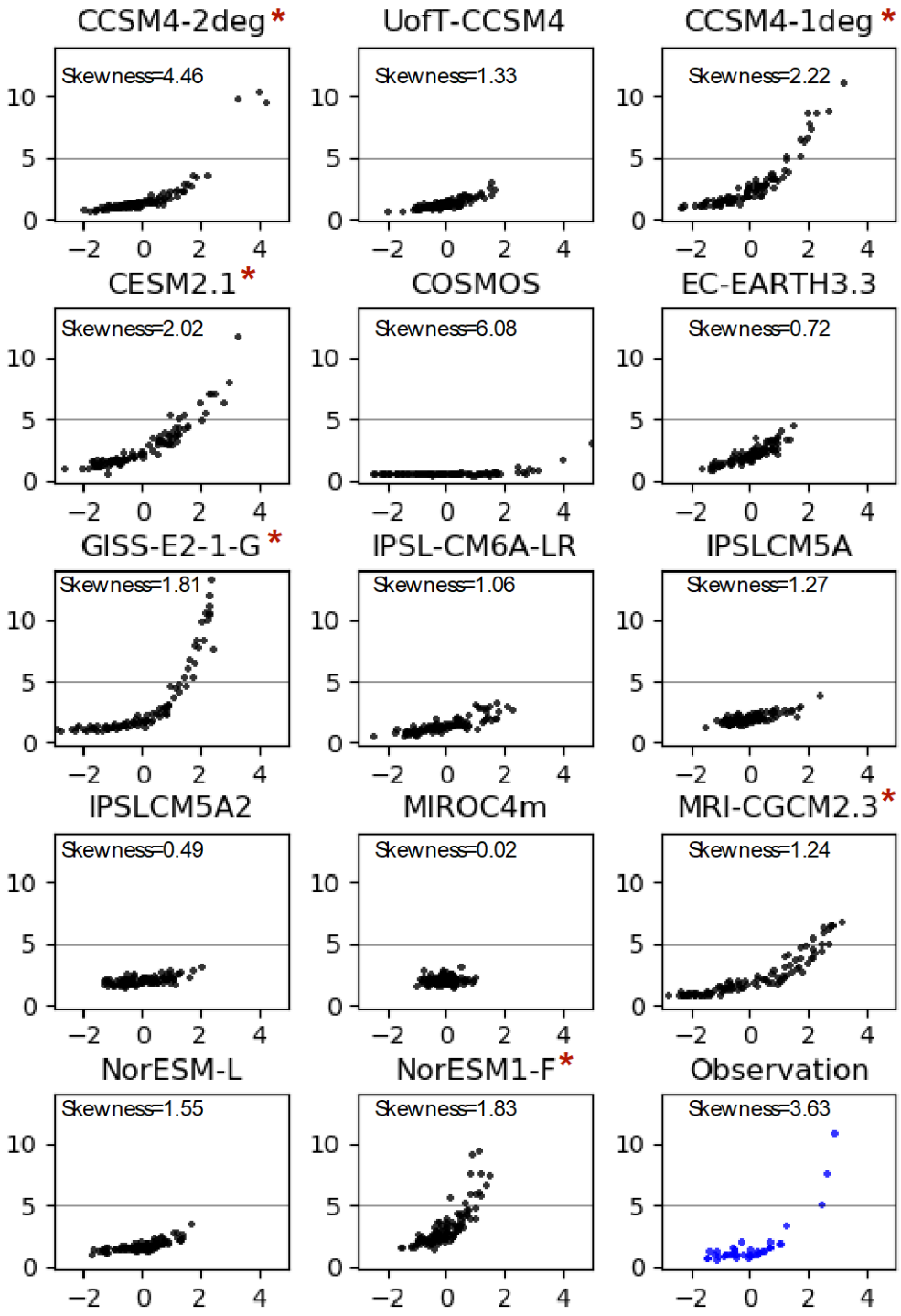


**Figure C6. ENSO non-linear characteristics for each PlioMIP2 model.** Relationship between Niño3 SST anomalies (x-axis, ºC) and Niño3 rainfall (y-axis, mm/day) for the last 100 years of the pre-industrial control simulation of each model. Observed relationship was computed from GPCP and ERSSTv5 datasets from 1979 to 2020. Models that simulate rainfall skew greater than 1 and rainfall anomalies greater than 5mm/day are marked with a 'red star'.

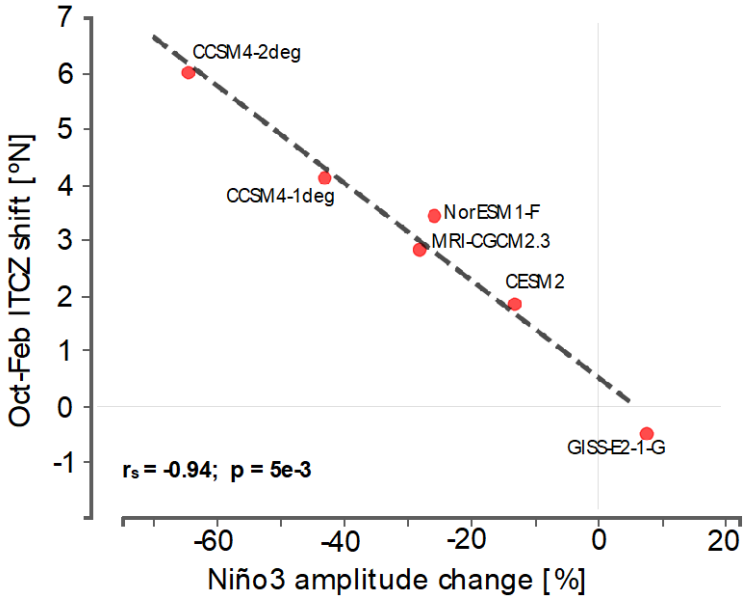


**Figure C7. ITCZ-ENSO relationship for selected models.** Relationship between the change in the Niño3 amplitude and the mean October-to-February ITCZ shift for the models that correctly captured ENSO non-linear characteristics.

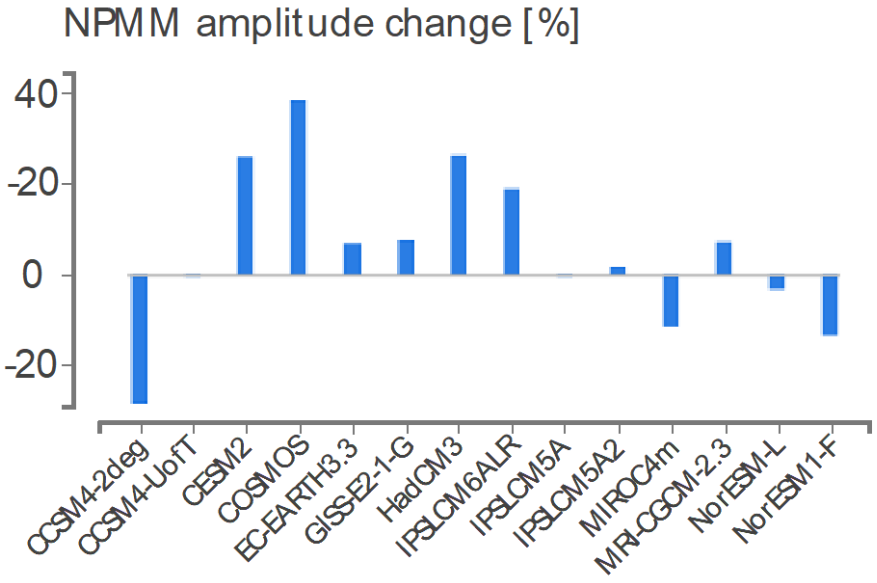


**Figure C8. NPMM amplitude change.** Simulated change in the amplitude of the North Pacific Meridional Mode.

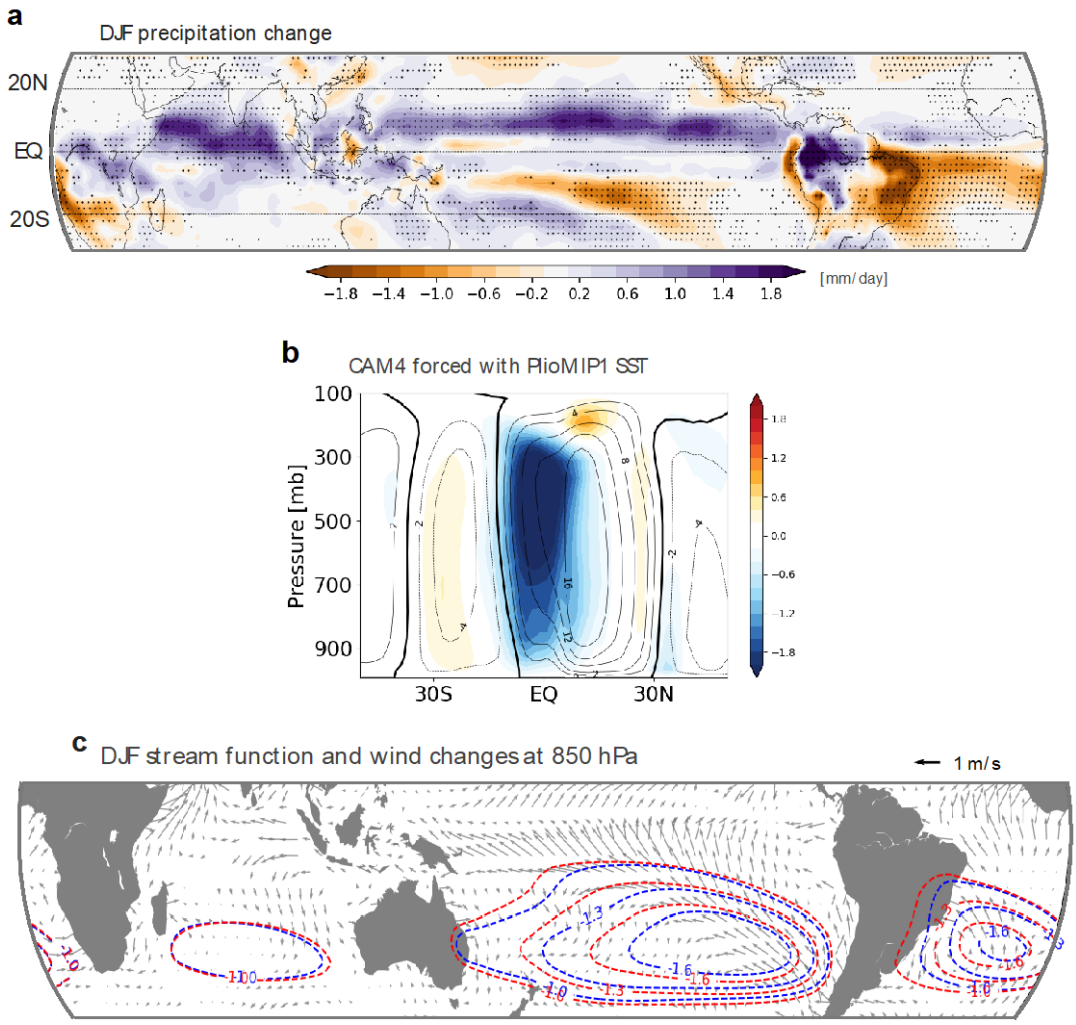


**Figure C9. Atmospheric circulation changes for PlioMIP1 models. a** multi-model mean DJF precipitation change (mPWP minus pre-industrial). Stippling indicates where changes are significant at the 95% level. **b** Changes in the meridional streamfunction in the AGCM experiment forced with climatological PlioMIP1 SST and sea-ice (see Methods). **c** multi-model mean change in low-level (850 hPa) winds and streamfunction. Wind changes are only plotted where there is a significant change at the 95% level.